Mechanisms and pathways of ocean heat anomalies in the Arctic-Atlantic region

Helene Asbjørnsen

Thesis for the degree of Philosophiae Doctor (PhD)
University of Bergen, Norway
2020

UNIVERSITY OF BERGEN

Mechanisms and pathways of ocean heat anomalies in the Arctic-Atlantic region

Helene Asbjørnsen

Thesis for the degree of Philosophiae Doctor (PhD)
at the University of Bergen

Date of defense: 10.12.2020

Year: 2020

Title: Mechanisms and pathways of ocean heat anomalies in the Arctic-Atlantic region

Name: Helene Asbjørnsen

Print: Skipnes Kommunikasjon / University of Bergen

Scientific environment

This study was carried out at the Geophysical Institute, University of Bergen, where I have been a part of the Physical Oceanography group. Additionally, I have been affiliated with the Bjerknes Centre for Climate Research, belonging to the Polar research theme. A three month research stay at the Department of Earth Science, University of Oxford has also been valuable to the presented research and the progress made. The work presented here was funded by the Norwegian Research Council project PATHWAY (grant 263223). The work has also been supported by the Nansen Legacy project (Norwegian Research Council; grant 276730), the Blue Action project (European Unions Horizon 2020 research and innovation program; grant 727852), and the Trond Mohn Foundation (grant BFS2018TMT01). I have also been enrolled in the Research School on Changing Climates in the Coupled Earth System (CHESS), which provided several relevant and interesting short-courses and meetings that I participated in.

CHESS
Research school on changing climates in the coupled earth system

UNIVERSITAS BERGENSIS

BJERKNES CENTRE
for Climate Research

Acknowledgements

I would like to take the opportunity to thank everyone that has made the work presented here possible. First and foremost, I want to thank my supervisor, Marius Årthun, for guiding me through the phd-experience. Thanks for letting me be a part of PATHWAY and for introducing me to the exciting world of oceanographic research. Your input has been invaluable, and your enthusiasm and general optimism has made the process all the more fun. I would also like to thank my two co-supervisors, Tor Eldevik and Øystein Skagseth, for contributing with ideas and for putting my research to the test. Thank you for including me in the 'cooling machine'-work and for sharing your knowledge about the complex processes in the Barents Sea. Last but not least, thank you to Helen Johnson for generously welcoming me to Oxford for a research stay during the spring of 2019. Thanks for showing interest in my research and for being a big help with the (sometimes confusing) Lagrangian trajectories.

A big thank you to the phd-community at GFI – there is no better group to have coffees or beers with. Shoutouts to Ailin and Stefanie for sticking with me at Målestuen towards the end, and to Elina for insisting on being my GFI bestie. More generally, thank you to friends and family for being a welcome distraction after long days at the office. A special thanks to mamma, pappa, and the girls in 'flokken' for your support through some frustrating home office months. Also, thank you to my former university classmates turned long-term friends for always being enthusiastic about my current endeavours.

I feel privileged to have been a part of the excellent climate research community in Bergen. I am grateful for the (pre-korona) trips to conferences and summer schools, and, most importantly, for all the friends I made along the way – you have made this a great experience!

Helene Asbjørnsen
Bergen, 16/09-2020

Abstract

Along the Atlantic water pathway, from the Gulf Stream in the south to the Arctic Ocean in the north, variability in ocean heat content is pronounced on interannual to decadal time scales. Ocean heat anomalies in this Arctic-Atlantic sector are known to affect Arctic sea ice extent, marine ecosystems, and continental climate. However, there is at present neither consensus nor any complete understanding of the mechanisms causing such heat anomalies. This dissertation obtains a more robust understanding of regional ocean heat content variability by assessing the mechanisms and pathways of ocean heat anomalies in the Arctic-Atlantic region. The results are presented in three papers.

The first paper investigates the link between a variable Nordic Seas inflow and large-scale ocean circulation changes upstream. Using a global, eddy-permitting ocean hindcast together with a Lagrangian analysis tool, numerical particles are seeded at the Iceland-Scotland Ridge and tracked backward in time. Water from the subtropics supplied by the North Atlantic Current (NAC) is found to be the main component of the Nordic Seas inflow (64%), while 26% of the inflow has a subpolar or Arctic origin. Different atmospheric patterns are seen to affect the circulation strength along the advective pathways, as well as the supply of subtropical and Arctic-origin water to the ridge through shifts in the NAC and the subpolar front. A robust link between a high transport of Arctic-origin water and a cold and fresh inflow is furthermore established, while a high transport of subtropical water leads to higher inflow salinities. The second paper investigates the mechanisms of interannual heat content variability in the Norwegian Sea downstream of the Iceland-Scotland Ridge, using a state-of-the-art ocean state estimate and closed heat budget diagnostics. Ocean advection is found to be the primary contributor to heat content variability in the Atlantic domain of the Norwegian Sea, although local surface fluxes also play an active role. Anomalous heat advection furthermore depends on the strength of the Atlantic water inflow and the conditions upstream of the ridge. Combined, the two papers demonstrate the importance of gyre dynamics and large-scale wind forcing in causing variability at the ridge, while highlighting the impacts on Norwegian Sea heat content downstream.

For the third paper, warming trends in the Barents Sea and Fram Strait are explored, and, thus, the mechanisms underlying recent Atlantification of the Arctic Ocean. The Barents Sea is seen to transition to a warmer state, with reduced sea ice concentrations and Atlantic water extending further poleward. The mechanisms driving the warming are, however, found to be regionally dependent and not stationary in time. In the ice-free region, ocean advection is found to be a major driver of the warming trend due

to increasing inflow temperatures in the late 1990s and early 2000s, while reduced ocean heat loss is contributing to the warming trend from the mid-2000s and onward. A considerable upper-ocean warming and a weakened stratification is seen in the ice-covered northwestern Barents Sea. However, in contrast to what has been previously hypothesized, the results do not point to increased upward heat fluxes from the Atlantic water layer to the Arctic surface layer as the source of the upper-ocean warming.

The supply of Atlantic heat to the Nordic Seas and the Arctic Ocean has been scrutinized using both Lagrangian methods and heat budget diagnostics. Combined, the three papers demonstrate the important role of ocean heat transport in causing regional heat content variability and change in the Arctic-Atlantic region. A better understanding of interannual to decadal ocean heat content variability has implications for future prediction efforts, and for how we understand the ocean's role in ongoing and future climate change.

List of abbreviations

BSO: Barents Sea Opening

EAP: East Atlantic Pattern

NAC: North Atlantic Current

NAO: North Atlantic Oscillation

NwAC: Norwegian Atlantic Current

OGCM: Ocean general circulation model

SPG: Subpolar Gyre

SPNA: Subpolar North Atlantic

SSS: Sea surface salinity

SST: Sea surface temperature

STG: Subtropical Gyre

Outline

This dissertation consists of an introductory part and three scientific papers. Chapter 1 describes the circulation in the Arctic-Atlantic region, and introduces the topic of poleward heat transport and ocean heat content variability. Objectives are stated and methods are described in chapter 2. A brief summary of the papers is given in chapter 3, while perspectives and outlook are provided in chapter 4. The three papers included in the dissertation (chapter 5; Paper I–III) are listed below. Additional contributions relevant to the presented work have been included as an addendum (chapter 6; Paper A).

List of papers

I. Asbjørnsen, H., Johnson, H., Årthun, M., (in prep.) *Linking variable Nordic Seas inflow to upstream circulation anomalies*, manuscript for submission to Journal of Climate.

II. Asbjørnsen, H., Årthun, M., Skagseth, Ø. Eldevik, T., (2019) *Mechanisms of ocean heat anomalies in the Norwegian Sea*, Journal of Geophysical Research: Oceans, 124(4), 2908-2923. doi: 10.1029/2018JC014649.

III. Asbjørnsen, H., Årthun, M., Skagseth, Ø. Eldevik, T., (2020) *Mechanisms underlying recent Arctic Atlantification*, Geophysical Research Letters, 47(15), 1-9. doi: 10.1029/2020GL088036.

Additional contributions

A) Skagseth, Ø., Eldevik, T., Årthun, M. Asbjørnsen, H., Lien, V. S., Smedsrud, L. H., (2020) *Reduced efficiency of the Barents Sea cooling machine*, Nature Climate Change, 10, 661-666, doi: 10.1038/s41558-020-0772-6.

Contents

Chapter 1

Introduction

Along the Atlantic water pathway, from the Gulf Stream in the south to the Barents Sea and Fram Strait in the north, ocean heat content variability is pronounced on interannual to decadal time scales. This chapter introduces the role of poleward ocean heat transport in our climate system (section 1.1), describes the main circulation features in the Arctic-Atlantic region (section 1.2), and discusses mechanisms of regional ocean heat content variability (section 1.3).

1.1 Poleward ocean heat transport

The equator receives more solar radiation than the high-latitudes, creating a net radiation surplus in the tropics and a net deficit at the poles. As a result, poleward transport of heat in the atmosphere and ocean is necessary to balance the Earth's energy budget (*Trenberth and Caron*, 2001). While a large part of the poleward heat transport is carried by the atmosphere, the ocean is also making a sizeable contribution (Figure 1.1). The ocean heat transport from the tropics to the subpolar and polar regions has implications for both high-latitude marine ecosystems, marine and continental climate, and Arctic sea ice, and is therefore an integral part of the climate system (*Palter*, 2015; *Rhines et al.*, 2008).

The temperature gradients that arise due to differential heating of the Earth's surface induce horizontal pressure gradients, ultimately resulting in the major wind patterns seen in the atmosphere. The ocean circulation is, in-part, driven by winds exerting stress on the ocean surface and thus transferring momentum to the upper-ocean (*Ekman*, 1905; *Sverdrup*, 1947). Fluxes of heat and salt are also driven by surface heat loss at high latitudes, causing convection and ventilation of the deep ocean (e.g. *Lambert et al.*, 2016; *Stommel*, 1961). This is the buoyancy-driven circulation, also termed the thermohaline circulation. The wind-driven and the buoyancy-driven circulation are intertwined and not easily disentangled (*Wunsch*, 2002), though typically considered to dominate oceanic variability on different time scales – wind-forcing on intra-annual to interannual time scales, and buoyancy forcing on decadal time scales and longer (*Buckley and Marshall*, 2016).

In the Atlantic Ocean there is net northward heat transport at all latitudes (Figure 1.2), also south of the equator because cold deep water formed in the polar and subpolar

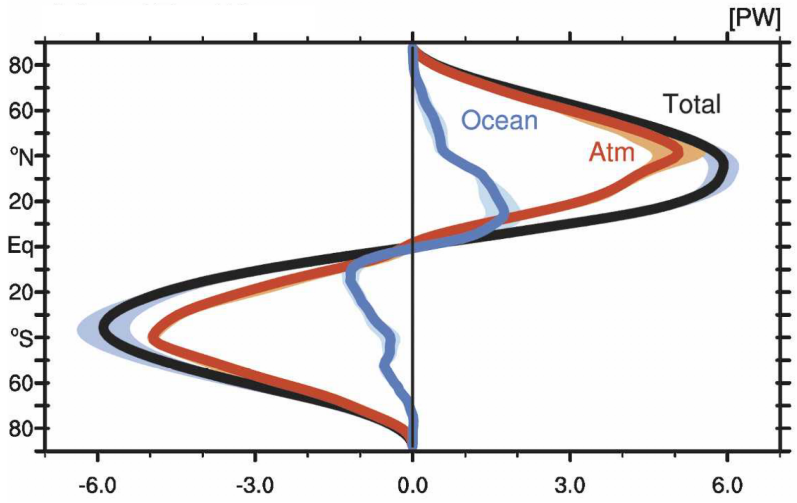

Figure 1.1: Oceanic and atmospheric poleward heat transport. *The median annual mean northward heat transport by latitude inferred from top of the atmosphere satellite measurements (ERBE), atmospheric reanalysis (NCEP-NCAR), and ocean heat content (GODAS). Total northward heat transport is drawn in black, with atmospheric (red) and oceanic (blue) contributions ($\pm 2\sigma$ in shadings). Positive vaules indicate northward heat transport and negative values indicate southward heat transport. 1 PW equals* 10^{15} *J/s. From Fasullo and Trenberth (2008).*

North Atlantic (SPNA) flows southward at depth (*Trenberth and Caron*, 2001). The net northward heat transport is characteristic for the Atlantic circulation, which is often viewed as an overturning cell transporting warm and saline water northward in its upper limb, and cold, dense water southward in its lower limb (e.g. *Buckley and Marshall*, 2016; *Frajka-Williams et al.*, 2019).

In the northern hemisphere, it is evident from Figure 1.2 that a large part of the total oceanic poleward heat transport occurs in the Atlantic Ocean, particularly dominating the overall oceanic heat transport at latitudes north of 40°N. This leaves the high-latitude ocean regions notably warmer than its Pacific counterpart. Here, the focus is mainly the upper-ocean circulation along the Atlantic water pathway from the subtropics to the Arctic (Figure 1.3) – a region where warm and saline water masses are transported northward down the temperature gradient seen in Figure 1.4. The Atlantic heat is known to inhibit sea ice growth, making the Norwegian coast and the southwestern Barents Sea largely ice-free, also in winter (*Helland-Hansen and Nansen*, 1909). The temperate eastern North Atlantic also provides heat and moisture energizing the Atlantic storm tracks, and is responsible for creating maritime climates downwind of the ocean in the northwestern Europe (*Palter*, 2015; *Rhines et al.*, 2008).

1.2 Circulation in the Arctic-Atlantic region

The Gulf Stream transports large amounts of warm, saline water from the tropics to subpolar latitudes, and is a detrimental part of our climate system. As a narrow western

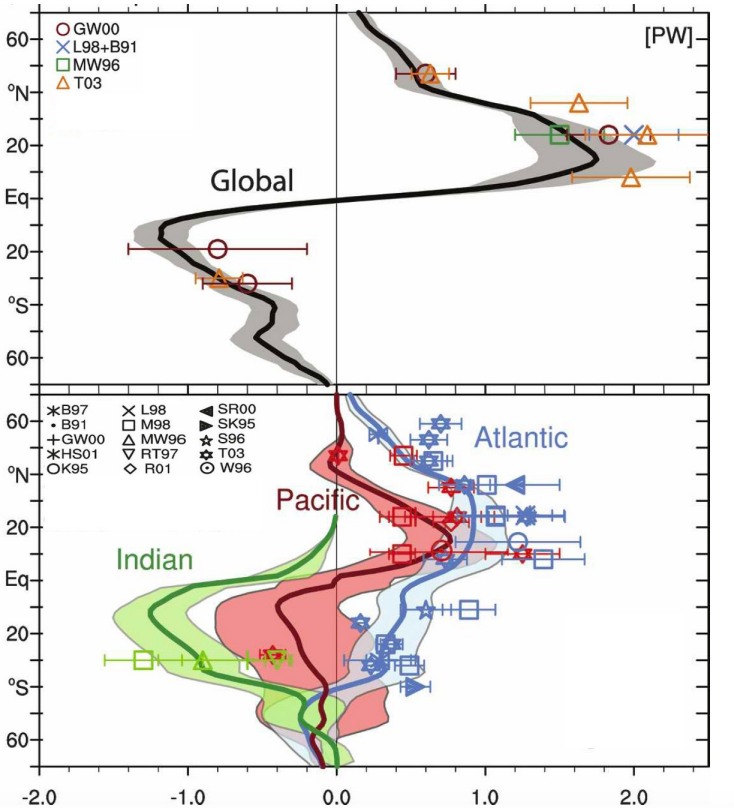

Figure 1.2: Oceanic poleward heat transport. *The median annual mean northward ocean heat transport by latitude inferred from top of the atmosphere satellite measurements (ERBE), atmospheric reanalysis (NCEP-NCAR), and ocean heat content (GODAS). Total oceanic northward heat transport is drawn in black, with the contributions from the Pacific Ocean (red), Indian Ocean (green), and Atlantic Ocean (blue) in the lower panel ($\pm 2\sigma$ in shadings). The different markers represents mean values from a range of observational estimates. Positive vaules indicate northward heat transport and negative values indicate southward heat transport. 1 PW equals* 10^{15} *J/s. From Trenberth and Fasullo (2008).*

boundary current, the Gulf Stream flows from the Gulf of Mexico through the Florida Straits and north along the eastern coast of the United States (Figure 1.3). After separating from the coast at 35°N and turning east, the Gulf Stream broadens and reaches a maximum transport of roughly 150 Sv at 60°W (*Hogg*, 1992). The North Atlantic Current (NAC) is the northeastward extension of the Gulf Stream, and represents the northern boundary of the Subtropical Gyre (STG) with the colder and fresher Subpolar Gyre (SPG) to the north (Figure 1.3). After crossing the Mid-Atlantic Ridge, the NAC flows via the Rockall Trough or via the Iceland Basin further north, and reaches the Greenland-Scotland Ridge (*Daniault et al.*, 2016).

The Greenland-Scotland Ridge has a mean sill depth of roughly 500m, and functions as a topographic barrier for the warm Atlantic water by constricting the exchanges between the SPNA and the Nordic Seas (e.g. *Hansen and Østerhus*, 2000; *Rheinlaender*

et al., 2020). The Nordic Seas consists of the Norwegian Sea, the Iceland Sea, and the Greenland Sea. The inflow into the Nordic Seas largely occurs between Iceland and Scotland over the Iceland-Faroe Ridge and through the deeper Faroe-Shetland Channel, with an average estimated transport of 3.8 Sv and 2.7 Sv into the Norwegian Sea respectively (*Østerhus et al.*, 2019). Exchanges across the Iceland-Scotland Ridge are observed to occur on a broad range of time scales (*Bringedal et al.*, 2018; *Hansen et al.*, 2008), and high mesoscale activity leads to particularly high transport variability on short time scales (*Sherwin et al.*, 2006; *Zhao et al.*, 2018).

After crossing the Iceland-Scotland Ridge, Atlantic water enters the Norwegian Sea and flows poleward with the Norwegian Atlantic Current (NwAC) following two main pathways; the Norwegian Atlantic Slope Current and the Norwegian Atlantic Front Current (*Bosse and Fer*, 2019; *Orvik and Niiler*, 2002; *Orvik and Skagseth*, 2003). The Norwegian Sea acts as a transition zone between the temperate SPNA and the cold Arctic Ocean. While progressing northward, the Atlantic water experiences considerable along-path modification due to heat loss to the atmosphere and lateral eddy exchanges with the colder and fresher Greenland and Iceland seas (*Chafik et al.*, 2015; *Furevik*, 2001; *Segtnan et al.*, 2011). The pronounced along-path cooling is apparent in Figure 1.4 from the strong temperature gradient between the eastern SPNA and the northern Norwegian Sea.

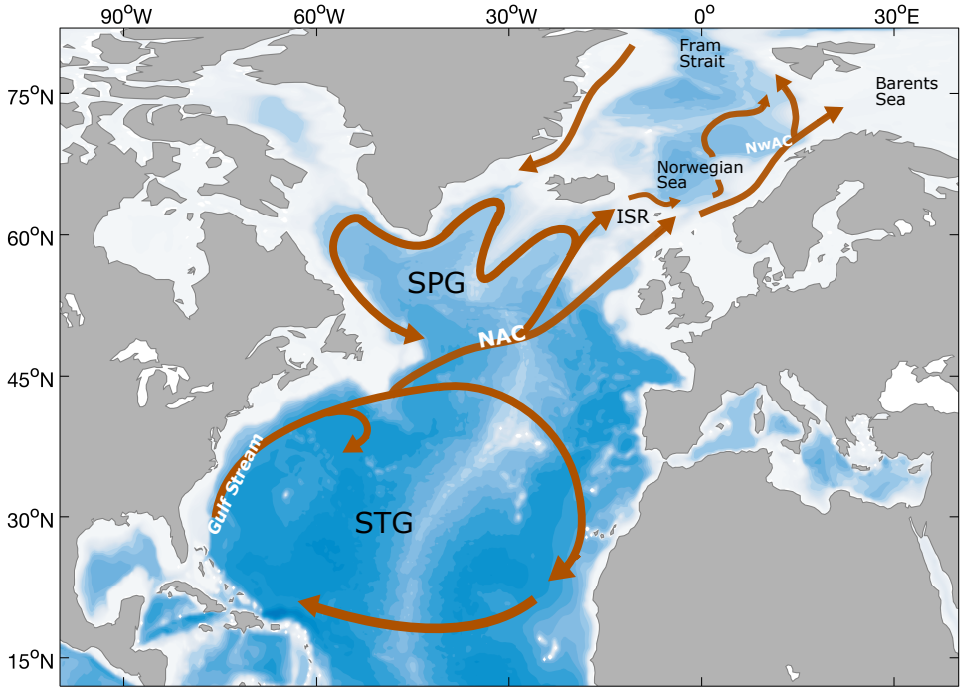

Figure 1.3: North Atlantic and Nordic Seas circulation. *Bathymetry with the main upper-ocean circulation features in the North Atlantic and Nordic Seas indicated (STG; Subtropical Gyre, SPG; Subpolar Gyre, NAC; North Atlantic Current, ISR; Iceland-Scotland Ridge, NwAC; Norwegian Atlantic Current). Bathymetry indicated by white (shallow) to blue (deep) color scale.*

In leaving the Norwegian Sea, parts of the Atlantic water enter the Barents Sea and the Arctic Ocean through the Barents Sea Opening (BSO) and the Fram Strait respectively (*Schauer et al.*, 2004; *Skagseth et al.*, 2008), and parts will recirculate within the Nordic Seas (*Eldevik et al.*, 2009). In the Barents Sea, the Atlantic water continues on its poleward journey following two main pathways – one going east into the Central Basin before turning north and exiting through the St. Anna Trough, and one shorter pathway turning north along the Hopen Trench (*Loeng*, 1991). The Barents Sea has a winter ice cover that reaches a maximum extent in March/April, and is practically ice-free during summer (*Signorini and McClain*, 2009). The ice cover is sensitive to Atlantic water heat transport inhibiting winter ice growth to an extent that skillful prediction of the ice extent from observed heat transport through the BSO is possible (*Årthun et al.*, 2012; *Onarheim et al.*, 2015).

The long-term warming trend (*Skagseth et al.*, 2020) and unprecedented winter sea ice loss (*Onarheim et al.*, 2018) observed in the Barents Sea are characteristics of what has been termed an 'Atlantification' of the Arctic (*Årthun et al.*, 2012; *Lind et al.*, 2018; *Polyakov et al.*, 2017; *Reigstad et al.*, 2002). The concept of Atlantification embodies both Atlantic water extending further poleward and/or occupying a larger part of the water column – both resulting in a warming and salinification of the upper-ocean. While pronounced internal variability in Atlantic water temperature and transport will give rise to variability in the Barents Sea heat content and ice cover on interannual to decadal time scales, future projections show the Barents Sea to move toward increasingly ice-free conditions, with an Atlantification signal gradually extending northeastward into the Kara and Laptev seas (*Årthun et al.*, 2019; *Onarheim and Årthun*, 2017).

In the Eurasian Basin of the Arctic Ocean, downstream of the Barents Sea and Fram Strait, the Atlantic water is found below a cold halocline layer that separates it from the cold and fresh surface layer and the Arctic sea ice (e.g. *Aagaard et al.*, 1981; *Fer*, 2009; *Steele and Boyd*, 1998). The heat loss from the Atlantic water layer (warmer than $0°C$) to the cold surface layer is typically small due to the stable stratification. As a consequence of ongoing climate change and the observed reductions in Arctic sea ice area, the Arctic Ocean absorbs more heat in summer, warming the upper-ocean (*Perovich et al.*, 2007). While surface heating and summer ice loss receive a lot of attention, an increasingly important role for oceanic heat has been proposed as the Arctic ice volume continues to decline (*Carmack et al.*, 2015). For instance, signs of enhanced upward heat fluxes from the Atlantic water layer have been observed in the Eurasian Basin due to changes in the stratification, consequently warming the surface layer from below (*Polyakov et al.*, 2010, 2017, 2020). Future projections show increased heat transport through the BSO due to increasing Atlantic water temperatures in a warming climate (*Årthun et al.*, 2019). The Arctic Ocean is projected to warm as a result of both increased poleward ocean heat transport and warming by surface heat fluxes, though which mechanism will dominate future warming is still unknown (*Burgard and Notz*, 2017).

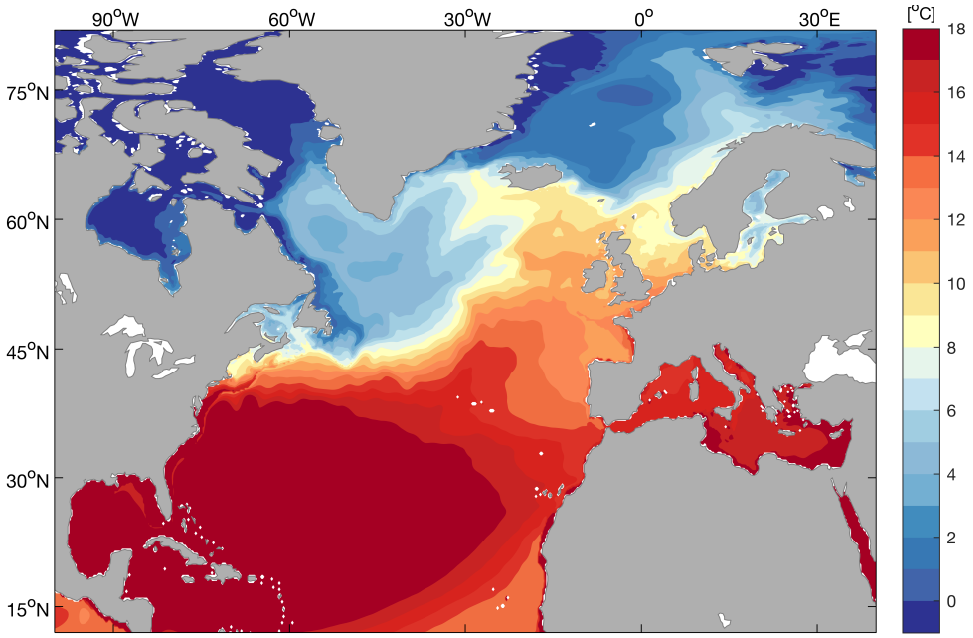

***Figure 1.4: North Atlantic and Nordic Seas temperatures**. Climatological annual mean upper-ocean (0–400m) temperature for the period 1976–2015 in the ORCA025 ocean hindcast simulation used in Paper I.*

1.3 Mechanisms of ocean heat content variability

The North Atlantic Ocean and Nordic Seas exhibit pronounced variability in regional heat content on interannual, decadal, and multidecadal time scales (*Deser and Blackmon*, 1993; *Furevik*, 2001; *Holliday et al.*, 2008; *Kushnir*, 1994). From the low-frequency variability arises a potential for predicting changes in marine ecosystem habitats and populations (*Årthun et al.*, 2018a; *Fossheim et al.*, 2015; *Hátún et al.*, 2016), Arctic sea ice (*Onarheim et al.*, 2015; *Schlichtholz*, 2019), and decadal climate in terms of precipitation and surface air-temperatures (*Årthun et al.*, 2018b; *Keenlyside et al.*, 2008; *Yeager and Robson*, 2017). There is, however, no consensus or complete understanding of the causal mechanisms of heat content variability in the Arctic-Atlantic sector. A better understanding of such mechanisms is therefore important for future prediction efforts.

Changes in the heat content of an oceanic volume is a result of ocean heat transport convergence and/or changes in the surface heat fluxes. Both horizontal and vertical advective and diffusive processes can give rise to ocean heat transport convergence through increased volume- or temperature fluxes. Volume transport variability can be a local adjustment to wind forcing, or be reflective of more dynamical changes in the ocean circulation. Temperature anomalies can be created locally due to anomalous air-sea heat fluxes, or be advected by the ocean currents from remote regions. Interannual variability in regional heat content often occurs on top of decadal trends, and different

mechanisms can dominate on different time scales (e.g. *Buckley et al.*, 2015; *Deser and Blackmon*, 1993; *Lozier et al.*, 2008). Untangling these relationships is necessary to fully understand the underlying causes of regional heat content variability.

A common approach to assess the mechanisms causing heat content variability is to construct a heat budget detailing the convergence of advective, diffusive, and surface heat fluxes for the region of interest (e.g. *Buckley et al.*, 2015; *Carton et al.*, 2011; *Mork et al.*, 2014; *Piecuch et al.*, 2017; *Roberts et al.*, 2017). Capturing the temporal variability is nevertheless challenging because the observational record is limited in time and space, particularly in terms of long-term measurements of oceanic volume transport. As a result, heat budgets constructed directly from observations usually infer the ocean heat transport convergence as a residual (*Carton et al.*, 2011; *Mork et al.*, 2014; *Roberts et al.*, 2017). Observation-based, closed heat budget diagnostics have, however, been made possible from the development of ocean state estimates in recent decades (*Buckley et al.*, 2015; *Piecuch et al.*, 2017), combining the physical consistency of an ocean model with ocean observations (*Heimbach et al.*, 2019; *Wunsch and Heimbach*, 2007).

There are multiple mechanisms that can contribute to regional heat content variability in the North Atlantic Ocean. On interannual time scales, the North Atlantic Oscillation (NAO), which is the dominant mode of atmospheric variability, is a major player (*Visbeck et al.*, 2003). The NAO reflects the strength of the westerlies (*Hurrell*, 1995), and is known to force ocean circulation changes as well as air-sea heat flux anomalies in the North Atlantic (e.g. *Bersch*, 2002; *Marshall et al.*, 2001; *Sarafanov*, 2009). Another frequently highlighted mechanism is the SPG controlling the relative supply of subpolar and subtropical water to the eastern SPNA and the Nordic Seas inflow (*Häkkinen et al.*, 2011; *Hátún et al.*, 2005; *Koul et al.*, 2020). *Hátún et al.* (2005) find a weak SPG to be associated with a northwestward shifted subpolar front, high NAC transport of subtropical waters, and higher salinities in the eastern SPNA. *Häkkinen et al.* (2011) further link variable STG/SPG exchanges to North Atlantic wind stress curl variability (not always attributable to the NAO) modulating the gyres. The ambiguity of the SPG index used to describe the SPG state has in recent years spurred discussions on what is the best metric to capture variability in the SPG strength and extent, and how such variability affects water mass properties in the eastern SPNA (*Foukal and Lozier*, 2017; *Hátún and Chafik*, 2018; *Koul et al.*, 2020).

The Nordic Seas receiving thermohaline anomalies from the SPNA is a robust finding in both observations (*Chepurin and Carton*, 2012; *Holliday et al.*, 2008; *Sutton and Allen*, 1997) and models (*Årthun and Eldevik*, 2016; *Krahmann et al.*, 2001; *Langehaug et al.*, 2019). Downstream of the Iceland-Scotland Ridge, conflicting views exist on whether heat anomalies are actively formed and/or modified within the Norwegian Sea, or whether the region is merely a passive receiver of anomalies advected from the SPNA (*Carton et al.*, 2011; *Mork et al.*, 2014). A 3–4 year lag time in thermohaline characteristics between the northeastern SPNA and the Fram Strait has been reported from observations (*Holliday et al.*, 2008). From this lagged relationship arises a prediction potential for heat reaching the Arctic and the Arctic sea ice several years in advance. Along-path modification of the thermohaline anomalies can, however, limit the predictability, and the effects of lateral mixing and air-sea heat exchanges are there-

fore important to assess.

The North Atlantic Ocean is also subject to decadal variability in both heat- and freshwater content. During the 1990s and early 2000s the SPNA was warming, followed by a trend reversal and cooling after 2005 (*Piecuch et al.*, 2017; *Robson et al.*, 2016). *Robson et al.* (2016) link the trend reversal to changes in the Atlantic Meridional Overturning Circulation (AMOC) as a lagged response to conditions in the Labrador Sea. *Piecuch et al.* (2017), on the other hand, link the trend reversal to anomalous gyre circulation due to changes in the wind stress curl. Such a trend reversal has interestingly not been observed in the Norwegian Sea heat content despite colder Atlantic water temperatures in the Faroe-Shetland Channel since the mid-2000s (*Broome et al.*, 2019; *Mork et al.*, 2019). Both reduced ocean heat loss during 2011–2018 (*Mork et al.*, 2019), and a 'disconnect' between the SPNA and the Norwegian Sea after 2005 due to shifts in the subpolar front (*Broome et al.*, 2019), have been proposed as potential mechanisms. During 2012–2016 a record-breaking freshening of the SPNA was observed (*Holliday et al.*, 2020). Unlike the Great Salinity Anomaly of the late 1960s caused by enhanced freshwater export from the Arctic, *Holliday et al.* (2020) explain the freshening by anomalous winter wind patterns re-routing Arctic-origin water off the North West Atlantic Continental Shelf and into the subpolar basins. This freshening was also subsequently seen in the Norwegian Sea, leaving it in the rare combination of a warm and fresh state (*Mork et al.*, 2019).

The predictability of regional ocean heat content variability in the Arctic-Atlantic sector, and the associated impacts on climate, sea ice, and marine ecosystems, depends on the causal mechanisms driving the variability. Variability dominated by changes in local wind stress (Ekman forcing) or air-sea heat fluxes is considered less predictable because it is a response to local stochastic atmospheric forcing (*Roberts et al.*, 2017). Variability dominated by ocean dynamics/nonlocal forcing, for instance related to advection of heat anomalies, wave propagation, or geostrophic circulation anomalies, has a potential for skillful prediction through accurate initialization of the ocean state (*Robson et al.*, 2012; *Yeager et al.*, 2012). In understanding the mechanisms involved in creating and maintaining heat anomalies in different regions, we can improve both predictions and our understanding of the ocean's role in the climate system.

Chapter 2

Objectives and methods

This dissertation aims to obtain a more robust understanding of interannual heat content variability in the Arctic-Atlantic region, particularly focusing on the upstream sources feeding warm Atlantic water across the Iceland-Scotland Ridge, the Norwegian Sea directly downstream of the ridge, and the Atlantic sector of the Arctic Ocean where Atlantic heat meets the Arctic sea ice. This chapter states the main objectives and the motivation for the presented work (section 2.1), in addition to describe the methods applied to achieve said objectives (section 2.2).

2.1 Objectives

Redistribution of oceanic heat by the ocean currents, and the interaction with the atmosphere above, give rise to regional ocean heat content variability on multiple time scales. The causal mechanisms driving interannual to decadal heat content variability in the Arctic-Atlantic region are, however, not fully understood. As a result, the key objectives are summarized by the following research questions:

- How is variability in water mass characteristics and volume transport at the Iceland-Scotland Ridge related to circulation changes in the North Atlantic Ocean?
- Which mechanisms control interannual ocean heat content variability in the Norwegian Sea?
- What are the mechanisms underlying recent Atlantification of the Arctic Ocean?

While the key objectives focus on improving our mechanistic understanding of heat content variability in the Arctic-Atlantic sector, implications for prediction is a main motivation for the work presented here. Low-frequency variability in the ocean is generally a source of climate predictability, arising from the ocean's inertia and systematic poleward heat transport (*Årthun et al.*, 2017). The sensitivity of the Barents Sea ice cover and dense water properties to variable Atlantic water properties and volume transport, is another main motivation, in which a prediction potential also resides (*Onarheim et al.*, 2015; *Skagseth et al.*, 2020). Changes in ocean heat content caused by oceanic circulation changes appear more predictable than those caused by surface heat fluxes

(*Yeager and Robson*, 2017). As a result, understanding the processes involved in creating and modifying ocean heat anomalies, the potential for prediction of regional ocean heat content variability, as well as the limitations, can be better understood.

2.2 Methods

Ocean general circulation models (OGCMs) simulate the time-evolving, three-dimensional ocean circulation in a dynamically and kinematically consistent framework (e.g. *Fox-Kemper et al.*, 2019; *McWilliams*, 1996; *Wunsch and Ferrari*, 2018). In comparison, ocean observation systems are expensive and logistically challenging to organize (*Weller et al.*, 2019), and often suffer from either giving information about temporal variability (e.g. mooring measurements) or spatial variability (e.g. surveys using CTD measurements). The observational record therefore does not have the temporal and spatial coverage, or the dynamical consistency required, to provide a full mechanistic view of interannual ocean heat content variability. Analysing oceanic fields from OGCMs allows for thorough descriptions of regional heat content variability and the underlying causal mechanisms. However, numerical models are imperfect. The primitive equations at the core of an OGCM are discretized in time and space according to the model time step and spatial grid. Processes acting on spatial or temporal scales not resolved by the model, such as diffusion, turbulent mixing, and often mesoscale eddies, are parameterized. Additionally, OGCMs are typically forced by an atmospheric reanalysis product (e.g. ERA-Interim, MERRA, JRA-55) carrying its own set of approximations and uncertainties (*Chaudhuri et al.*, 2013). As a result, ocean model products should be evaluated against the observational record to discuss weaknesses and strengths, and assess the suitability for the research questions posed.

In order to address the research questions above, a number of model products and analysis tools have been used in the papers presented in this dissertation. The main products and tools used are described briefly in the following sections.

2.2.1 ORCA025 ocean hindcast

ORCA025 is a global, eddy-permitting configuration of the NEMO model (*Madec*, 2015) coupled to the thermodynamic sea-ice model LIM2 (*Bouillon et al.*, 2009), and is developed by the Drakkar project (*Barnier et al.*, 2006). The hindcast simulation used spans 1958–2015 with no spin-up, and the first 10–15 years should therefore be treated with caution. The ORCA025 hindcast is forced by the Drakkar forcing set 5.2 (*Dussin et al.*, 2016), constructed from ERA-Interim (*Dee et al.*, 2011) and ERA40 (*Uppala et al.*, 2005) surface fields. The advection and diffusion schemes used in the ORCA025 configuration are described in *Grégorio et al.* (2015). The ORCA025 grid is tripolar, with a 1/4° horizontal resolution (27km at the equator, 12km in the Arctic), 75 unevenly spaced vertical levels, and a partial step representation of bottom topography (*Barnier et al.*, 2006).

The ORCA025 hindcast provides a multidecadal simulation of the global ocean circulation of high spatial and temporal resolution. In Paper I, 5-day mean ORCA025 fields

are used together with a Lagrangian analysis tool to investigate the link between variable inflow (volume transport and properties) at the Iceland-Scotland Ridge between 1986–2015 and large-scale ocean circulation anomalies upstream.

2.2.2 ARIANE Lagrangian analysis tool

In contrast to Eulerian kinematics where the motion of a fluid is described in a reference frame that is fixed in space, Lagrangian kinematics describes the fluid motion in a reference frame that is moving with an infinitesimal fluid particle (e.g. *van Sebille et al.*, 2018). While Eulerian kinematics form the basis for OGCMs (grid cells fixed in space), the Lagrangian approach is a powerful supplement where the trajectories of numerical particles representing oceanic volumes can be estimated (Figure 2.1).

ARIANE is a Lagrangian analysis tool developed for offline calculations of Lagrangian trajectories from the output of OGCMs (*Blanke and Raynaud*, 1997; *Döös*, 1995). ARIANE utilizes a purely advective scheme where streamlines are computed analytically, along which numerical particles are evolved forward or backward in time. The streamlines represent true trajectories under the assumption of three-dimensional nondivergence and temporal stationarity over the sampling period of the velocity field. Particle volume is conserved along the individual trajectories, while the properties of the numerical particles (temperature and salinity) evolve according to the linearly interpolated Eulerian fields of the ocean model. As the ARIANE scheme is purely advective, subgrid-scale processes parameterized in the OGCM (e.g. diffusion and turbulent mixing) are not factored in when calculating the Lagrangian trajectories (*Wagner et al.*, 2019). These processes still affect the Eulerian temperature and salinity fields the particles are translated through, and therefore indirectly the particle properties (*Lique et al.*, 2010).

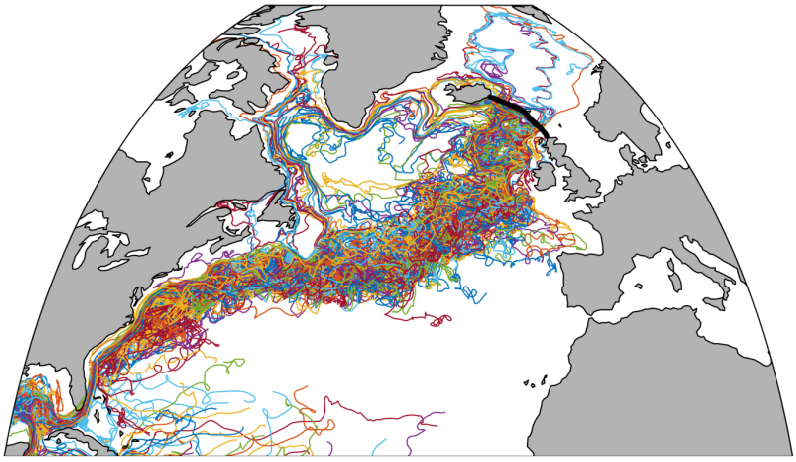

Figure 2.1: Lagrangian trajectories with ARIANE. *Trajectories of 150 randomly selected particles seeded at the Iceland-Scotland Ridge (marked in black) between 2006-2015. 7 years of backtracking is displayed.*

ARIANE allows for offline tracking of oceanic volumes forward and backward in time,

efficiently calculating Lagrangian trajectories from stored OGCM velocity fields. In Paper I, the temporal and spatial variability in the advective pathways of the Nordic Seas inflow is explored by tracking numerical particles seeded at the Iceland-Scotland Ridge backward in time. Using the fields from the ORCA025 hindcast together with ARIANE, particles distributed in space to represent the full column of inflowing water at the ridge are released at every time step during 1986–2015. The number of particles released in each grid cell at the ridge is scaled with the volume transport at the release time, and each particle is tagged with a transport. Particle trajectories from the Lagrangian experiment are visualized in Figure 2.1, with the Iceland-Scotland Ridge release section marked in black.

2.2.3 ECCOv4-r3 ocean state estimate

ECCO version 4 release 3 (hereafter referred to as ECCOv4-r3) is an ocean state estimate of the 1992–2015 global ocean-circulation and sea-ice state (*Forget et al.*, 2015a; *Fukumori et al.*, 2017). The ECCO state estimation framework was developed to synthesize nearly all available observations with an ocean model, to get a description of the ocean's time-evolving state in the modern era (*Wunsch and Heimbach*, 2007).

The ECCOv4-r3 state estimate is generated by the ice-ocean component of the Massachusetts Institute of Technology general circulation model (MITgcm) solving the primitive equations for a time-evolving, Boussinesq, hydrostatic ocean, with a nonlinear free surface. Through the adjoint method, the modeled fields are fitted to satellite and in-situ ocean observations in a least-square sense (*Heimbach et al.*, 2005). Profiles from Argo floats, Ice-Tethered Profilers, and a large number of individual CTD stations are used as constraints in ECCOv4-r3 (*Fukumori et al.*, 2017). Additionally, satellite observations of sea surface temperature (SST), sea surface salinity (SSS), sea level, sea ice concentration, and ocean bottom pressure are used. ERA-Interim reanalysis fields (*Dee et al.*, 2011) are used as the initial near surface atmospheric state (air temperature, humidity, precipitation, downward radiation, and wind stress), while air-sea heat fluxes are calculated from bulk formulae (*Large and Yeager*, 2004). The ECCOv4-r3 grid has a 1° nominal horizontal resolution and 50 unevenly spaced vertical levels. The grid is split into five faces, one of which is the Arctic cap (Figure 2.2a). The effect of subgrid-scale flow is parameterized as a bolus velocity, and turbulent transport parameters are estimated within the ECCOv4-r3 framework under the constraints of observations (*Forget et al.*, 2015a,b).

ECCOv4-r3 is an ideal framework for heat budget analysis as the physical consistency of an OGCM is combined with actual observational data (*Buckley et al.*, 2014, 2015; *Piecuch et al.*, 2017). In contrast to ocean reanalysis products also assimilating observational data (e.g. SODA3; *Carton et al.* (2018), ORAS5; *Zuo et al.* (2019)), the ECCO state estimation framework conserves ocean momentum, heat, and salt. The practical closure of the heat budget is demonstrated in Figure 2.2b, displaying the vertically intergated monthly mean heat budget for a selected grid cell in the Norwegian Sea. Ocean heat transport convergence is represented explicitly (Figure 2.2b), and is not calculated as a residual, which is often the case for observational heat budgets (e.g. *Carton et al.*, 2011; *Mork et al.*, 2014). Heat budgets constructed from ECCOv4-r3 are

used in Paper II to determine the mechanisms of interannual heat content variability in the Norwegian Sea. Additionally, heat budgets are used in Paper III to explore warming trends in the Barents Sea and Fram Strait, and assess the mechanisms underlying recent Atlantification of the Arctic Ocean.

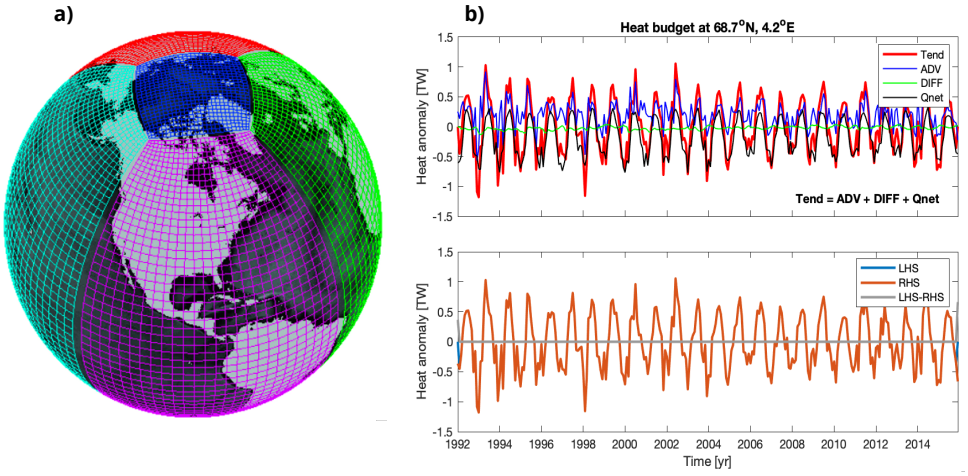

Figure 2.2: Heat budgets with ECCOv4-r3. ***(a)*** *ECCOv4 lon-lat-cap grid used for budget analysis. The global grid is split into five faces indicated by the different mask colors. From Forget et al. (2015a).* ***(b)*** *Vertically integrated monthly mean heat budget for grid cell at 68.7°N, 4.2°E in the Norwegian Sea. Tend is the heat content tendency, ADV is the advective heat transport convergence, DIFF is the diffusive heat transport convergence, and Qnet is the net air-sea heat fluxes. Practical budget closure is demonstrated showing the difference between the left-hand side (LHS) and the right-hand side (RHS) of the budget equation (Tend=ADV+DIFF+Qnet). 1 TW equals* 10^{12} *J/s.*

Chapter 3

Summary of papers

Paper I: **Linking variable Nordic Seas inflow to upstream circulation anomalies**

Asbjørnsen, H., Johnson, H., Årthun, M., in prep. for Journal of Climate.

Paper I investigates interannual variability in the Nordic Seas inflow by assessing how variable upstream sources and advective pathways impact volume transport and water mass properties at the Iceland-Scotland Ridge. Using an eddy-resolving ocean hindcast simulation and a Lagrangian analysis tool, numerical particles are released at the ridge during 1986-2015 and tracked backward in time for 10 years. Of the annual mean inflow, 64% comes from the subtropics and 26% has a subpolar or Arctic origin. However, the inflowing water masses are well-mixed, and the source waters cannot be identified by hydrographic properties alone. Interannual variability in transport across the ridge and the relative fraction of subtropical and Arctic-origin waters are associated with distinct atmospheric circulation anomalies at different locations along the advective pathways. At the time of inflow, the local response to the NAO is important for the overall inflow of both subtropical and Arctic waters – a strong inflow being associated with NAO^{+} conditions. In the years before reaching the Iceland-Scotland Ridge, the subtropical particles are influenced by atmospheric circulation anomalies in the boundary region between the subtropical and subpolar gyre, and over the SPNA. These atmospheric circulation anomalies lead to meridional shifts in the NAC and zonal shifts in the subpolar front, respectively – an equatorward shift of the NAC and westward shift of the subpolar front corresponding to a warmer and more saline inflow at the ridge. Wind stress curl anomalies over the SPNA also influence the pathway of Arctic-origin waters, affecting the number of particles re-routed from the Labrador Current into the subpolar basins and toward the Nordic Seas. A high transport of Arctic-origin water is furthermore associated with a colder and fresher inflow. The results presented here thus demonstrate the importance of gyre dynamics and large-scale wind forcing in affecting the properties and transport of Atlantic water across the Iceland-Scotland Ridge.

Paper II: **Mechanisms of ocean heat anomalies in the Norwegian Sea**

Asbjørnsen, H., Årthun, M., Skagseth, Ø., Eldevik, T., (2019), Journal of Geophysical Research: Oceans, 124(4), 2908-2923.

Paper II investigates the mechanisms of interannual heat content variability in the Norwegian Sea through closed heat budget diagnostics, using a state-of-the-art ocean state estimate constrained by ocean observations for the period 1992–2015. We find both ocean advection and air-sea heat fluxes to play an active role in the formation of heat content anomalies. Ocean advection is the primary contributor to heat content variability in the Atlantic domain of the Norwegian Sea. Spatial and temporal decompositions of the advection budget term show that non-Ekman dynamics dominate the advective heat transport in the region. Furthermore, advection by the resolved velocities dominates, while eddy-driven transports have an overall dampening effect. Anomalous heat advection depends on the strength of the Atlantic water inflow rather than the temperature variability, and a strong Atlantic water inflow is associated with a weakened SPG upstream. The importance of nonlocal forcing identified implies a prediction potential for ocean heat content changes on interannual time scales, as skillful predictions generally arise from the realistic initialization of ocean circulation anomalies associated with ocean dynamics. However, local surface forcing (air-sea heat fluxes and Ekman forcing) within the Norwegian Sea can substantially modify the phase and amplitude of ocean heat anomalies along their poleward pathway, and therefore likely limits predictability.

Paper III: Mechanisms underlying recent Arctic Atlantification

Asbjørnsen, H., Årthun, M., Skagseth, Ø., Eldevik, T., (2020), Geophysical Research Letters, 47(15).

Paper III investigates warming trends in the Barents Sea and Fram Strait in order to identify the mechanisms underlying recent Atlantification of the Arctic Ocean. We find the Barents Sea transitioning to a warmer state during the 1993–2014 period analysed, with reduced sea ice concentrations and Atlantic water extending further poleward. In the Fram Strait, we find no significant warming trend. Heat budgets along the main poleward pathways of Atlantic water reveal a complex Arctic climate system where the underlying mechanisms driving the Atlantification are found to be regionally dependent and not stationary in time. In the ice-free region of the Barents Sea, ocean advection is found to be a major driver of the warming trend due to increasing inflow temperatures between 1996 and 2006. Reduced ocean heat loss is contributing to the warming trend in the ice-free region towards the end of the period. A significant upper-ocean warming and a weakened stratification in the ice-covered northwestern Barents Sea is identified. However, in contrast to what has been previously hypothesized, the heat budget analysis does not point to enhanced vertical mixing and increased upward heat fluxes from the Atlantic water layer as the source of the warming. An improved understanding of the recent warming trends in the Barents Sea and Fram Strait has implications for how we understand the mechanisms driving ongoing and future warming of the Arctic Ocean and, thus, Arctic climate change.

Chapter 4

Perspectives and outlook

This dissertation assesses key mechanisms and pathways of ocean heat anomalies in the Arctic-Atlantic region. The study area spans the subtropical and the subpolar North Atlantic, the intermediate Norwegian Sea, and the Atlantic sector of the Arctic Ocean. The presented papers establish an important role of poleward ocean heat transport in causing regional heat content variability and change, while also detailing the complex relationship between advective ocean heat transport and atmospheric forcing. The three papers take a mechanistic view, investigating the role of variability in oceanic temperatures, volume transport, and air-sea heat fluxes, while also discussing the implications for predictability. The results of the presented work furthermore naturally point toward a number of open questions, some of which will be discussed here.

In Paper I, the Nordic Seas inflow is tracked from the Iceland-Scotland Ridge to its subtropical and subpolar sources. The Lagrangian method used allows for an assessment of source region fractions, spatial shifts in the advective pathways, and other processes giving rise to variability in temperature or volume transport at the ridge. To what degree coherent thermohaline anomalies propagate from the Gulf Stream, along the NAC, and into the Norwegian Sea, has not been addressed directly. However, the particle transit times from the Lagrangian analysis are within the range of observed propagation speeds of thermohaline anomalies (*Årthun et al.*, 2017; *Chepurin and Carton*, 2012; *Sutton and Allen*, 1997). This indicates that an oceanic volume is likely to travel from the Gulf Stream region to the Iceland-Scotland Ridge at speeds far slower than the mean NAC speed due to along-path horizontal and vertical displacements and eddying features, visible in the individual particle trajectories. Further evaluation of the particles' ability to retain anomalous characteristics along the advective pathways remains, and could be an important contribution to the debate regarding the apparent poleward propagation of thermohaline anomalies.

The importance of the inflow over the Iceland-Scotland Ridge for Norwegian Sea heat content is highlighted in Paper II. Through observation-based, closed heat budget diagnostics, mechanisms of interannual Norwegian Sea heat content variability are thoroughly evaluated. Spatial analysis of the individual heat budget terms shows that ocean advection is the primary contributor to heat content variability in the Atlantic domain of the Norwegian Sea, and that anomalous heat advection depends on the strength of the Atlantic water inflow. The relationship between the inflow strength and the Nor-

wegian Sea heat content emphasizes the importance of continuous monitoring of volume fluxes both upstream at the OSNAP array (*Lozier et al.*, 2019), at the ridge in the Faroe-Shetland Channel (*Berx et al.*, 2013), and downstream at the Svinøy section in the NwAC (*Orvik and Skagseth*, 2003). While the results in Paper II suggest a potential for predicting Norwegian Sea heat content based on upstream conditions, local surface forcing actively modifying the phase and amplitude of the ocean heat anomalies, likely limits the predictability.

Variability at the Iceland-Scotland Ridge, and the link to large-scale atmospheric forcing and ocean circulation changes upstream, is addressed in both Paper I and Paper II. Paper II connects a strong Atlantic water inflow to a weak SPG and a strengthened and poleward shifted NAC. The inflow strength is correlated to the NAO and, more strongly, to the East Atlantic Pattern (EAP), often interpreted as a meridionally shifted NAO (higher inflow associated with poleward shifted westerlies). While the barotropic stream function-based SPG index used in Paper II reflects the strength of the gyre center in the western SPNA, it might not capture variability in SPG extent in the east (*Koul et al.*, 2020). The ambiguity of the SPG index pointed out in several recent studies (*Foukal and Lozier*, 2017; *Hátún and Chafik*, 2018; *Koul et al.*, 2020) makes it difficult to compare and consolidate findings from previous studies using different metrics to describe variability in the SPNA. Paper I avoids using a SPG index altogether, but variability in the extent of the SPG can be inferred from the Lagrangian trajectory analysis.

In Paper I, a strong inflow at the Iceland-Scotland Ridge is found to consist of high transports of both subtropical and subpolar/Arctic-origin water, and is associated with NAO^+ conditions at the time of inflow. A strong inflow is furthermore linked to high transports of subtropical water associated with a negative wind stress curl anomaly over the SPNA two years before reaching the ridge – a pattern often connected to a weak and contracted SPG (*Häkkinen et al.*, 2011). Additionally, a cyclonic sea level pressure anomaly in the intergyre region four years prior to the subtropical water reaching the ridge is associated with a strong inflow, potentially by enhancing the southwest-northeast tilt of the NAC. While the strong inflow, weak SPG, and enhanced NAC transport mechanism from Paper II is consistent with the results in Paper I, the connection between the EAP and the inflow over the ridge is not found in Paper I. It is not known whether this discrepancy is due to differences between the two model frameworks, e.g., resolution, or whether it is due to differences between the two Nordic Seas inflow sections compared and other calculation metrics.

Paper I and II mainly focus on mechanisms causing variability at the Iceland-Scotland Ridge and in the Norwegian Sea on interannual time scales. However, from the two papers interesting questions regarding decadal trends emerge, noting that decadal variability in Norwegian Sea heat content is not necessarily dominated by the same mechanisms as interannual variability. For instance, temperature variability is expected to be more important for driving heat transport variability on longer time scales (*Orvik and Skagseth*, 2005). The Norwegian Sea has interestingly retained a warm state in the years after the 2005 offset of a decadal cooling trend in the SPNA (*Broome et al.*, 2019; *Mork et al.*, 2019). From the apparent disconnect between the SPNA and the

Norwegian Sea, and the decoupling of salinity and temperature anomalies seen, a number questions emerge. To what degree is the disconnect caused by reduced surface heat loss in the Norwegian Sea as suggested by *Mork et al.* (2019)? To what degree is gyre dynamics and associated shifts in the subpolar front important? Finally, what role does the Iceland-Scotland Ridge play in terms of being a physical barrier between the SPNA and the Norwegian Sea?

Heat budgets are also constructed for the Barents Sea and Fram Strait, directly downstream of the Norwegian Sea (Paper III), motivated by the observed warming trend (*Skagseth et al.*, 2020) and sea ice loss (*Onarheim et al.*, 2018) characterizing an Atlantification of the Arctic. The heat budgets reveal a complex Arctic climate system where the underlying mechanisms driving the Atlantification are found to be regionally dependent and not stationary in time. The results highlight the different dynamical regions (open-ocean, marginal ice zone, ice-covered ocean), finding that despite a significant warming trend everywhere in the Barents Sea, the mechanisms driving the warming trends differ. Consequently, areas in the Arctic over which to evaluate future heat or freshwater budgets need to be chosen carefully with these findings in mind.

The ocean state estimate used in Paper III adequately reproduces a weakened stratification and an upper-ocean warming of the northwestern Barents Sea similar to what is seen in observations (*Lind et al.*, 2018). However, in contrast to the hypothesis in *Lind et al.* (2018), no evidence is found suggesting that enhanced upward heat fluxes from the Atlantic water layer to the Arctic surface layer is the source of the upper-warming. The coarse vertical resolution in the model framework means that vertical heat fluxes are to a large degree parameterized, and could be underrepresented. The results in Paper III nevertheless demonstrate that an upper-ocean warming in the ice-covered Barents Sea, such as the one observed, can be caused by a combination of horizontal oceanic processes (warmer inflow and reduced sub-zero throughflow) and air-sea heat fluxes (periods of reduced surface heat loss). Direct flux measurements over time is likely needed to get a definite answer to whether or not vertical heat fluxes are important for the upper-ocean warming. Such measurements will be central in the Nansen Legacy project (https://arvenetternansen.com), where understanding heat fluxes and mixing processes in the northwestern Barents Sea is a key objective.

The Arctic is a region where the effects of externally forced climate change are very much present in the observational record in terms of oceanic and atmospheric temperatures, as well as sea ice extent and thickness (e.g. *Carmack et al.*, 2015). Extending the heat budget analysis in Paper III into the Arctic basins utilizing upcoming ECCO-products with higher resolution, more observational constraints, and an improved circulation in the Arctic Ocean (e.g. ECCOv5; *Heimbach et al.* (2019) and ASTE; *Nguyen et al.* (2017)), would be another step toward understanding recent climate change better. How changes in the freshwater supply affect the stratification in the Eurasian Basin, and how important enhanced upward mixing of Atlantic heat (e.g. *Polyakov et al.*, 2017) is for the overall upper-ocean warming, are relevant questions that can be addressed through heat- and freshwater budget analysis.

In the three presented papers, modeled Lagrangian trajectories (Paper I) and heat bud-

get analysis (Paper II and III) are used to determine the pathways and processes of ocean heat anomalies in the Arctic-Atlantic region. While the mechanistic understanding of ocean heat anomalies aimed for required a model approach, the heat budgets are constructed from a model framework that relies on observational constraints (e.g. Argo profiles, CTD measurements, satellite observations of SST, SSS, sea level, and sea ice). Furthermore, the two different model products used (ECCOv4-r3 and ORCA025) have been evaluated against available observational records to discuss weaknesses and strengths, and assess the accuracy of the simulated oceanic fields. It is therefore clear that continued monitoring of the North Atlantic and Arctic regions, especially in terms of the Argo program and different mooring arrays, is crucial for constraining and evaluating the output of OGCMs. As the field of state estimation and other forms of data assimilation continues to evolve, improved simulations of the global ocean circulation, and potentially also the coupled Earth system (*Heimbach et al.*, 2019), will be invaluable to improve our understanding of ocean processes. By assessing anomalous exchanges across the Iceland-Scotland Ridge (Paper I and II), and detailing heat content variability and change in the Norwegian Sea and Barents Sea in recent decades (Paper II and III), this dissertation asserts the important role of Atlantic water variability in the Arctic-Atlantic climate system.

Chapter 5

Scientific results

Paper II

Mechanisms of ocean heat anomalies in the Norwegian Sea

Asbjørnsen, H., Årthun, M., Skagseth, Ø., Eldevik, T.
Journal of Geophysical Research: Oceans, **124** (2019)

JGR Oceans

RESEARCH ARTICLE
10.1029/2018JC014649

Mechanisms of Ocean Heat Anomalies in the Norwegian Sea

Helene Asbjørnsen[1], Marius Årthun[1], Øystein Skagseth[2], and Tor Eldevik[1]

[1]Geophysical Institute, University of Bergen and Bjerknes Centre for Climate Research, Bergen, Norway, [2]Institute of Marine Research, and Bjerknes Centre for Climate Research, Bergen, Norway

Key Points:
- We document interannual variability of the Norwegian Sea heat content using the ECCOv4 ocean state estimate
- Ocean advection explains the majority of interannual heat content variability in the Norwegian Sea's Atlantic domain
- Ocean advection is related to the Atlantic water inflow strength, and inversely linked to the subpolar gyre strength

Correspondence to:
H. Asbjørnsen,
H.Asbjornsen@uib.no

Citation:
Asbjørnsen, H., Årthun, M., Skagseth, Ø., & Eldevik, T. (2019). Mechanisms of ocean heat anomalies in the Norwegian Sea. *Journal of Geophysical Research: Oceans*, *124*, 2908–2923. https://doi.org/10.1029/2018JC014649

Received 8 OCT 2018
Accepted 2 APR 2019
Accepted article online 10 APR 2019
Published online 29 APR 2019

Abstract Ocean heat content in the Norwegian Sea exhibits pronounced variability on interannual to decadal time scales. These ocean heat anomalies are known to influence Arctic sea ice extent, marine ecosystems, and continental climate. It nevertheless remains unknown to what extent such heat anomalies are produced locally within the Norwegian Sea, and to what extent the region is more of a passive receiver of anomalies formed elsewhere. A main practical challenge has been the lack of closed heat budget diagnostics. In order to address this issue, a regional heat budget is calculated for the Norwegian Sea using the ECCOv4 ocean state estimate—a dynamically and kinematically consistent model framework fitted to ocean observations for the period 1992–2015. The depth-integrated Norwegian Sea heat budget shows that both ocean advection and air-sea heat fluxes play an active role in the formation of interannual heat content anomalies. A spatial analysis of the individual heat budget terms shows that ocean advection is the primary contributor to heat content variability in the Atlantic domain of the Norwegian Sea. Anomalous heat advection furthermore depends on the strength of the Atlantic water inflow, which is related to large-scale circulation changes in the subpolar North Atlantic. This result suggests a potential for predicting Norwegian Sea heat content based on upstream conditions. However, local surface forcing (air-sea heat fluxes and Ekman forcing) within the Norwegian Sea substantially modifies the phase and amplitude of ocean heat anomalies along their poleward pathway, and, hence, acts to limit predictability.

1. Introduction

Ocean heat content variability plays an important role in our climate system. In the Arctic-Atlantic region, ocean heat anomalies have been shown to affect sea ice (e.g., Årthun et al., 2012; Yeager et al., 2015), marine ecosystems (Hátún et al., 2009), and potentially also continental climate (Årthun et al., 2017). There is, however, at present neither consensus nor any complete understanding of the mechanisms causing and maintaining such heat anomalies. One primary question regarding the nature of ocean heat anomalies in the North Atlantic is whether the anomalies are related to upstream ocean circulation changes (e.g., Årthun & Eldevik, 2016; Dong & Kelly, 2003; Hátún et al., 2005; Jungclaus et al., 2014; Sutton & Allen, 1997), or whether they are more the surface ocean signature of evolving large-scale atmospheric patterns such as the North Atlantic Oscillation (NAO; Foukal & Lozier, 2016; Krahmann et al., 2001; Saravanan & McWilliams, 1998). Understanding the mechanisms of ocean heat anomalies, with a special emphasis on quantifying the relative influence of ocean advection and air-sea heat fluxes, has implications for climate predictability, as heat anomalies caused by ocean circulation changes appear more predictable than those caused by surface heat fluxes (Yeager & Robson, 2017).

The Norwegian Sea (Figure 1a) is a key component of the North Atlantic climate system, as it acts as a transition zone between the temperate North Atlantic and the cold Arctic Ocean. The oceanographic conditions are influenced by the northward flowing Norwegian Atlantic Current (NwAC) transporting warm, saline Atlantic water into the region (Orvik & Niiler, 2002; Skagseth et al., 2008). After entering the Norwegian Sea, the Atlantic water is modified along its poleward pathway due to heat loss to the atmosphere and lateral eddy exchanges with the colder and fresher Greenland and Iceland Seas (Chafik et al., 2015; Furevik, 2001; Segtnan et al., 2011). In leaving the Norwegian Sea, parts of the Atlantic water will enter the Barents Sea and the Arctic Ocean through the Barents Sea Opening (BSO) and the Fram Strait respectively, and parts will recirculate within the Nordic Seas (Eldevik et al., 2009; Skagseth et al., 2008).

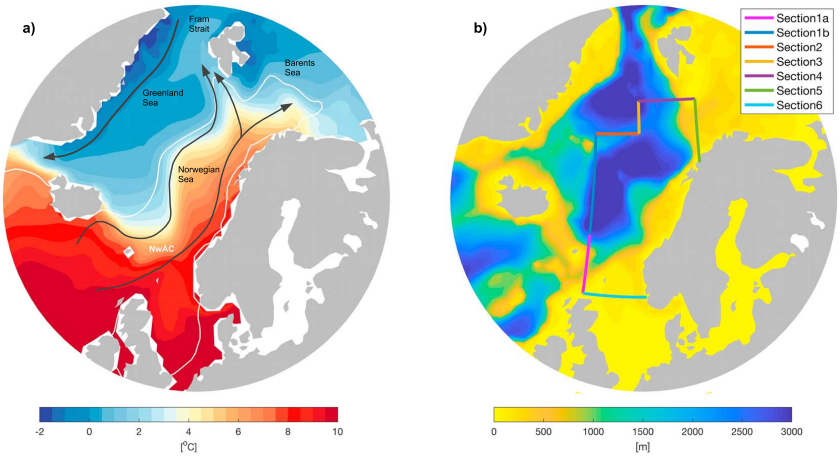

Figure 1. North Atlantic-Nordic Seas temperature and bathymetry. (a) Upper-ocean (0–350 m) mean potential temperature and 35 isohaline (white contour line), with main circulation features indicated. (b) Ocean depth, with Norwegian Sea domain boundary Sections1–6 marked. NwAC = Norwegian Atlantic Current.

Heat exchanges between the Norwegian Sea and neighboring oceans have been studied ever since the first budget estimate was put forward by Mosby (1962). While early work (as summarized in Simonsen & Haugan, 1996) was based on mean ocean transports to and from the Nordic Seas, more recent budget studies have additionally applied atmospheric reanalysis fields to estimate mean heat exchanges with the atmosphere (Segtnan et al., 2011; Simonsen & Haugan, 1996). An alternative approach has been to use air-sea heat fluxes from atmospheric reanalysis together with ocean heat content from hydrography and calculate the ocean heat transport component as a residual (Carton et al., 2011; Mork et al., 2014), something which allows for heat content changes to be assessed.

The Norwegian Sea exhibits pronounced variability in ocean heat content on interannual to decadal timescales. It is, however, not known to what extent the region is a passive receiver of heat anomalies formed elsewhere and to what extent the anomalies are produced locally, for instance, by anomalies in the regional atmospheric circulation (Lien et al., 2014), or a varying influence of the East Icelandic Current (Mork et al., 2014). Focusing on the Atlantic domain of the Nordic Seas, Carton et al. (2011) find ocean advection to be the dominant cause of interannual to decadal heat content variability for the time period 1950–2009, with local air-sea heat fluxes only having a weak reinforcing effect on the anomalies. Mork et al. (2014), on the other hand, find local air-sea heat fluxes to explain about half of the observed heat content variability in the Norwegian Sea between 1951 and 2010. However, these studies, based on comparisons between observed heat content variations (from hydrography) and air-sea fluxes from different reanalysis products, suffer from the inability to close the heat budget, as ocean heat transport is not a well-observed quantity. The role of ocean advection in observation-based studies can therefore only be obtained as a residual, and a detailed examination of the relative contributions of ocean dynamics and local surface forcing has yet to be performed.

In this paper we identify the mechanisms responsible for ocean heat content variability in the Norwegian Sea, using the physically consistent ECCOv4 ocean state estimate (Forget et al., 2015a; Fukumori et al., 2017; Wunsch & Heimbach, 2007). First, we quantify the contribution from air-sea heat fluxes and ocean advection. Then, the contribution of ocean advection is elucidated in more detail by exploring the relative importance of resolved (Eulerian) and eddy-driven (bolus) advection in driving ocean heat transport convergences, as well as the importance of wind-driven Ekman dynamics. A temporal and spatial decomposition furthermore identifies the main sources of advective heat transport variability. Finally, we assess the dominant large-scale oceanic and atmospheric circulation anomalies associated with a variable heat transport to the Norwegian Sea.

2. Methods

2.1. ECCOv4 Ocean State Estimate

ECCO version 4 release 3 (hereafter referred to as ECCOv4) is an ocean state estimate of the 1992–2015 global ocean circulation and sea ice state, generated by fitting the Massachusetts Institute of Technology General Circulation Model (MITgcm) to satellite and in situ ocean observations in a least square sense (Forget et al., 2015a; Fukumori et al., 2017; Wunsch & Heimbach, 2007). The ocean-ice component of the MITgcm produces monthly fields by solving the primitive equations for a time-evolving, Boussinesq, hydrostatic ocean with a nonlinear free surface. Through the adjoint method (Heimbach et al., 2005), these model fields are constrained by ocean observations. Latent, sensible, and upward radiative heat fluxes are calculated from bulk formulae (Large & Yeager, 2004), with ERA-Interim reanalysis (Dee et al., 2011) used as the initial near surface atmospheric state (air temperature, humidity, precipitation, downward radiation, and wind stress). The MITgcm framework obeys the conservation laws of momentum, mass, heat, and salt, and the adjoint method avoids adding nonphysical source/sink terms to the model equations. Consequently, the ECCOv4 estimate is dynamically and kinematically consistent and allows for closed heat, salt, and volume budgets at each grid cell, to machine precision (Buckley et al., 2014, 2015; Piecuch et al., 2017).

The ECCOv4 state estimate is gridded at a LLC90 grid—a global lon-lat-cap (LLC) grid split into five "gcm-faces," one of which is the "Arctic cap" (Forget et al., 2015a). The four grid vertices of the Arctic cap are placed over land at 67°N, while for Antarctica two grid vertices are placed over land at 80°S and away from major ice shelves. The grid has a 1° nominal horizontal resolution, and 50 unevenly spaced vertical layers. The meridional resolution in the Norwegian Sea region is approximately 0.5°, which is larger than the internal deformation radius (Nurser & Bacon, 2014) and the dominant eddy scale (Poulain et al., 1996). The effect of unresolved mesoscale eddies is parameterized as a bolus velocity (Gent & Mcwilliams, 1990). Time-invariant three-dimensional turbulent transport parameters, such as the Gent-McWilliams bolus velocity (eddy) coefficient, are estimated within the ECCOv4 framework under the constraints of observations (Forget et al., 2015a). Constraining the turbulent transport parameters in ECCOv4 greatly improves the fit to in situ profiles compared to earlier ECCO solutions (Forget et al., 2015b).

2.2. Comparison to Observations

In combining the physical consistency of a GCM with actual observational data, ECCOv4 is ideal for a regional heat budget analysis of the Norwegian Sea. To test ECCOv4's general applicability for the Nordic Seas region, we compare to observed ocean heat and freshwater anomalies from the combined data sets of the Institute of Marine Research, the Polar Research Institute of Marine Fisheries and Oceanography, and the Argo Global Data Assembly Centre (Coriolis Data Centre), acquired from the ICES Report on Ocean Climate (González-Pola et al., 2018). The ECCOv4 heat and freshwater content is calculated by integrating temperature and freshwater (relative to a reference salinity of 34.8) over the Norwegian Sea domain seen in Figure 1b. The observed heat and freshwater content is an estimate over the Atlantic water layer of the topographically defined Norwegian Sea domain seen in Mork et al. (2014; mean Atlantic water depth between 1951 and 2010 is 409 m). We note, however, that the comparison is not sensitive to the exact definition of our domain.

The overall variability in heat and freshwater content for the 1992–2015 period is captured well by the ECCOv4 estimate (Figure 2; $r = 0.87$ for the upper 400 m). ECCOv4 does, however, appear slightly colder and fresher than the observations. Another noticeable difference is the delayed late 1990s warming trend in ECCOv4. Still, the comparison to hydrography is favorable, though not entirely surprising, as ECCOv4 is constrained to some of the same observational data (e.g., Argo data).

We furthermore compare temperature and volume transport estimates in ECCOv4 to observations from the Faroe-Shetland Channel (FSC; available from the ICES Report on Ocean Climate and Marine Scotland, UK, respectively) and the BSO (provided by the Institute of Marine Research, Norway). As seen in Figures 3c and 3d, the observed temperature compares well with the ECCOv4 estimate for both the FSC and the BSO. While the time-mean volume transport at the BSO is captured accurately by ECCOv4 (Figure 3b; 2.0 versus 2.1 Sv in observations), the interannual variability is not reproduced. The low correlation could, in part, be a result of insufficient horizontal resolution in both current measurements (Ingvaldsen et al., 2002) and ECCOv4, neither being able to resolve the internal radius of deformation in the BSO (Nurser & Bacon, 2014). We note that high-resolution (1/4°-4 km) ocean models also struggle to capture observed volume

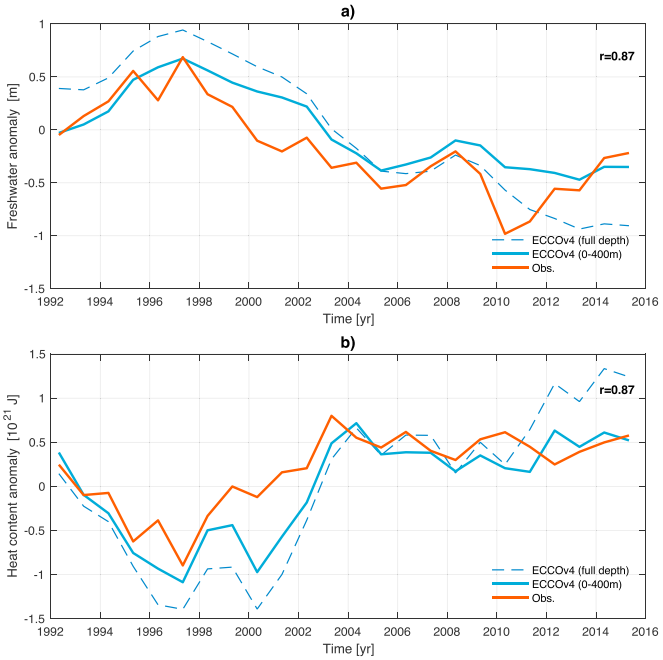

Figure 2. Comparison to hydrography. (a) May freshwater anomaly for the Norwegian Sea in ECCOv4 relative to 34.8, and May-centered freshwater anomaly for the Norwegian Sea Atlantic water layer in observations. (b) May heat content anomaly for the Norwegian Sea in ECCOv4, and May-centered heat content anomaly for the Norwegian Sea Atlantic water layer in observations. Correlations between the observations and the 0–400 m anomaly in ECCOv4 is noted in the upper right-hand corner. May-centered hydrography stems from annual internationally coordinated cruises between 15 April and 15 June and is acquired from the ICES Report on Ocean Climate.

transport variations in the BSO (Lien et al., 2016). The transport of Atlantic water through the FSC is, on the other hand, reproduced well by ECCOv4 (Figure 3a; $r = 0.68$). As the inflow through the FSC is the main provider of Atlantic heat to the Norwegian Sea, these results (Figures 3a and 3c), together with the favorable comparison to observed hydrography (Figure 2), provide confidence in the ability of ECCOv4 to assess ocean heat content variability in the Norwegian Sea, and its drivers.

2.3. Heat Budget

In order to identify the processes driving interannual heat content variability in the Norwegian Sea, a regional heat budget is calculated using the ECCOv4 ocean state estimate. The Norwegian Sea domain (Figure 1b) is enclosed by six boundary sections plus the Norwegian coast as the eastern boundary. Section1 is split into two parts and will be treated separately, as the inflow of warm Atlantic water occurs in Section1's southernmost part (Section1a; 6.1 Sv in), while small amounts of relatively cold water is exiting the domain through the northernmost part (Section1b; 0.6 Sv out). The northern section toward the Fram Strait (Section4; 8.2 Sv out) and the section at the BSO (Section5; 3.3 Sv out) are the main outflow regions where warm Atlantic water exits the Norwegian Sea domain and continues toward the Arctic (Figure 1a). Although the locations of the defined boundary sections make them not directly comparable to observations from the Fram Strait and the BSO, we note that the simulated transports toward the Arctic are in broad agreement with observational estimates (Schauer et al., 2004; Skagseth et al., 2008).

The heat content tendency for a given control volume is determined by convergence of advective, diffusive, and surface heat fluxes. The heat budget equation describing this relationship, originates from integrating

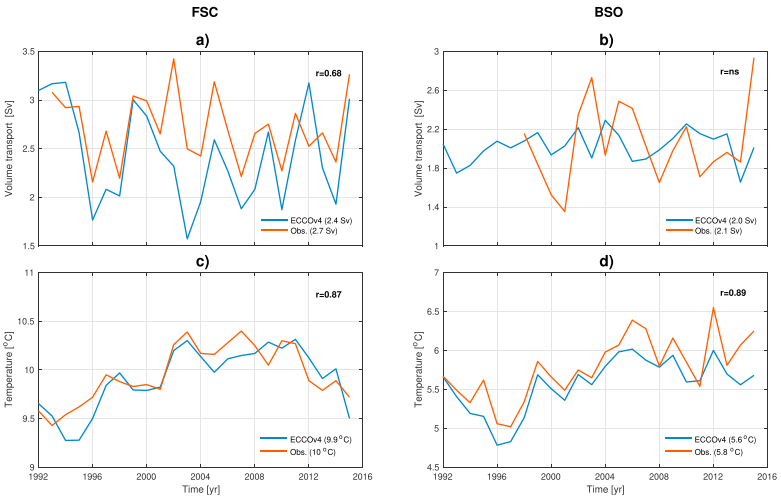

Figure 3. Comparison to observations. Annual mean volume transport in (a) the Faroe-Shetland Channel (Berx et al., 2013), and (b) the Barents Sea Opening (Skagseth et al., 2008), from observations and ECCOv4. Annual mean temperature at (c) the Faroe-Shetland Channel (0–200 m), and (d) the Barents Sea Opening (50–200 m), in observations (ICES Report on Ocean Climate) and ECCOv4. The time-mean volume transport (a, b) and temperature (c, d) are noted in parentheses in the lower right-hand corner. Correlations between the respective time series are noted in the upper right-hand corner ("ns" stands for "not significant").

the conservation of heat equation over a chosen geometric volume V:

$$\underbrace{\rho_o C_p \iiint_V \frac{\partial \theta}{\partial t} \mathrm{d}V}_{Tend} = \underbrace{\rho_o C_p \iiint_V (-\nabla \cdot \mathbf{u}\theta)\mathrm{d}V}_{ADV} + \underbrace{\rho_o C_p \iiint_V (-\nabla \cdot \mathbf{K})\mathrm{d}V}_{DIFF} + \underbrace{\rho_o C_p \iiint_V Q \mathrm{d}V}_{Qnet} \quad (1)$$

where ρ_o is a reference density of seawater, C_p is the specific heat capacity, θ is potential temperature, $\mathbf{u}$ is the three-dimensional velocity vector, $\mathbf{K}$ is the diffusive temperature flux vector, and Q is the net air-sea heat flux (sensible, latent, shortwave, and longwave). For conceptual and methodological simplicity and robustness, for example, to avoid effects of local vertical heaving, we choose to integrate the Norwegian Sea domain from the sea surface to the ocean bottom. However, we note that the heat budget is dominated by upper-ocean variability (Figure 2b). The budget terms will for simplicity be referred to as heat content tendency *Tend*, advective heat transport convergence *ADV*, diffusive heat transport convergence *DIFF*, and net air-sea heat fluxes *Qnet*.

Following the approach and terminology of Piecuch and Ponte (2012), we use "Variance Explained" (v) as a metric to quantify the amount of variability in heat content tendency *Tend* explained by the respective budget terms:

$$v(x, y) = 100\% \times (1 - \frac{\sigma^2(x - y)}{\sigma^2(x)}), \quad (2)$$

where σ^2 is the temporal variance. The $v(x, y)$ takes on values between $-\infty$ and 100 and gives the percentage of variance in variable x explained by variable y. A value of, for example, 40% indicates that 40% of the variance in x can be explained by variance in y, while a value of -40% means that the variance in y increases the variance in x by 40%. Large negative values ($< -100\%$) indicate that the signals are out of phase and/or that the variance in y is larger than the variance in x. Applying the metric to our heat budget ($Tend = ADV + DIFF + Qnet$), x equals the heat content tendency *Tend* and y equals one of the remaining budget terms, depending on which one is being analyzed.

In order to explore the link between Atlantic water inflow and large-scale atmospheric forcing, the leading modes of atmospheric variability for the ECCOv4 time period (1992–2015) are identified by calculating

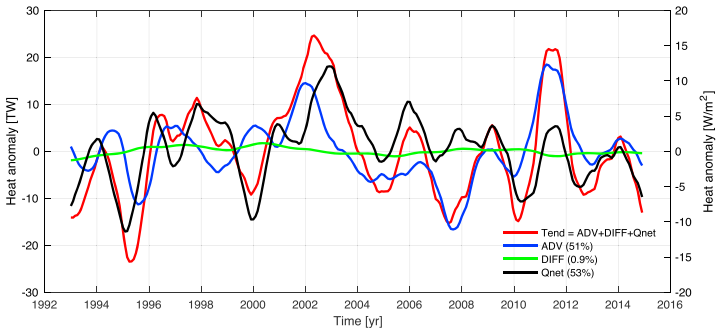

Figure 4. Norwegian Sea heat budget. Deseasoned, detrended, and 1-year low-pass-filtered heat budget (1993–2014) for the Norwegian Sea domain, where *Tend* is the heat content tendency, *ADV* is the advective heat transport convergence, *DIFF* is the diffusive heat transport convergence, and *Qnet* is the net air-sea heat fluxes; 1 TW equals 10^{12} J/s. Variance in *Tend* explained by the respective budget terms is noted in parentheses.

empirical orthogonal functions for area-weighted sea level pressure over the North Atlantic region, using the original ERA-Interim reanalysis fields used to force the MITgcm (the adjusted fields are not available as output). The two leading modes are the NAO (41% of the variance) and the East Atlantic Pattern (EAP; Barnston and Livezey (1987); 17% of the variance). NAO and EAP indexes are defined using the principal component time series. Our empirical orthogonal function-based NAO index is strongly correlated ($r = 0.85$) with the station-based index of Hurrell (1995).

As we focus on interannual variability, seasonal cycles and linear trends are removed from all time series from here and onward. In order to accentuate interannual variability, the time series are smoothed by applying a 1-year low-pass triangular filter (24-month filter width). To avoid edge effects from filtering, the first and last 12 months of the time series are removed, leaving us with the 1993–2014 time period that will be analyzed here.

3. Results

3.1. Norwegian Sea Heat Budget

The Norwegian Sea heat budget shows pronounced interannual variability, with standard deviations of 10.3 TW for *Tend*, 6.8 TW for *ADV*, 7.1 TW for *Qnet*, and 0.8 TW for *DIFF* (Figure 4). Fifty-one percent of the variability in *Tend* is explained by variability in *ADV*, and 53% is explained by variability in *Qnet*. *DIFF* is practically negligible, explaining only 0.9% of the variability. These results translate to an equal contribution from ocean advection and air-sea heat fluxes in driving the interannual Norwegian Sea heat content variability, consistent with the findings of Mork et al. (2014).

While *ADV* and *Qnet* are found to be equally important when integrating the heat budget over the Norwegian Sea domain in its entirety, this does not exclude the possibility of large spatial variations in the importance of the individual budget terms. Consequently, a spatial analysis is carried out by calculating the depth-integrated heat budget for each horizontal grid cell within the Norwegian Sea domain and neighboring areas, and mapping the relative importance of the budget terms (Figure 5). Note that summing the depth-integrated budgets within the Norwegian Sea domain gives the volume-integrated budget in Figure 4.

Figure 5a shows pronounced spatial variations in the ability of *ADV* to explain the variability in *Tend*. Toward the center of the Norwegian Sea domain (southwest to northeast), *ADV* explains the majority of the variability in *Tend* (60–80%). This area largely coincides with the extent of the Atlantic water (defined here as the horizontal area with salinity ≥35 in the upper 350 m within the Norwegian Sea domain), along which *ADV* explains 62% and *Qnet* 39% of the interannual heat content variability. A branching pattern is also visible at the northern boundary, indicating that heat content variability along the NwAC is closely related to advective heat transport. As *ADV* and *Tend* are largely positively correlated (Figure 5b), areas with large negative ν values are generally due to a larger temporal variance σ^2 in *ADV* compared to that in *Tend* (equation (2)).

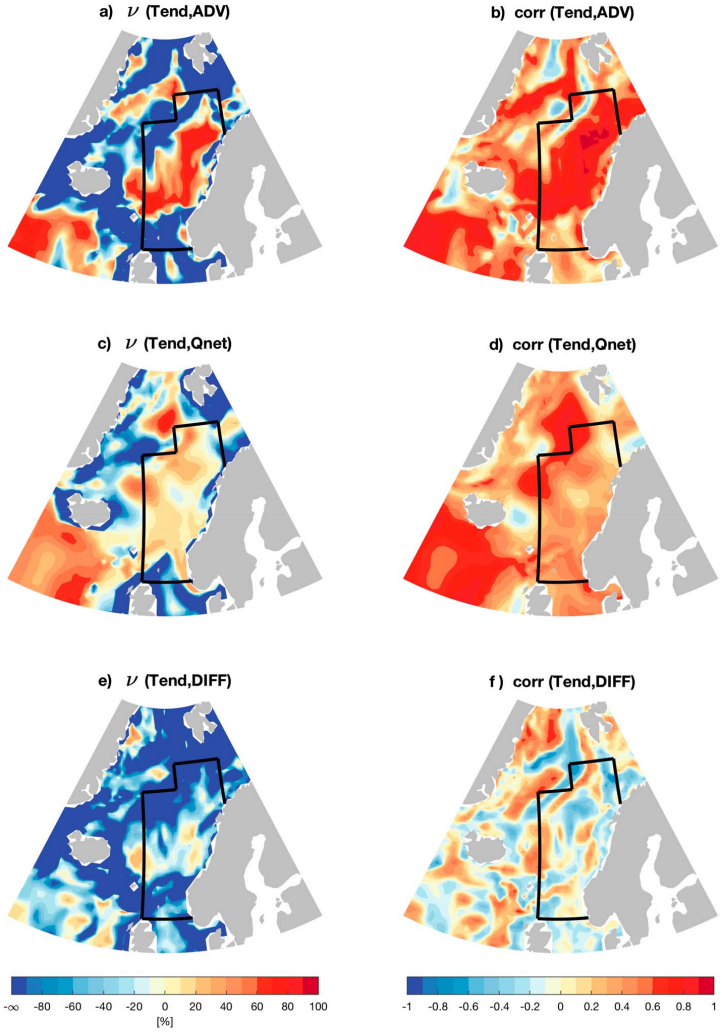

Figure 5. Spatial heat budget analysis. (a, c, and e) Variance in *Tend* explained by respective budget terms in each horizontal grid cell, and (b, d, and f) correlation between *Tend* and respective budget terms. The analysis is based on deseasoned, detrended, and 1-year low-pass-filtered depth-integrated heat budgets. The Norwegian Sea domain is indicated by the solid black lines.

A noticeable feature in Figure 5a is the discontinuity at the Iceland-Scotland Ridge, separating high ν values in the subpolar North Atlantic and within the Nordic Seas. The Atlantic inflow across the ridge takes place through narrow channels, and the flow is characterized by high mesoscale activity, leading to high transport variability (Sherwin et al., 2006; Zhao et al., 2018). Closer inspection of the region shows that the discontinuity in ν values across the ridge is much reduced if we consider unfiltered monthly time series. While exchanges between the Norwegian Sea and the North Atlantic south of the ridge are observed to occur on a broad range of time scales (Bringedal et al., 2018; Hansen & Østerhus, 2000), the processes driving local heat content change at the ridge is thus found to act predominantly on subannual time scales.

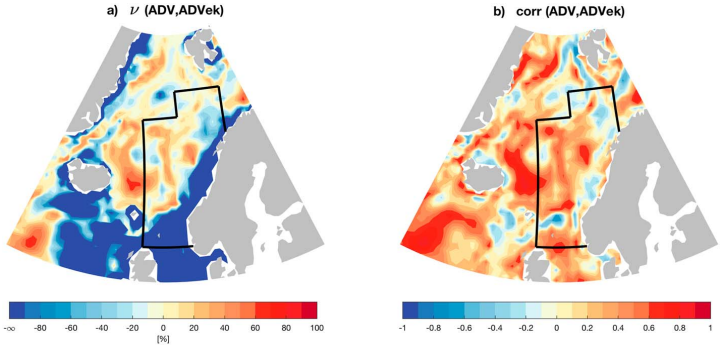

Figure 6. Role of Ekman forcing. (a) Variance in *ADV* explained by Ekman forcing ADV_{ek} in each horizontal grid cell, and (b) correlation between *ADV* and ADV_{ek}. The analysis is based on deseasoned, detrended, and 1-year low-pass-filtered depth-integrated heat budgets. The Norwegian Sea domain is indicated by the solid black lines.

Within the Norwegian Sea domain, *Qnet* is positively correlated to *Tend* (Figure 5d), though the correlations are slightly weaker compared to *ADV* (Figure 5b). Figure 5c shows higher ν values in the eastern Nordic Seas, compared to the western Nordic Seas, implying that air-sea heat fluxes acts as a source of interannual heat content variability throughout the Norwegian Sea domain.

The ability of *DIFF* to explain variability in *Tend* is modest (Figure 5e). Figure 5f shows a highly fractioned spatial pattern, with the highest correlations near the northwestern boundaries of the Norwegian Sea domain, something which could be related to lateral heat loss from the warm NwAC by isopycnal diffusion observed in the region (e.g., Isachsen et al., 2012; Nilsen et al., 2006).

3.2. Role of Local Wind Forcing

Ocean advection appears to be the dominant driving mechanism of ocean heat content variability in the Atlantic domain within the Norwegian Sea domain. However, some fraction of this advective heat transport variability is likely directly attributable to local wind forcing (Ekman forcing). In order to quantify this contribution, we calculate the advective heat transport convergence by Ekman transport ADV_{ek}.

Following the approach of Buckley et al. (2014), we assume that the horizontal velocity $\mathbf{u_h}$ can be decomposed into a geostrophic part $\mathbf{u_g}$ and an Ekman part $\mathbf{u_{ek}}$: $\mathbf{u_h} \approx \mathbf{u_g} + \mathbf{u_{ek}}$. The horizontal Ekman velocity is given by

$$\mathbf{u_{ek}} = \frac{\mathbf{M_{ek}}}{D_{ek}} = \frac{\boldsymbol{\tau} \times \hat{\mathbf{z}}}{\rho_o f D_{ek}} \tag{3}$$

where $\mathbf{M_{ek}}$ is the Ekman transport, D_{ek} is the Ekman depth (here 50 m is used; e.g., Rio & Hernandez, 2003), τ is the wind stress, and f is the Coriolis parameter. The vertical Ekman transport vanishes, as we consider the full ocean depth. Advective heat transport convergence by Ekman transport for a horizontal grid cell is then given by

$$ADV_{ek} = \rho_o C_p \int_{-D_{ek}}^{\eta} (-\nabla \cdot \bar{\mathbf{u}}_{\mathbf{ek}} \bar{\theta}) \mathrm{d}z \tag{4}$$

where $\bar{\mathbf{u}}_{\mathbf{ek}}$ and $\bar{\theta}$ is the time-evolving Ekman velocity and potential temperature, averaged over the Ekman layer. The lack of difference between using time-evolving $\bar{\theta}$ and climatological $\bar{\theta}$ (not shown), indicates that local wind variability dominates over temperature field changes in causing interannual variability in ADV_{ek}. The shallow areas along the Norwegian coast and at the southern boundary (Figure 1b) will not be discussed, as the approximation $\mathbf{u_h} \approx \mathbf{u_g} + \mathbf{u_{ek}}$ breaks down for shallow regions due to lateral friction and bottom Ekman layers (Buckley et al., 2014).

Figure 6 shows that *ADV* and ADV_{ek} are largely positively correlated, and ADV_{ek} is found to contribute to interannual variability in *ADV* toward the center of the Norwegian Sea domain, explaining 30–40% or less of the variability. These results suggest that Ekman dynamics is important, but not dominant, in driving

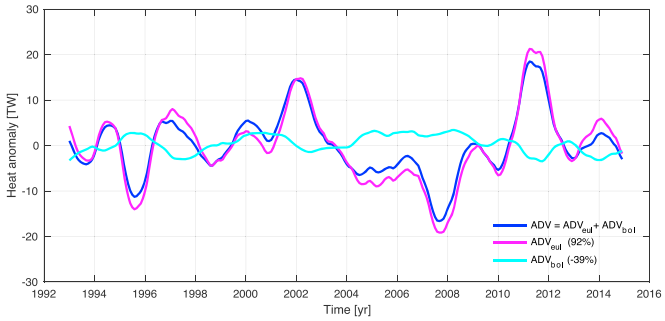

Figure 7. Role of eddy-scale processes. Decomposition of the Norwegian Sea heat budget term *ADV* into advection by resolved (ADV_{eul}) and bolus (ADV_{bol}) velocities. Variance in *ADV* explained by ADV_{eul} and ADV_{bol} is noted in parentheses.

advective heat transport convergence *ADV*. Forcing by local wind variability within the Norwegian Sea particularly acts to enhance the variance of heat anomalies advected into the domain with the North Atlantic Current/NwAC.

3.3. Decomposition of Advection

Advection of heat anomalies into the Norwegian Sea domain has been shown to be a driving mechanism of Norwegian Sea heat content variability comparable in size to that of local surface forcing (air-sea heat fluxes and Ekman forcing). In order further to understand the advection mechanism, spatial and temporal decompositions of the volume-integrated Norwegian Sea heat budget term *ADV* from Figure 4 are now carried out.

3.3.1. Eulerian and Eddy-Driven Advection

Advection by both resolved (Eulerian) and parameterized (bolus) velocities constitute the advective heat transport convergence budget term: $ADV = ADV_{eul} + ADV_{bol}$ (Buckley et al., 2014; Piecuch et al., 2017). Considering the two model velocities separately, we find that *ADV* largely originates from temperature advection by the resolved velocity field ADV_{eul} (Figure 7). The eddy-driven advection ADV_{bol} acts in the opposite direction of ADV_{eul} but has a small magnitude in comparison. ADV_{bol} acting to compensate for ADV_{eul} is consistent with eddies cooling the NwAC by transporting the warm Atlantic water away from the mean current (Isachsen et al., 2012). A stronger Atlantic water current would then imply increased eddy activity, and more heat loss from the Atlantic water core. The importance of eddy exchanges with the colder and fresher neighboring Iceland and Greenland Seas has been highlighted in previous budget studies (Segtnan et al., 2011) and is consistent with ADV_{bol} contributing to heat transport convergence along the northwestern and northern boundaries of our Norwegian Sea domain.

3.3.2. Source of Advective Heat Transport Variability

The heat transport convergence term *ADV* accounts for heat transport variations through six boundary sections encompassing the Norwegian Sea. The sections capture the different branches of the NwAC; the Atlantic water inflow across the Greenland-Scotland Ridge (Section1a; AWin), and the two northern branches entering the Fram Strait (Section4; FS) and the Barents Sea (Section5; BS). By analyzing the importance of the different branches and their driving mechanisms, we aim to identify the source of advective heat transport variability for the Norwegian Sea.

For individual sections where the volume transport is not balanced, heat transport is not well defined (Schauer & Beszczynska-Möller, 2009), but a relative value can be calculated by using a reference temperature. Because we are concerned with the heat transport (*HT*) that actually alters the heat content of the Norwegian Sea domain, we use the time-evolving volume-averaged Norwegian Sea temperature as a reference temperature θ_{ref}, following the approach of Lee et al. (2004):

$$\theta_{ref}(t) = \iiint_V \theta(t,x,y,z)\mathrm{d}V \tag{5}$$

$$HT = \rho_o C_p \int_S (\mathbf{v}\cdot\mathbf{n})(\theta - \theta_{ref})\mathrm{d}S \tag{6}$$

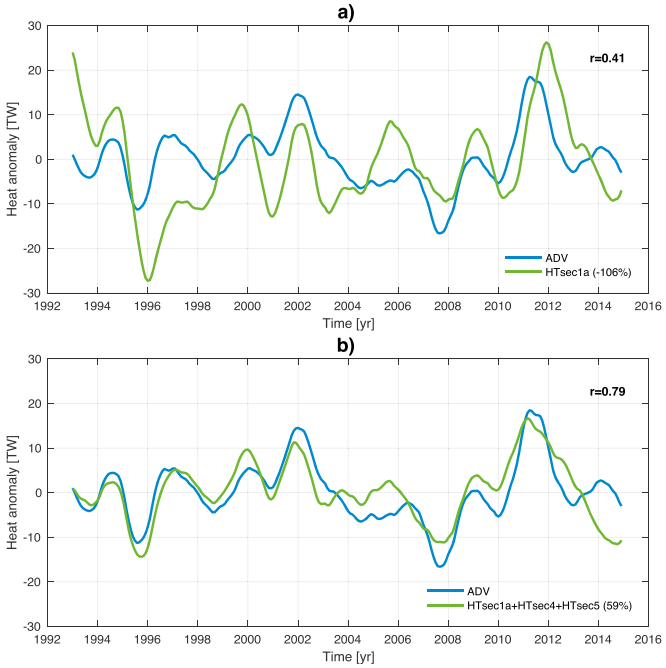

Figure 8. Atlantic water inflow as source of *ADV* variability. Norwegian Sea heat budget term *ADV* versus (a) heat transport through Section1a (AWin), and (b) summed heat transport through Section1a (AWin), Section4 (FS), and Section5 (BS). Heat transport is positive when warm water (relative to θ_{ref}; equation (6)) is brought into, or cold water out of, the Norwegian Sea domain. Correlations are noted in the upper right-hand corner. Variance in *ADV* explained by the heat transport through the respective boundary sections are noted in parenthesis.

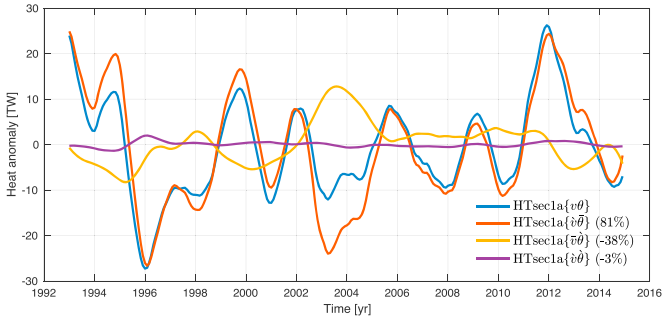

Figure 9. Decomposition of heat transport $HT\{v\theta\}$ through Section1a (AWin) into a velocity component $HT\{v'\bar{\theta}\}$, a temperature component $HT\{\bar{v}\theta'\}$, and a covariance component $HT\{v'\theta'\}$. Heat transport is positive when warm water (relative to θ_{ref}; equation (6)) is brought into, or cold water out of, the Norwegian Sea domain. Variance in $HT\{v\theta\}$ explained by the respective terms is noted in parentheses.

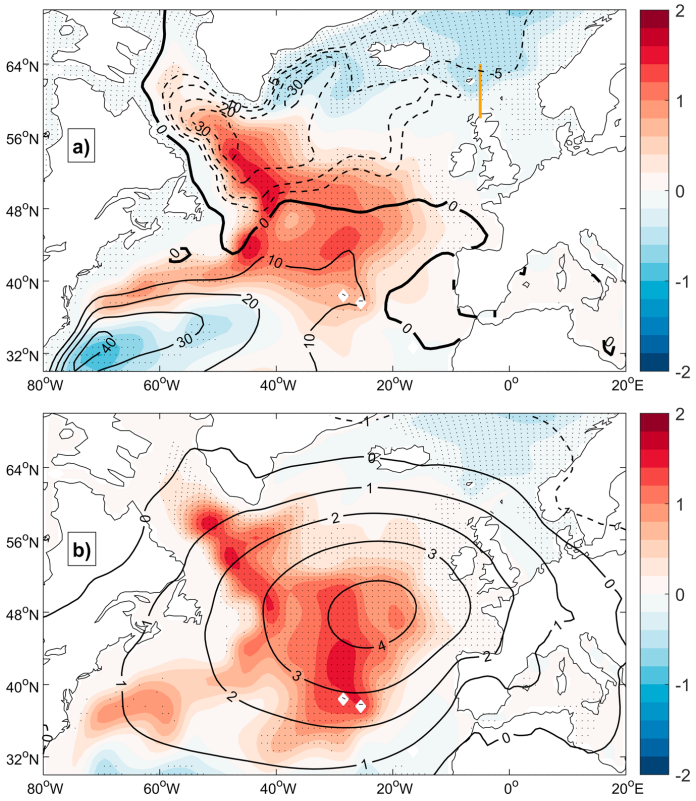

Figure 10. Linear regression between (a) $HT\{v'\bar{\theta}\}$ and the barotropic stream function and (b) between the East Atlantic Pattern and the barotropic stream function (units: Sv/std[index]). All time series were detrended and filtered prior to analysis. In (a) the mean barotropic stream function (Sv) is also shown by the black contours. The subpolar and the subtropical gyres are characterized by cyclonic (negative) and anticyclonic (positive) circulation, respectively. In (b) the black contours show the sea level pressure anomalies (hPa) associated with the East Atlantic Pattern. The location of Section1a (AWin) used to calculate $HT\{v'\bar{\theta}\}$ is shown in (a) by the orange line. Dots indicate where the correlation is significant at the 95% confidence level (Ebisuzaki, 1997).

where V is the Norwegian Sea volume and S is the surface area of the boundary section analyzed. We note that the volume-averaged Norwegian Sea temperature is practically 0 °C, regardless of averaging over the full ocean depth or over the upper ocean (e.g., 0–550 m), or using the corresponding time-mean value. The applied reference temperature is thus close to that used by previous studies on heat transport in the Nordic Seas (e.g., Årthun et al., 2012; Orvik & Skagseth, 2005), and our results are not noticeably sensitive to the assessed methods of choosing θ_{ref}.

The heat transport through Section1a (AWin) is more related to ADV ($r = 0.41$; Figure 8a) than any of the other boundary sections (HTsec4 and HTsec5 are not correlated to ADV). This supports an important contribution to the Norwegian Sea heat budget from upstream ocean heat anomalies transported by the North Atlantic Current/NwAC. The negative ν value (−106%) arises from HTsec1a having a higher variance than ADV (10.3 and 6.8 TW, respectively). To capture the correct phase and amplitude of the basin-scale heat anomalies, it is necessary to include the outflow regions Section4 (FS) and Section5 (BS; Figure 8b). Such a finding highlights the important role of local surface forcing in modifying the heat anomalies within the Norwegian Sea domain (Furevik, 2001).

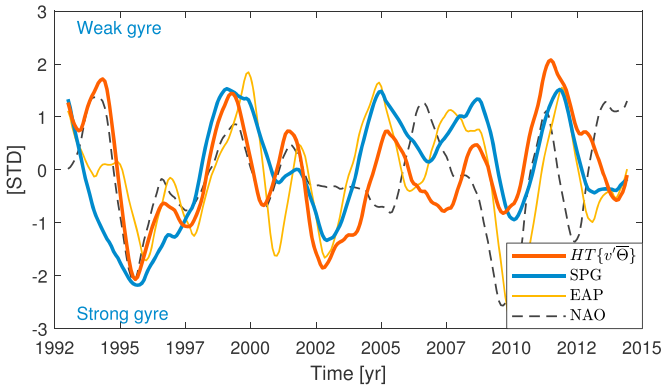

Figure 11. Standardized time series of the Atlantic inflow to the Nordic Seas ($HT\{v'\bar{\theta}\}$), the SPG strength (inverted), and the NAO and EAP indexes (calculated as the principal components of the first two modes of sea level pressure variability). SPG = subpolar gyre; EAP = East Atlantic Pattern; NAO = North Atlantic Oscillation.

In order to determine the driver of Atlantic water inflow variability, a temporal decomposition of the heat transport through Section1a is carried out. The Atlantic water inflow variability can originate from anomalous velocities $\{v'\bar{\theta}\}$, changes in the temperature of the advected water mass $\{\bar{v}\theta'\}$, or the covariance between the two $\{v'\theta'\}$: $HT\{v\theta\} = HT\{v'\bar{\theta}\} + HT\{\bar{v}\theta'\} + HT\{v'\theta'\}$, where overbar denotes the time mean and prime denotes the time anomaly. As seen in Figure 9, the Atlantic water inflow variability is dominated by velocity fluctuations v' (explain 81% of the variability) rather than temperature fluctuations. This is in agreement with observations from the NwAC (Orvik & Skagseth, 2005), and modeled heat transport at the Greenland-Scotland Ridge (Årthun & Eldevik, 2016). For the two outflow regions, the same decompositions show that velocity fluctuations v' play a leading role at Section5 (66%), though temperature fluctuations T' are also important (58%). At Section4, on the other hand, temperature fluctuations T' take the leading role (85%), but with velocity fluctuations v' also being important (42%).

3.3.3. Relation to Large-Scale Forcing

Having identified volume transport fluctuations $HT\{v'\bar{\theta}\}$ in the Atlantic inflow to play a leading role in the Norwegian Sea heat budget, we now aim to identify the dominant mechanisms of anomalous Atlantic water circulation in ECCOv4. To assess the dynamic variations in North Atlantic circulation associated with $HT\{v'\bar{\theta}\}$, Figure 10a shows the regression between $HT\{v'\bar{\theta}\}$ and the barotropic stream function in the North Atlantic. A stronger inflow to the Nordic Seas is associated with a weakened subpolar gyre (SPG) and a strengthening, and northward shift, of the North Atlantic Current that flows along the zero line of the stream function. The covariability between the Atlantic inflow to the Nordic Seas and ocean circulation in the subpolar North Atlantic can be quantified by calculating the SPG strength, defined as the absolute value of the minimum barotropic stream function in the subpolar region. For the time period covered by ECCOv4 the SPG strength shows a good connection to $HT\{v'\bar{\theta}\}$ (r=-0.54), and especially after the late 1990s the covariability is strong (Figure 11). These results support a close coupling between the subpolar North Atlantic and the Nordic Seas (Hátún et al., 2005; Langehaug et al., 2012; Yeager et al., 2015).

The origin of ocean circulation variability in the subpolar North Atlantic has been much studied (e.g., Häkkinen et al., 2011; Lohmann et al., 2009; Piecuch et al., 2017; Robson et al., 2012). Several studies have, for instance, previously related inflow changes to large-scale wind forcing associated with the NAO (e.g., Bringedal et al., 2018; Hansen & Østerhus, 2000; Sandø et al., 2012). In ECCOv4, the correlation between $HT\{v'\bar{\theta}\}$ and the NAO index is significant for the full time period (Figure 11; $r = 0.45$). However, this mostly reflects covariability during the 1990s, and the inflow variability appears not to have been driven by the NAO in the latter part of the time series (correlation not significant for 2000–2014). This supports the finding that the ocean circulation in the subpolar North Atlantic has been decoupled from the NAO in recent decades (Foukal & Lozier, 2017; Lohmann et al., 2009). The regression pattern between the Atlantic inflow strength and the barotropic stream function (Figure 10a) does, however, closely resemble the circulation anomalies associated with the EAP index (Figure 10b). The EAP reflects changes in the wind stress curl over the

subpolar North Atlantic (Barnston & Livezey, 1987) and is known to modulate ocean circulation in the subpolar North Atlantic (Foukal & Lozier, 2017; Häkkinen et al., 2011). For the ECCOv4 time period, the EAP reflects well the SPG strength (Figure 11; $r = -0.70$). Our results thus support a modulation of the gyre strength through wind stress curl variability associated with the EAP.

4. Discussion and Conclusions

In this study, a regional heat budget for the Norwegian Sea has been calculated using the ECCOv4 ocean state estimate in order to quantify the relative importance of ocean dynamics and local surface forcing. We find ocean advection and air-sea heat fluxes to be equally important in driving interannual heat content variability between 1993 and 2014, consistent with the findings of Mork et al. (2014). A further spatial analysis shows advection to be dominant (60–80%) in the Atlantic domain within the Norwegian Sea domain. While this dominance of advection in the Atlantic domain is along the lines of Carton et al. (2011), we note that, unlike Carton et al. (2011), our results suggest an active role of air-sea heat fluxes in generating heat anomalies also within the Atlantic domain. This discrepancy could be a result of the 2-year low-pass filter applied in Carton et al. (2011), which emphasizes multiannual variability more influenced by ocean advection (Buckley et al., 2014).

Spatial and temporal decompositions of the advection budget term show that non-Ekman dynamics dominate the advective heat transport in the region, consistent with the findings of Furevik and Nilsen (2005) and Raj et al. (2018). Furthermore, advection by Eulerian velocities dominates, while eddy-driven transports appear to have a dampening effect. The Atlantic water inflow is found to be a major source of the advection-driven convergence of heat within the Norwegian Sea domain (Figure 8a). However, we also find that the outflow regions are necessary to capture the correct magnitude and phase of the basin-scale heat anomalies (Figure 8b), suggesting that local surface forcing (air-sea heat fluxes and Ekman forcing) is important for modifying the anomalies along their poleward pathway. Furthermore, while velocity fluctuations are found to control heat transport variability at the Atlantic water inflow region, temperature fluctuations become increasingly more important at the outflow regions—a result that also points to surface forcing within the Norwegian Sea domain being important.

The ECCOv4 time period is relatively short, and, as highlighted in Mork et al. (2014), the relative amount of heat content change caused by ocean advection and air-sea heat fluxes is likely not stationary in time. For the Norwegian Sea this can for instance be a varying influence of the East Icelandic Current. In this paper we have focused on analyzing overall heat content variability for the ECCOv4 time period. It is, however, evident from our heat budget (Figure 4) that some of the warming/cooling events are purely advection driven (e.g., 2007), some are purely air-sea heat flux driven (e.g., 1999), and some are a mix of the two (e.g., 2002).

Our results indicate that the strength of the Atlantic inflow ($HT\{v'\bar{\theta}\}$) is related to ocean circulation variability in the subpolar North Atlantic, as expressed by the SPG strength—a strong/weak inflow being associated with a weak/strong gyre. Increased northward transport of Atlantic water in the northeastern Atlantic as a result of a weakened SPG is in agreement with previous studies (Häkkinen et al., 2011; Hátún et al., 2005). A weakened SPG is commonly associated with a northwest shift of the subpolar front, that is, a smaller gyre, allowing an increased northward advection of warm subtropical water into the eastern subpolar North Atlantic and Norwegian Sea (Hátún et al., 2005). However, in ECCOv4, changes in the strength of the gyre associated with increased Atlantic inflow to the Norwegian Sea are mostly confined to the western SPG region (Figure 10a), and not to a large degree related to the zonal extent of the gyre along the eastern boundary. Hence, the eastward expansions and contractions of the gyre do not control the strength of the Atlantic inflow to the Norwegian Sea.

In line with our results, heat budget estimates from the eastern subpolar North Atlantic, just upstream of the Norwegian Sea, find variations in ocean heat transport to be a major source of heat content variability (Desbruyères et al., 2015; Foukal & Lozier, 2018). These studies demonstrate that anomalous northward heat transport in the eastern subpolar North Atlantic is strongly influenced by the strength of the inter-gyre connection between the subtropical and SPGs. This is consistent with our finding of a wind-driven strengthening and northward shift of the North Atlantic Current when the Atlantic inflow to the Norwegian Sea is high (Figure 10; Marshall et al., 2001).

We note that unlike gyre indexes inferred from sea surface height (SSH; e.g., Häkkinen & Rhines, 2004; Hátún et al., 2005), the gyre strength in ECCOv4 (calculated directly from the barotropic stream function)

shows no decline in SPG circulation. The trend in the SSH-based SPG index comes from a basin-wide sea level rise in the North Atlantic (Foukal & Lozier, 2017; Hátún & Chafik, 2018), which does not translate into dynamical SPG changes. Constructing an SPG index based on detrended SSH in ECCOv4 yields similar gyre variations as to that obtained from the barotropic stream function ($r = 0.67$ if the SSH-based index leads by 1 year). For a recent, more detailed discussion on the calculation and interpretation of SSH-based SPG indexes, see Hátún and Chafik (2018).

The accuracy of the ECCOv4 ocean state estimate depends on the model fields being well constrained to actual observational data. The good match to observed variability in Norwegian Sea heat and freshwater content (Figure 2), and FSC and BSO temperatures (Figures 3c and 3d), implies a well-constrained ocean state estimate in our region of interest. As the Atlantic inflow strength is found to be a major source of Norwegian Sea heat content variability, the good fit to observed FSC volume transport is encouraging (Figure 3a), despite the poor representation of BSO transport variability (Figure 3b). The applied air-sea heat fluxes represent an additional source of uncertainty (Carton et al., 2011). However, ERA-Interim reanalysis, which provides ECCOv4 with its initial atmospheric state, has been shown to perform well in the Nordic Seas region (Lindsay et al., 2014). The mean turbulent heat fluxes calculated within the ECCOv4 framework are higher than in ERA-Interim (93 and 77 W/m^2, respectively, when averaged over the Norwegian Sea), but the variance (6 and 5 W/m^2) and interannual variability are similar ($r = 0.84$). As the effect of mesoscale eddies are largely parametrized, eddy-driven transport of heat could be underrepresented and thus lead to an elevated heat loss to the atmosphere. Lastly, although we have demonstrated the realism of ECCOv4 for our region of interest, our results are based on a single model, and the robustness of our results therefore need to be further established.

By performing a detailed heat budget analysis for the Norwegian Sea, we have identified an important role of ocean dynamics/nonlocal forcing in the Atlantic domain. This finding implies a potential for prediction of ocean heat content on interannual time scales, as skillful predictions of ocean heat content generally arise from the realistic initialization of ocean circulation anomalies associated with ocean dynamics (e.g., Yeager & Robson, 2017). Our results thus support and detail the findings from initialized climate prediction models, which demonstrate that large-scale circulation changes in the subpolar North Atlantic are communicated toward the Arctic via the Norwegian Sea (Langehaug et al., 2017; Yeager et al., 2015; Yeager & Robson, 2017). We find that interannual heat content anomalies in the Norwegian Sea are more related to the variable strength of the Atlantic water inflow than to temperature changes of the inflowing water. Observations nevertheless show that on multiannual to decadal time scales, temperature anomalies are able to propagate into and through the Norwegian Sea (Årthun et al., 2017; Broomé & Nilsson, 2018), something which suggests that temperature anomalies advected by the mean current could play a more important role in the heat budget on longer time scales. The time period covered by ECCOv4 is, however, too short to assess decadal variability in Norwegian Sea heat content. Our results furthermore highlight the importance of air-sea fluxes in generating and modifying ocean heat anomalies within the Norwegian Sea, which, at times, can mask the predictable oceanic variability. As the predictability of individual warming/cooling events is expected to vary depending on their dominant driver, heat budget diagnostics, such as those presented here, provide valuable benchmarks for assessing the skill of climate prediction models (e.g., Robson et al., 2012; Yeager et al., 2012).

Acknowledgments
The authors thank two anonymous reviewers for useful comments that improved the manuscript. This research was supported by the Research Council of Norway project PATHWAY (grant 263223), the Blue-Action project (European Union's Horizon 2020 research and innovation program, grant 727852), and the Trond Mohn Foundation (project number BFS2018TMT01). The ECCOv4 ocean state estimate is available at https://ecco.jpl.nasa.gov/products/all/ website. ERA-Interim reanalysis is available at https://www.ecmwf.int/en/forecasts/datasets/archive-datasets/reanalysis-datasets/era-interim website. Time series of Norwegian Sea heat and freshwater content and FSC temperature are available at https://ocean.ices.dk/iroc/ website. Volume transport estimates from the FSC were provided by Bee Berx, Marine Scotland, UK.

References

Årthun, M., & Eldevik, T. (2016). On anomalous ocean heat transport toward the Arctic and associated climate predictability. *Journal of Climate*, *29*(2), 689–704. https://doi.org/10.1175/JCLI-D-15-0448.1

Årthun, M., Eldevik, T., Smedsrud, L. H., Skagseth, Ø., & Ingvaldsen, R. B. (2012). Quantifying the influence of Atlantic heat on Barents sea ice variability and retreat. *Journal of Climate*, *25*(13), 4736–4743. https://doi.org/10.1175/JCLI-D-11-00466.1

Årthun, M., Eldevik, T., Viste, E., Drange, H., Furevik, T., Johnson, H. L., & Keenlyside, N. S. (2017). Skillful prediction of northern climate provided by the ocean. *Nature Communications*, *8*, 15875. https://doi.org/10.1038/ncomms15875

Barnston, A. G., & Livezey, R. E. (1987). Classification, seasonality and persistence of low-frequency atmospheric circulation patterns. *Monthly Weather Review*, *115*(6), 1083–1126. https://doi.org/10.1175/1520-0493(1987)115<1083:CSAPOL>2.0.CO;2

Berx, B., Hansen, B., Østerhus, S., Larsen, K. M., Sherwin, T., & Jochumsen, K. (2013). Combining in situ measurements and altimetry to estimate volume, heat and salt transport variability through the Faroe-Shetland Channel. *Ocean Science*, *9*(4), 639–654. https://doi.org/10.5194/os-9-639-2013

Bringedal, C., Eldevik, T., Skagseth, Ø., Spall, M. A., & Østerhus, S. (2018). Structure and forcing of observed exchanges across the Greenland-Scotland Ridge. *Journal of Climate*, *31*(24), 9881–9901. https://doi.org/10.1175/JCLI-D-17-0889.1

Broomé, S., & Nilsson, J. (2018). Shear dispersion and delayed propagation of temperature anomalies along the Norwegian Atlantic Slope Current. *Tellus A: Dynamic Meteorology and Oceanography*, *70*(1), 1453215. https://doi.org/10.1080/16000870.2018.1453215

Buckley, M. W., Ponte, R. M., Forget, G., & Heimbach, P. (2014). Low-frequency sst and upper-ocean heat content variability in the North Atlantic. *Journal of Climate*, *27*(13), 4996–5018. https://doi.org/10.1175/JCLI-D-13-00316.1

Buckley, M. W., Ponte, R. M., Forget, G., & Heimbach, P. (2015). Determining the origins of advective heat transport convergence variability in the North Atlantic. *Journal of Climate*, *28*(10), 3943–3956. https://doi.org/10.1175/JCLI-D-14-00579.1

Carton, J. A., Chepurin, G. A., Reagan, J., & Häkkinen, S. (2011). Interannual to decadal variability of Atlantic water in the Nordic and adjacent seas. *Journal of Geophysical Research*, *116*, C11035. https://doi.org/10.1029/2011JC007102

Chafik, L., Nilsson, J., Skagseth, Ø., & Lundberg, P. (2015). On the flow of Atlantic water and temperature anomalies in the Nordic Seas toward the Arctic Ocean. *Journal of Geophysical Research: Oceans*, *120*, 7897–7918. https://doi.org/10.1002/2015JC011012

Dee, D. P., Uppala, S. M., Simmons, A. J., Berrisford, P., Poli, P., Kobayashi, S., et al. (2011). The ERA-Interim reanalysis: Configuration and performance of the data assimilation system. *Quarterly Journal of the Royal Meteorological Society*, *137*(656), 553–597. https://doi.org/10.1002/qj.828

Desbruyères, D., Mercier, H., & Thierry, V. (2015). On the mechanisms behind decadal heat content changes in the eastern subpolar gyre. *Progress in Oceanography*, *132*, 262–272. https://doi.org/10.1016/J.POCEAN.2014.02.005

Dong, S., & Kelly, K. A. (2003). Heat budget in the gulf stream region: The importance of heat storage and advection. *Journal of Physical Oceanography*, *34*, 1214–1231. https://doi.org/10.1175/1520-0485(2004)034<1214:HBITGS>2.0.CO;2

Ebisuzaki, W. (1997). A method to estimate the statistical significance of a correlation when the data are serially correlated. *Journal of Climate*, *10*, 2147–2153. https://doi.org/10.1175/1520-0442(1997)010<2147:AMTETS>2.0.CO;2

Eldevik, T., Nilsen, J. E. Ø., Iovino, D., Anders Olsson, K., Sandø, A. B., & Drange, H. (2009). Observed sources and variability of Nordic seas overflow. *Nature Geoscience*, *2*(6), 406–410. https://doi.org/10.1038/ngeo518

Forget, G., Campin, J.-M, Heimbach, P., Hill, C. N., Ponte, R. M., & Wunsch, C. (2015a). ECCO version 4: An integrated framework for non-linear inverse modeling and global ocean state estimation. *Geoscientific Model Development*, *8*, 3071–3104. https://doi.org/10.5194/gmd-8-3071-2015

Forget, G., Ferreira, D., & Liang, X. (2015b). On the observability of turbulent transport rates by Argo: Supporting evidence from an inversion experiment. *Ocean Science*, *11*(5), 839–853. https://doi.org/10.5194/os-11-839-2015

Foukal, N. P., & Lozier, M. S. (2016). No inter-gyre pathway for sea-surface temperature anomalies in the North Atlantic. *Nature Communications*, *7*, 11333. https://doi.org/10.1038/ncomms11333

Foukal, N. P., & Lozier, M. S. (2017). Assessing variability in the size and strength of the North Atlantic subpolar gyre. *Journal of Geophysical Research: Oceans*, *122*, 6295–6308. https://doi.org/10.1002/2017JC012798

Foukal, N. P., & Lozier, M. S. (2018). Examining the origins of ocean heat content variability in the eastern North Atlantic subpolar gyre. *Geophysical Research Letters*, *45*, 11,275–11,283. https://doi.org/10.1029/2018GL079122

Fukumori, I., Wang, O., Fenty, I., Forget, G., Heimbach, P., & Ponte, R. M. (2017). ECCO version 4 release 3. 1721.1/110380.

Furevik, T. (2001). Annual and interannual variability of Atlantic Water temperatures in the Norwegian and Barents Seas: 1980–1996. *Deep Sea Research Part I: Oceanographic Research Papers*, *48*(2), 383–404. https://doi.org/10.1016/S0967-0637(00)00050-9

Furevik, T., & Nilsen, J. E. Ø. (2005). Large-scale atmospheric circulation variability and its impacts on the Nordic Seas Ocean Climate—A review. In H. Drange (Ed.), *The Nordic Seas: An integrated perspective, Geophysical Monograph Series* (Vol. 158, pp. 105–136). Washington, DC: American Geophysical Union. https://doi.org/10.1029/158GM09

Gent, P. R., & Mcwilliams, J. C. (1990). Isopycnal mixing in ocean circulation models. *Journal of Physical Oceanography*, *20*(1), 150–155. https://doi.org/10.1175/1520-0485(1990)020<0150:IMIOCM>2.0.CO;2

González-Pola, C., Larsen, K. M. H., Fratantoni, P., Beszczynska-Möller, A., & Hughes, S. L. (Eds.) (2018). ICES Report on Ocean Climate 2016. ICES Cooperative Research Report No. 339 (110 pp.). Copenhagen, Denmark. https://doi.org/10.17895/ices.pub.4069

Häkkinen, S., & Rhines, P. B. (2004). Decline of subpolar north atlantic circulation during the 1990s. *Science*, *304*(5670), 555–559. https://doi.org/10.1126/science.1094917

Häkkinen, S., Rhines, P. B., & Worthen, D. L. (2011). Warm and saline events embedded in the meridional circulation of the northern North Atlantic. *Journal of Geophysical Research*, *116*, C03006. https://doi.org/10.1029/2010JC006275

Hansen, B., & Østerhus, S. (2000). North Atlantic-Nordic Seas exchanges. *Progress in Oceanography*, *45*(2), 109–208. https://doi.org/10.1016/S0079-6611(99)00052-X

Hátún, H., & Chafik, L. (2018). On the recent ambiguity of the North Atlantic subpolar gyre index. *Journal of Geophysical Research: Oceans*, *123*, 5072–5076. https://doi.org/10.1029/2018JC014101

Hátún, H., Payne, M. R., Beaugrand, G., Reid, P. C., Sandø, A. B., Drange, H., et al. (2009). Large bio-geographical shifts in the north-eastern Atlantic Ocean: From the subpolar gyre, via plankton, to blue whiting and pilot whales. *Progress in Oceanography*, *80*, 149–162. https://doi.org/10.1016/j.pocean.2009.03.001

Hátún, H., Sandø, A. B., Drange, H., Hansen, B., & Valdimarsson, H. (2005). Influence of the Atlantic subpolar gyre on the thermohaline circulation. *Science*, *309*, 1841–1844. https://doi.org/10.1126/science.1114777

Heimbach, P., Hill, C., & Giering, R. (2005). An efficient exact adjoint of the parallel MIT General Circulation Model, generated via automatic differentiation. *Future Generation Computer Systems*, *21*(8), 1356–1371. https://doi.org/10.1016/J.FUTURE.2004.11.010

Hurrell, J. W. (1995). Decadal trends in the North Atlantic Oscillation: Regional temperatures and precipitation. *Science*, *269*(5224), 676–679. https://doi.org/10.1126/science.269.5224.676

Ingvaldsen, R., Loeng, H., & Asplin, L. (2002). Variability in the Atlantic inflow to the Barents Sea based on a one-year time series from moored current meters. *Continental Shelf Research*, *22*(3), 505–519. https://doi.org/10.1016/S0278-4343(01)00070-X

Isachsen, P. E., Koszalka, I., & LaCasce, J. H. (2012). Observed and modeled surface eddy heat fluxes in the eastern Nordic Seas. *Journal of Geophysical Research*, *117*, C08020. https://doi.org/10.1029/2012JC007935

Jungclaus, J. H., Lohmann, K., & Zanchettin, D. (2014). Enhanced 20th-century heat transfer to the Arctic simulated in the context of climate variations over the last millennium. *Climate of the Past*, *10*, 2201–2213. https://doi.org/10.5194/cp-10-2201-2014

Krahmann, G., Visbeck, M., & Reverdin, G. (2001). Formation and propagation of temperature anomalies along the North Atlantic Current. *Journal of Physical Oceanography*, *31*(5), 1287–1303. https://doi.org/10.1175/1520-0485(2001)031<1287:FAPOTA>2.0.CO;2

Langehaug, H. R., Matei, D., Eldevik, T., Lohmann, K., & Gao, Y. (2017). On model differences and skill in predicting sea surface temperature in the Nordic and Barents Seas. *Climate Dynamics*, *48*(3-4), 913–933. https://doi.org/10.1007/s00382-016-3118-3

Langehaug, H. R., Medhaug, I., Eldevik, T., & Otterå, O. H. (2012). Arctic/atlantic exchanges via the subpolar gyre. *Journal of Climate*, *25*(7), 2421–2439. https://doi.org/10.1175/JCLI-D-11-00085.1

Large, W., & Yeager, S. G. (2004). Diurnal to decadal global forcing for ocean and sea-ice models: The data sets and flux climatologies, (Tech. Rep.). https://doi.org/10.5065/D6KK98Q6

Lee, T., Fukumori, I., & Tang, B. (2004). Temperature advection: Internal versus External Processes. *Journal of Physical Oceanography*, *34*(8), 1936–1944. https://doi.org/10.1175/1520-0485(2004)034<1936:TAIVEP>2.0.CO;2

Lien, V. S., Gusdal, Y., & Vikebø, F. B. (2014). Along-shelf hydrographic anomalies in the Nordic Seas (1960-2011): Locally generated or advective signals? *Ocean Dynamics*, *64*(7), 1047–1059. https://doi.org/10.1007/s10236-014-0736-3

Lien, V. S., Hjøllo, S. S., Skogen, M. D., Svendsen, E., Wehde, H., Bertino, L., et al. (2016). An assessment of the added value from data assimilation on modelled Nordic Seas hydrography and ocean transports. *Ocean Modelling*, *99*, 43–59. https://doi.org/10.1016/j.ocemod.2015.12.010

Lindsay, R., Wensnahan, M., Schweiger, A., & Zhang, J. (2014). Evaluation of seven different atmospheric reanalysis products in the Arctic. *Journal of Climate*, *27*(7), 2588–2606. https://doi.org/10.1175/JCLI-D-13-00014.1

Lohmann, K., Drange, H., & Bentsen, M. (2009). A possible mechanism for the strong weakening of the North Atlantic subpolar gyre in the mid-1990s. *Geophysical Research Letters*, *36*, L15602. https://doi.org/10.1029/2009GL039166

Marshall, J., Johnson, H., & Goodman, J. (2001). A study of the interaction of the North Atlantic Oscillation with ocean circulation. *Journal of Climate*, *14*(7), 1399–1421. https://doi.org/10.1175/1520-0442(2001)014<1399:ASOTIO>2.0.CO;2

Mork, K. A., Skagseth, Ø., Ivshin, V., Ozhigin, V., Hughes, S. L., & Valdimarsson, H. (2014). Advective and atmospheric forced changes in heat and fresh water content in the Norwegian Sea, 1951–2010. *Geophysical Research Letters*, *41*, 6221–6228. https://doi.org/10.1002/2014GL061038

Mosby, H. (1962). Water, salt and the heat balance of the North Polar Sea and of the Norwegian Sea. *Geophysica Norvegica*, *24*, 289–313.

Nilsen, F., Gjevik, B., & Schauer, U. (2006). Cooling of the west spitsbergen current: Isopycnal diffusion by topographic vorticity waves. *Journal of Geophysical Research*, *111*, C08012. https://doi.org/10.1029/2005JC002991

Nurser, A. J. G., & Bacon, S. (2014). The Rossby radius in the Arctic Ocean. *Ocean Science*, *10*(6), 967–975. https://doi.org/10.5194/os-10-967-2014

Orvik, K. A., & Niiler, P. (2002). Major pathways of Atlantic water in the northern North Atlantic and Nordic Seas toward Arctic. *Geophysical Research Letters*, *29*(19), 1896. https://doi.org/10.1029/2002GL015002

Orvik, K. A., & Skagseth, Ø. (2005). Heat flux variations in the eastern Norwegian Atlantic Current toward the Arctic from moored instruments. *Geophysical Research Letters*, *32*, L14610. https://doi.org/10.1029/2005GL023487

Piecuch, C. G., & Ponte, R. M. (2012). Importance of circulation changes to atlantic heat storage rates on seasonal and interannual time scales. *Journal of Climate*, *25*(1), 350–362. https://doi.org/10.1175/JCLI-D-11-00123.1

Piecuch, C. G., Ponte, R. M., Little, C. M., Buckley, M. W., & Fukumori, I. (2017). Mechanisms underlying recent decadal changes in subpolar North Atlantic Ocean heat content. *Journal of Geophysical Research: Oceans*, *122*, 7181–7197. https://doi.org/10.1002/2017JC012845

Poulain, P.-M., Warn-Varnas, A., & Niiler, P. P. (1996). Near-surface circulation of the Nordic Seas as measured by Lagrangian drifters. *Journal of Geophysical Research*, *101*(C8), 18,237–18,258. https://doi.org/10.1029/96JC00506

Raj, R. P., Nilsen, J. E., Johannessen, J. A., Furevik, T., Andersen, O. B., & Bertino, L. (2018). Quantifying Atlantic water transport to the Nordic seas by remote sensing. *Remote Sensing of Environment*, *216*, 758–769. https://doi.org/10.1016/J.RSE.2018.04.055

Rio, M.-H., & Hernandez, F. (2003). High-frequency response of wind-driven currents measured by drifting buoys and altimetry over the world ocean. *Journal of Geophysical Research*, *108*(C8), 3283. https://doi.org/10.1029/2002JC001655

Robson, J. I., Sutton, R. T., & Smith, D. M. (2012). Initialized decadal predictions of the rapid warming of the North Atlantic Ocean in the mid 1990s. *Geophysical Research Letters*, *39*, L19713. https://doi.org/10.1029/2012GL053370

Sandø, A. B., Nilsen, J. E. Ø., Eldevik, T., & Bentsen, M. (2012). Mechanisms for variable North Atlantic-Nordic seas exchanges. *Journal of Geophysical Research*, *117*, C12006. https://doi.org/10.1029/2012JC008177

Saravanan, R., & McWilliams, J. C. (1998). Advective ocean-atmosphere interaction: An analytical stochastic model with implications for decadal variability. *Journal of Climate*, *11*(2), 165–188. https://doi.org/10.1175/1520-0442(1998)011<0165:AOAIAA>2.0.CO;2

Schauer, U., & Beszczynska-Möller, A. (2009). Problems with estimation and interpretation of oceanic heat transport–Conceptual remarks for the case of Fram Strait in the Arctic Ocean. *Ocean Science*, *5*, 487–494.

Schauer, U., Fahrbach, E., Osterhus, S., & Rohardt, G. (2004). Arctic warming through the Fram Strait: Oceanic heat transport from 3 years of measurements. *Journal of Geophysical Research*, *109*, C06026. https://doi.org/10.1029/2003JC001823

Segtnan, O. H., Furevik, T., & Jenkins, A. D. (2011). Heat and freshwater budgets of the Nordic seas computed from atmospheric reanalysis and ocean observations. *Journal of Geophysical Research*, *116*, C11003. https://doi.org/10.1029/2011JC006939

Sherwin, T. J., Williams, M. O., Turrell, W. R., Hughes, S. L., & Miller, P. I. (2006). A description and analysis of mesoscale variability in the Färoe-Shetland Channel. *Journal of Geophysical Research*, *111*, C03003. https://doi.org/10.1029/2005JC002867

Simonsen, S. K., & Haugan, P. M. (1996). Heat budgets of the Arctic Mediterranean and sea surface heat flux parameterizations for the Nordic Seas. *Journal of Geophysical Research*, *101*(15), 6553–6576. https://doi.org10.1029/95JC03305

Skagseth, Ø., Furevik, T., Ingvaldsen, R., Loeng, H., Mork, K. A., Orvik, K. A., & Ozhigin, V. (2008). Volume and heat transports to the Arctic Ocean via the Norwegian and Barents Seas, *Arctic-subarctic ocean fluxes* (pp. 45–64). Dordrecht, Netherlands: Springer. https://doi.org/10.1007/978-1-4020-6774-7_3

Sutton, R. T., & Allen, M. R. (1997). Decadal predictability of North Atlantic sea surface temperature and climate. *Nature*, *388*, 563–567. https://doi.org/:10.1038/41523

Wunsch, C., & Heimbach, P. (2007). Practical global oceanic state estimation. *Physica D*, *230*, 197–208. https://doi.org/10.1016/j.physd.2006.09.040

Yeager, S. G., Karspeck, A. R., & Danabasoglu, G. (2015). Predicted slowdown in the rate of Atlantic sea ice loss. *Geophysical Research Letters*, *42*, 704–10. https://doi.org/10.1002/2015GL065364

Yeager, S., Karspeck, A., Danabasoglu, G., Tribbia, J., & Teng, H. (2012). A decadal prediction case study: Late twentieth-century north atlantic ocean heat content. *Journal of Climate*, *25*, 5173–5189. https://doi.org/10.1175/JCLI-D-11-00595.1

Yeager, S. G., & Robson, J. I. (2017). Recent progress in understanding and predicting atlantic decadal climate variability. *Current Climate Change Reports*, *3*(2), 112–127. https://doi.org/10.1007/s40641-017-0064-z

Zhao, J., Bower, A., Yang, J., Lin, X., & Penny Holliday, N. (2018). Meridional heat transport variability induced by mesoscale processes in the subpolar North Atlantic. *Nature Communications*, *9*(1), 1124. https://doi.org/10.1038/s41467-018-03134-x

Paper III

Mechanisms underlying recent Arctic Atlantification

Asbjørnsen, H., Årthun, M., Skagseth, Ø., Eldevik, T.
Geophysical Research Letters, **47** (2020)

Geophysical Research Letters

RESEARCH LETTER
10.1029/2020GL088036

Mechanisms Underlying Recent Arctic Atlantification

Helene Asbjørnsen[1,2], Marius Årthun[1,2], Øystein Skagseth[2,3], and Tor Eldevik[1,2]

[1]Geophysical Institute, University of Bergen, Bergen, Norway, [2]Bjerknes Centre for Climate Research, Bergen, Norway, [3]Institute of Marine Research, Bergen, Norway

Key Points:
- Atlantification of the Barents Sea and Fram Strait is documented using the ECCOv4-r3 ocean state estimate
- Mechanisms driving the warming trends along Atlantic water pathways are regionally dependent and not stationary in time
- Stratification is weakened in the northern Barents Sea, but increased vertical temperature fluxes are not driving the upper-ocean warming

Supporting Information:
- Supporting Information S1

Correspondence to:
H. Asbjørnsen,
H.Asbjornsen@uib.no

Citation:
Asbjørnsen H., Årthun, M., Skagseth, Ø., & Eldevik, T. (2020). Mechanisms underlying recent Arctic Atlantification. *Geophysical Research Letters*, *47*, e2020GL088036. https://doi.org/10.1029/2020GL088036

Received 9 APR 2020
Accepted 4 JUN 2020
Accepted article online 20 JUN 2020

Abstract Recent warming and reduced sea ice concentrations in the Atlantic sector of the Arctic Ocean are the main signatures of ongoing Arctic "Atlantification." The mechanisms driving the warming trends are nevertheless still debated, particularly regarding the relative importance of oceanic and atmospheric heat fluxes. Here, heat budgets along main Atlantic water pathways through the Barents Sea and Fram Strait are constructed to investigate the mechanisms of Atlantification during 1993–2014. The largest warming trends occur south of the winter ice edge, with ocean advection as the main driver. Warming in the marginal ice zone is mainly due to low surface heat loss from the 1990s to the mid-2000s. In the ice-covered northwestern Barents Sea, ocean advection and air-sea heat fluxes act in concert to drive a gradual warming of the upper ocean. Despite a weakened stratification, no evidence is found of vertical oceanic temperature fluxes driving this upper-ocean warming.

Plain Language Summary Recent "Atlantification" of the Arctic is characterized by warmer ocean temperatures and a reduced sea ice cover. The Barents Sea is a "hot spot" for these changes, something which has broad socioeconomic and environmental impacts in the region. However, there is, at present, no complete understanding of what is causing the ocean warming. Here, we determine the relative importance of transport of heat by ocean currents (ocean advection) and heat exchanges between the atmosphere and the ocean (air-sea heat fluxes) in warming the Barents Sea and Fram Strait. In the ice-free region, ocean advection is found to be the main driver of the warming trend due to increasing inflow temperatures between 1996 and 2006. In the marginal ice zone and the ice-covered northern Barents Sea, ocean advection and air-sea heat fluxes are found to be of interchanging importance in driving the warming trend through the 1993–2014 period analyzed. A better understanding of the recent warming trends in the Barents Sea and Fram Strait has implications for how we understand the ocean's role in ongoing and future Arctic climate change.

1. Introduction

The Arctic is currently experiencing rapid climate change manifested in the ocean and cryosphere (Carmack et al., 2015), as well as in the atmosphere and on land (Elmendorf et al., 2012; Kohnemann et al., 2017). The Barents Sea is a "hot spot" for Arctic climate change (Lind et al., 2018; Schlichtholz, 2019; Skagseth et al., 2020), with pronounced upper-ocean warming and a retreating sea ice cover over the past two decades (Figures 1a and 1b). Associated changes to the surface energy budget have implications for atmospheric circulation patterns, with potential impacts outside the immediate Arctic climate system (e.g., Screen et al., 2018; Sorokina et al., 2016). Additionally, the changing environmental conditions in the region alter distribution and migration patterns of local fish communities (Fossheim et al., 2015) and reduces the habitats of ice-dependent mammals (Descamps et al., 2017).

The Barents Sea is a shallow shelf sea in the Atlantic sector of the Arctic Ocean. With a seasonal ice cover, the sea ice reaches its maximum extent in March/April and minimum in September (Signorini & McClain, 2009). Warm and saline Atlantic water enters the western Barents Sea through the Barents Sea Opening (BSO) and flows northward following two main pathways—one going east into the Central Basin before turning north and eventually exiting through the St. Anna Trough and one shorter pathway turning north along the Hopen Trench (Loeng, 1991). Additionally, the West Spitsbergen Current transports Atlantic water poleward through the Fram Strait along the west coast of Svalbard (Aagaard et al., 1987). Considerable cooling and freshening occur along these pathways—cooling in the ice-free region where the water column loses heat to the Arctic atmosphere and freshening when the Atlantic water meets the fresh surface layer in the marginal ice zone (Smedsrud et al., 2010).

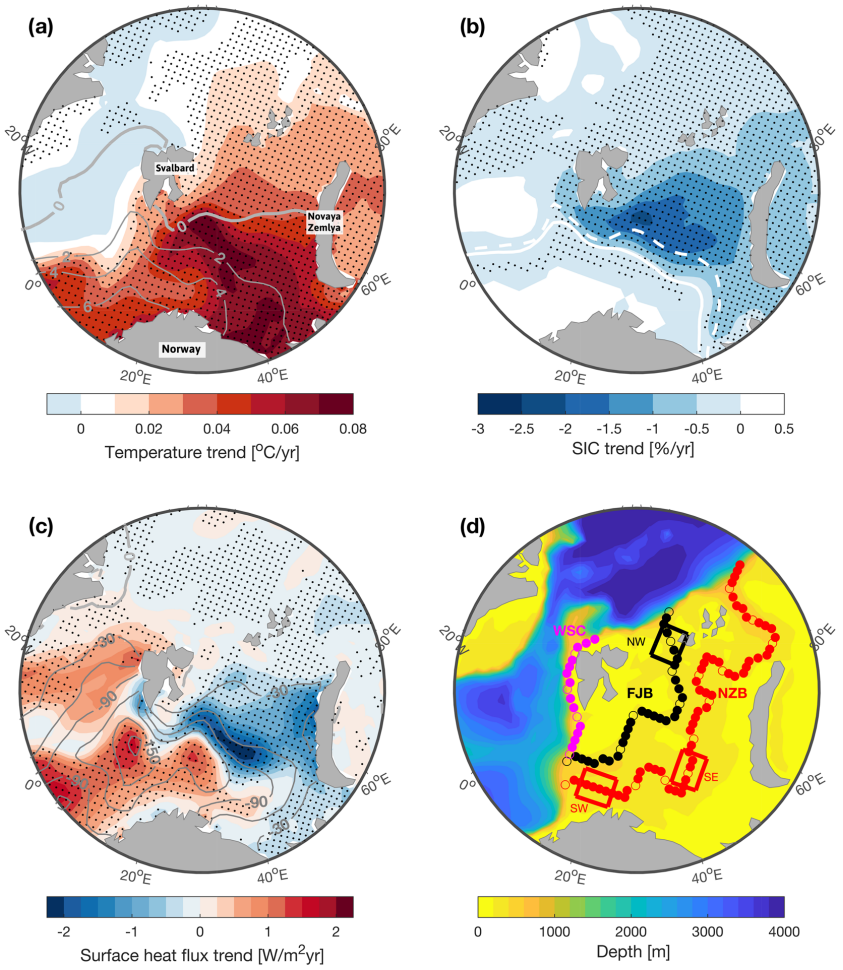

Figure 1. Linear trends over the 1993–2014 period. (a) Upper-ocean (0–100 m) temperature trend (shadings) with time mean temperature (gray contour lines: −2:2:6°C). (b) Sea ice concentration trend (shadings) with mean April ice edge (15% SIC) for 1993–2003 (solid white line) and 2004–2014 (dashed white line). (c) Net surface heat flux trend (shadings) with time mean net surface heat flux (gray contour lines: −180:30:0 W/m^2). Negative trend value indicates increased ocean heat loss (ocean cooling); positive trend value indicates reduced ocean heat loss (ocean warming). (d) Bathymetry, Atlantic water pathways, and regions defined for the heat budget analysis: Novaya Zemlya branch (NZB; red), Franz Josef branch (FJB; black), West Spitsbergen Current (WSC; magenta), southwestern box (SW), southeastern box (SE), and northwestern box (NW). Every 200 km has an open marker. Dots in (a)–(c) indicate where the trends are significant at the 95% confidence level.

With recent warming of the Atlantic water inflow and coinciding retreat of the ice cover, the increased influence of Atlantic water in the region has been termed an "Atlantification" of the Arctic Ocean (Årthun et al., 2012; Polyakov et al., 2017). This definition of Atlantification includes both Atlantic water extending further poleward and/or occupying a larger part of the water column—both resulting in a warming and salinification of the region. Different mechanisms have, however, been proposed explaining such Atlantification, and their relative importance in the overall warming of the Arctic Ocean is still debated. Changes in the strength

and properties of the inflowing Atlantic water have been shown to affect winter sea ice growth and consequently the size of the ice-free "Atlantic domain" in the Barents Sea (Årthun et al., 2012; Sandø et al., 2010). Changes in stratification, leading to an increased vertical oceanic heat flux from the submerged Atlantic water layer, have been proposed as an important mechanism for upper-ocean warming in the northwestern Barents Sea (Lind et al., 2018) and the Eurasian Basin of the Arctic Ocean (Polyakov et al., 2017). Additionally, changes in the atmospheric circulation can create oceanic heat anomalies through changes in local air-sea heat fluxes (Kim et al., 2019; Woods & Caballero, 2016).

To identify the mechanisms underlying recent Arctic Atlantification, we here present a first detailed spatio-temporal heat budget along the main poleward pathways of Atlantic water. We use the ECCO Version 4 Release 3 (referred to as ECCOv4-r3) ocean state estimate (Forget, Campin, et al., 2015; Fukumori et al., 2017), ideal for heat budget analysis due to its closed heat budget diagnostics (Asbjørnsen et al., 2019; Buckley et al., 2015; Foukal & Lozier, 2018; Piecuch et al., 2017). By quantifying the contribution of air-sea heat fluxes, and vertical and horizontal advective and diffusive oceanic temperature fluxes, we explore Barents Sea and Fram Strait warming trends in recent decades.

2. Methods

ECCOv4-r3 is an ocean state estimate of the 1992–2015 global ocean circulation and sea ice state, with a 1° nominal horizontal resolution (Forget, Campin, et al., 2015; Fukumori et al., 2017). The grid spacing in the Barents Sea region is roughly 45 km. The state estimate is generated by the ice-ocean component of the Massachusetts Institute of Technology general circulation model (MITgcm) solving the primitive equations for a time-evolving, Boussinesq, hydrostatic ocean, with solutions fitted to satellite and in situ ocean observations through the adjoint method (Heimbach et al., 2005). ERA-Interim reanalysis (Dee et al., 2011) is used as the initial near surface atmospheric state (air temperature, humidity, precipitation, downward radiation, and wind stress), while air-sea heat fluxes are calculated from bulk formulae (Large & Yeager, 2004). The long-term (1992–2015) mean turbulent heat fluxes calculated within the ECCOv4-r3 framework are consistent with ERA-Interim in both the southern (71–73°N, 20–30°E; -109 and $-102\,\mathrm{W/m^2}$, respectively) and northern Barents Sea (77–80°N, 30–40°E; $-21\,\mathrm{W/m^2}$ for both), and the interannual variability is similar ($r_{south} = 0.75$ and $r_{north} = 0.45$). The effect of unresolved eddies is parameterized as a bolus velocity (Gent & Mcwilliams, 1990). Turbulent transport parameters, such as the Gent-McWilliams bolus velocity (eddy) coefficient, are estimated within the ECCOv4-r3 framework under the constraints of observations (Forget, Campin, et al., 2015), something which greatly improves the fit to in situ profiles compared to earlier ECCO solutions (Forget, Ferreira, et al., 2015). The ECCOv4-r3 state estimate ensures closed heat, salt, and volume budgets, as the adjoint method avoids adding nonphysical source/sink terms to the model equations when constraining to observations.

The ECCOv4-r3 estimate reproduces well observed Atlantic water properties in the Nordic and Barents seas (Asbjørnsen et al., 2019; Carton et al., 2019), including temperature trends and variability in the BSO and Kola sections (supporting information Figure S2; $r_{BSO} = 0.89$ and $r_{Kola} = 0.93$). These are regions with relatively high observational data coverage (Figure S1), contributing to a well-constrained state estimate. Observations over the water column are fewer in the ice-covered regions, and satellite observations of sea ice concentration (SIC) therefore becomes a valuable constraint. Correct seasonal and interannual variability in the ice cover is, for instance, crucial for simulating stratification changes (e.g., Ellingsen et al., 2009). The comparison between observed and ECCOv4-r3 summer stratification in the northwestern Barents Sea (77–80°N, 30–40°E) is encouraging (Figure S3), with ECCOv4-r3 simulating the main features of the observed water masses: a warm and fresh surface layer, a cold and fresh Arctic layer, and a warm and saline Atlantic water layer at depth. ECCOv4-r3 nevertheless appears to be less stratified in both temperature and salinity compared to observations. However, as in observations (Figures S3a and S3b), a thinning Arctic layer is found during the 2000s (Figures S3c and S3d), in addition to a distinct surface warming and salinification over the 1993–2014 period.

The three Atlantic water pathways in Figure 1d are defined according to time mean barotropic stream function contours in ECCOv4-r3 and found to be consistent with the circulation patterns known from observations (e.g., Loeng, 1991). Following Aksenov et al. (2010), the three pathways will be referred to as the Novaya Zemlya branch (NZB), the Franz Josef branch (FJB), and the West Spitsbergen Current (WSC).

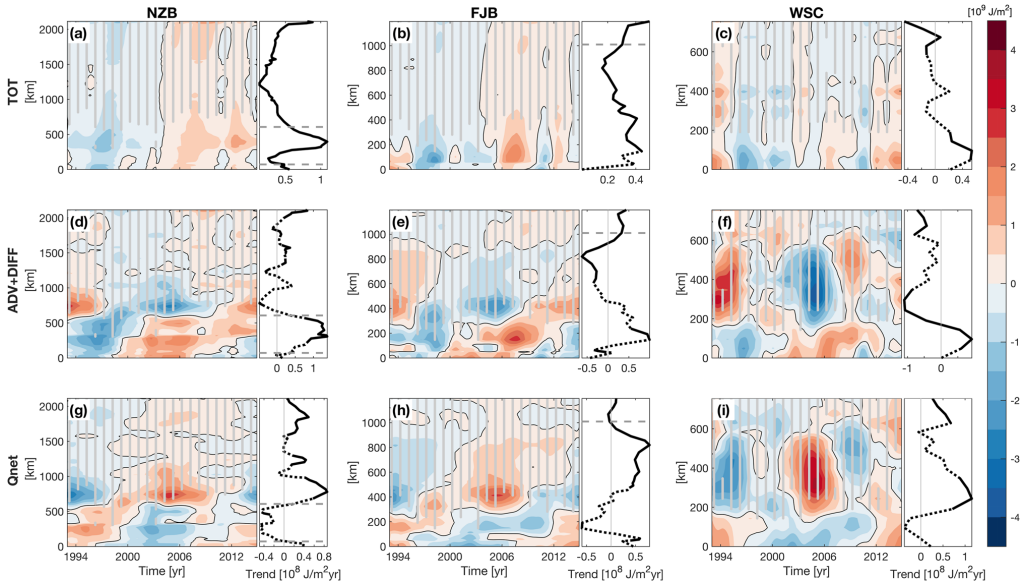

Figure 2. Along-path heat budget (full depth). (a–c) Heat content anomaly (per square meter) *TOT*. (d–f) Combined effect of advective and diffusive heat transport convergences *ADV+DIFF*. (g–i) Net air-sea heat fluxes *Qnet*. (a–i) Corresponding linear trend over the 1993–2014 period in black lines (dashed when not significant at the 95% confidence level). The center of the three boxes in Figure 1d is marked with gray horizontal dashed lines. Gray vertical lines mark areas with April sea ice concentrations higher than 15%. Note different scales on the *y* axes for the different pathways.

Start and end points of the pathways are chosen according to where the stream function contours come onto and off the continental shelf. Additionally, three boxes are defined in order to capture different regimes in the Barents Sea. The Southwestern box (SW) is located along the NZB and captures the ice-free Atlantic water inflow region. The Southeastern box (SE) is also located along the NZB but in the marginal ice zone. Finally, the Northwestern box captures the ice-covered northwest along the FJB.

The heat budget in J/m^2 is calculated by integrating the conservation of heat equation in time and depth z:

$$\underbrace{\rho_o C_p \int_t \int_z \frac{\partial \theta}{\partial t}\, dz\, dt}_{TOT} = \underbrace{\rho_o C_p \int_t \int_z \left(-\Delta \cdot \mathbf{u}\theta - \frac{\partial (w\theta)}{\partial z}\right) dz\, dt}_{ADV} + \underbrace{\rho_o C_p \int_t \int_z (-\Delta \cdot \mathbf{K})\, dz\, dt}_{DIFF} + \underbrace{\rho_o C_p \int_t \int_z Q\, dz\, dt}_{Qnet}, \quad (1)$$

where ρ_o is a reference density of seawater, C_P is the specific heat capacity, θ is potential temperature, $\mathbf{u}$ is the horizontal velocity vector, w is the vertical velocity, $\mathbf{K}$ is the three-dimensional diffusive temperature flux vector in °C m/s (from diapycnal diffusion and parameterized isopycnal diffusion), and Q is the net air-sea temperature flux in °C/s. For simplicity, the budget terms are referred to as total heat content *TOT*, advective heat transport convergence *ADV*, diffusive heat transport convergence *DIFF*, and net air-sea heat fluxes *Qnet*. The vertically integrated heat budgets displayed are time anomaly budgets, meaning that the time mean has been removed from each budget term in each horizontal grid cell after the depth integration. This implies that all budget results are relative to the mean rates of change over the study period. However, ocean heat content calculated directly from temperature shows practically the same trends and variability as *TOT* (not shown), and our interpretation and discussion of ocean heat content change and its drivers are therefore not impacted by the specific method of budget calculation used here. The along-path heat budgets (Figure 2) are integrated from the sea surface to the ocean bottom to focus on the relative roles of oceanic (*ADV+DIFF*) and atmospheric (*Qnet*) forcing on the water

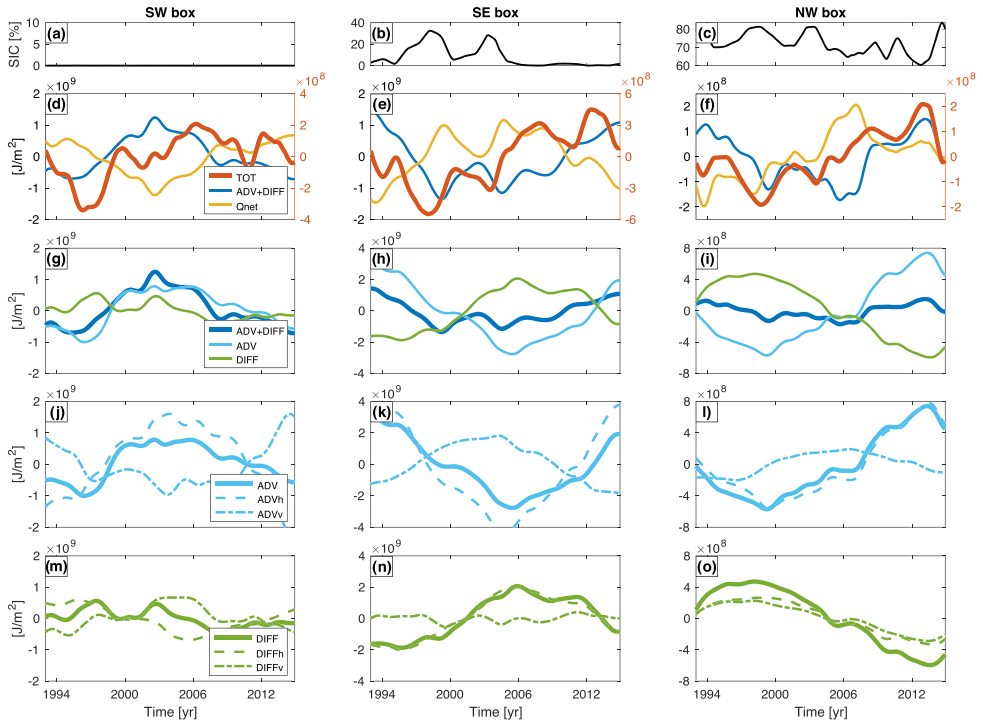

Figure 3. Upper-ocean heat budgets. (a–c) Sea ice concentration evolution in time, averaged over boxes in Figure 1d. (d–i) Heat budget (0–100 m) for boxes, with decomposition of advective heat transport convergence *ADV* (j–l) and diffusive heat transport convergence *DIFF* (m–o) into horizontal and vertical contributions. Note different scales on the *y* axes.

column, while the box heat budgets (Figure 3) are integrated over the upper 100 m in order to explore the effect of vertical advective heat transport in recent upper-ocean warming.

When diagnosing horizontal and vertical advection and diffusion (Figure 3), it is important to note that these are "temperature fluxes" relative to an arbitrary reference temperature, as the condition of zero net volume transport is not necessarily met. Here, we use 0°C as commonly used for the Barents Sea (Smedsrud et al., 2013; Wang et al., 2019). We have also calculated the temperature fluxes using the time-evolving volume-weighted temperature for the three boxes as reference temperature (Lee et al., 2004) and find that the relative contributions to *TOT* are largely unchanged.

All time series are smoothed by applying a 1-year low-pass triangular filter (24-month filter width), as we focus on interannual variability and change. The first and last 12 months of the 1992–2015 time series are removed to avoid edge effects from filtering, leaving us with the 1993–2014 time period analyzed here. Linear trends over the 1993–2014 period are calculated using the least squares method, and significance tested (95% confidence) with the modified Mann-Kendall trend test for autocorrelated data (Hamed & Rao, 1997).

3. Results and Discussion

For the Atlantic water pathways through the Barents Sea (NZB and FJB), a net warming of the water column is found along the entire pathway (Figures 2a and 2b). For the pathway through the Fram Strait (WSC), an overall warming trend is also seen in the southernmost part, although significant for only a limited part of

the pathway (Figure 2c). In the following sections we discuss the dominant mechanisms driving the warming along the three pathways according to three dynamically distinct regions: the open ocean, the marginal ice zone, and the ice-covered ocean.

3.1. Open Ocean

Because of the warm Atlantic water inflow through the BSO, the southwestern Barents Sea is ice-free, also in winter (Årthun et al., 2012; Loeng, 1991). It is also in this region the ocean climatologically loses the most heat to the Arctic atmosphere (Figure 1c), which is colder than the ocean most of the year (Smedsrud et al., 2010).

The open ocean domain is represented by the southernmost parts of the three Atlantic water pathways (Figure 2; 0–500 km along NZB, 0–250 km along FJB, and 0–150 km along WSC) and the SW box in Figure 3. As seen in Figures 2a–2c, the largest warming trends over the 1993–2014 period are found in this open ocean region. Advective and diffusive heat transport convergences (*ADV* + *DIFF*) in the 1990s and early 2000s are the main source of the overall warming (Figures 2d–2f), with an additional warming contribution from surface heat fluxes (*Qnet*) from the mid-2000s to the end of the period (Figures 2g–2i). For instance, in the open ocean domain along the NZB the mean cooling trend by *Qnet* is 23% of the mean warming trend by *ADV* + *DIFF*. The temporal evolution of the budget terms for the upper ocean (0–100 m; Figure 3) furthermore demonstrates that horizontal temperature flux convergence (*ADVh*) is the main contributor to changes in *ADV*+*DIFF* (Figures 3g and 3j; $r(ADVh, ADV + DIFF) = 0.86$). It is worth noting that *Qnet* and *ADV* + *DIFF* are strongly anticorrelated, and of opposing trends, in the open ocean domain (e.g., Figure 3d; $r = -0.97$). Often the large, but competing, budget terms leave a comparatively small heat content change. The competing budget terms reflect the opposing and close link between anomalous Atlantic heat transport and surface heat fluxes in the southern Barents Sea (Sandø et al., 2010; Smedsrud et al., 2010); for example, a warming by *ADV*+*DIFF* is followed by elevated heat loss to the atmosphere, which will be expressed in the heat budget as cooling by *Qnet*.

Horizontal advection of heat being an important driver in warming the southwestern Barents Sea is consistent with the traditional view of Atlantification by increased heat transport through the BSO (Årthun et al., 2012; Koenigk & Brodeau, 2014; Sandø et al., 2010). From observations, temperatures in the BSO have increased in recent decades, with a particular steep warming trend between 1996 and 2006 (Figure S2a). This period of enhanced warming in the BSO fits well with the period where warming of the open ocean domain in Figures 2d–2f is driven by *ADV* + *DIFF*. In a recent ocean-ice hindcast simulation the long-term trend in heat transport through the BSO is found to mainly stem from increasing ocean temperatures in the subpolar North Atlantic (Wang et al., 2019) and thus further connecting the warming of the southwestern Barents Sea to warm anomalies upstream.

Despite the Barents Sea being in a warm state, our results show a reduced ocean heat loss in the open ocean domain in recent years (Figure 1c). This particular mechanism has been highlighted in previous studies, connecting reduced regional heat loss since the mid-2000s to more southwesterly winds and consequently a warmer and more humid atmosphere (Skagseth et al., 2020; Woods & Caballero, 2016). Our heat budget confirms that reduced ocean heat loss contributes to the accumulated heat content anomaly since the mid-2000s (Figure 3d).

3.2. Marginal Ice Zone

The marginal ice zone is the transition between the open ocean and the ice-covered ocean. While there is large interannual variability in the Barents Sea ice extent and therefore the exact location of the marginal ice zone, the negative trend in SIC has led to an overall northward retreat of the ice edge (Figure 1b). As a result, the area in the vicinity of the ice edge has experienced an elevated ocean heat loss in recent years (Figure 1c).

Heat budgets from the marginal ice zone are here represented by the part of the three pathways in the proximity of the sea ice edge (Figure 2; 500–900 km along NZB, 250–500 km along FJB, and 150–400 km along WSC) and by the SE box in Figure 3. In the Barents Sea, a warming contribution from *Qnet* from the 1990s to the mid-2000s, together with a warming contribution from *ADV* + *DIFF* from the mid-2000s to the end of the period, explain the overall warming trend in the marginal ice zone. For the WSC pathway through the Fram Strait, *Qnet* also gives a warming contribution from the 1990s to the mid-2000s, but

opposing trends in *ADV+DIFF* compensate to the extent that the overall warming trend in Figure 2c is not significant in this region.

In the marginal ice zone, the trend and variability in ocean heat content is intrinsically linked to the trend and variability in the sea ice cover. The onset of the cooling contribution from *Qnet* in the southeastern Barents Sea during 2005–2014 (Figure 3e) notably coincides with the region becoming practically ice-free after 2005 (Figure 3b). The warming contribution from ADV+DIFF during the same period is due to gradually increasing temperatures of the inflowing water at the southwestern boundaries between 1998 and 2012, and the cold Arctic layer retreating out of the box as sea ice is retreating. This is consistent with the understanding of the Barents Sea as a "cooling machine," with higher ocean temperatures being damped by an increase in the open ocean area (less sea ice) and larger oceanic heat loss (Årthun et al., 2012; Smedsrud et al., 2013). However, this damping effect of the "cooling machine" has been called into question, as additional heat loss from sea ice loss will be marginal when the Barents Sea becomes increasingly ice-free in winter (Skagseth et al., 2020).

3.3. Ice-Covered Ocean

The northern Barents Sea has an Arctic climate and is ice-covered for most of the year. The hydrography is characterized by cold, fresh Arctic waters sitting on top of modified Atlantic water (e.g., Lind et al., 2018; Loeng, 1991). Although the Atlantic water is not in direct contact with the surface, also this region has experienced a warming of the upper ocean and reduced SICs over the 1993–2014 period (Figures 1a and 1b).

To assess the mechanisms responsible for warming the northern Barents Sea, we investigate heat budgets along the northernmost parts of the three pathways (Figure 2; north of 900 km along NZB, north of 500 km along FJB, and north of 400 km WSC) and for the NW box (Figure 3). The overall warming trend along NZB and FJB is in general weaker in the ice-covered domain than in the open ocean and the marginal ice zone (Figures 2a and 2b)—the very northernmost part of the pathways close to the shelf break being an exception. In contrast to the open ocean and marginal ice zone, oceanic and atmospheric forcing in the ice-covered domain are found to act in concert to drive the overall warming of the water column (Figures 2d, 2e, 2g, and 2h) and the upper ocean (Figure 3f; $r(TOT,ADV+DIFF)=0.49$, $r(TOT,Qnet)=0.56$). This regionally different behavior could result from the isolating effect of the seasonal ice cover and the more stratified water column in the northern Barents Sea, decoupling subsurface heat content anomalies from the atmosphere.

Although the Arctic layer in the northwestern Barents Sea is found to be thinning toward the end of the 1993–2014 period (Figures S3c and S3d), leading to reduced upper-ocean stratification, we find no evidence of vertical temperature fluxes from the underlying Atlantic water layer driving the upper-ocean warming (Figure 3l). Instead, horizontal temperature flux convergence (*ADVh*) largely determines changes in *ADV+DIFF* ($r = 0.64$), as for the ice-free SW box and the SE box in the marginal ice zone. For the NW box, the warming trend in *ADVh* between 1999 and 2013 is specifically explained by increasing temperatures of the inflowing water from the south and a reduced throughflow after 2006 (i.e., weaker transport of water with subzero temperatures).

Our results show an upper-ocean warming of the northern Barents Sea in line with Lind et al. (2018). However, in contrast to what is hypothesized in Lind et al. (2018), the heat budget analysis does not point to enhanced vertical mixing and increased upward fluxes as the source of the warming. We do interestingly find positive trends in vertical velocities over the 1993–2014 period in winter (Figure S4). The same dominance of *ADVh* is, however, found in January budgets as well as in August budgets for the NW box and for the larger 77–80°N, 30–40°E box (not shown). We therefore conclude that within the ECCOv4-r3 framework, vertical processes have not been a main driver of the upper-ocean warming of the Barents Sea. It is worth noting that the coarse vertical resolution (50 unevenly spaced vertical levels) means that processes related to vertical mixing are largely parameterized, and vertical transport of heat could therefore be underrepresented. However, in contrast to commonly used ocean reanalysis products, ECCOv4-r3 ensures vertical velocities and fluxes that are dynamically and kinematically consistent while constrained to available observational data (Forget, Ferreira, et al., 2015; Liang et al., 2017).

4. Summary and Conclusions

The Arctic Ocean has warmed significantly in recent decades (Figure 1a). During the 1993–2014 period analyzed here, the Barents Sea transitioned to a warmer state, with reduced SICs and Atlantic water extending further poleward in the latter half of the period compared to the first half of the period (Figures 1a and 1b). The mechanisms underlying this Atlantification have been investigated by constructing spatiotemporal heat budgets for three main Atlantic water pathways toward the Arctic Ocean basin. For the Atlantic water pathways through the Barents Sea, a significant warming of the water column is identified along the entire pathway (Figures 2a and 2b). The warming trend in the Fram Strait is, on the other hand, much less distinct and in general not significant (Figure 2c).

The heat budgets presented here reveal a complex Arctic climate system where the underlying mechanisms driving the recent Atlantification are found to be regionally dependent and not stationary in time. While the warming of the southern Barents Sea is largely due to a warming of the Atlantic water inflow between 1996 and 2006 (Figure 2a), reduced ocean heat loss to the atmosphere has also contributed to the warming trend toward the end of the 1993–2014 period. We find no evidence of vertical oceanic temperature fluxes driving the upper-ocean warming of the northwestern Barents Sea. However, increasing vertical velocities in winter over the 1993–2014 period are identified (Figure S4), which could suggest an increasingly important role for vertical oceanic temperature fluxes in the future, as the stratification is likely to weaken when the Barents Sea becomes increasingly ice-free (Onarheim & Årthun, 2017).

In this study we have focused on interannual variability and trends in ocean heat content. Seasonal variability in the Barents Sea is pronounced, for example, in Atlantic heat transport (Årthun et al., 2012), surface heat fluxes (Smedsrud et al., 2010), and sea ice cover (Signorini & McClain, 2009), and the annual budgets and associated mechanisms presented here represent the combined effect of different processes acting in different seasons. The upper-ocean warming in recent decades is nevertheless of similar magnitude in all seasons (not shown), consistent with winter temperatures determining the temperature in the Barents Sea for the rest of the year (Ottersen et al., 2000).

By presenting the first spatiotemporal heat budget for the Barents Sea and Fram Strait, our study has identified regionally different mechanisms underlying recent warming trends and thus contributes to bridge the gap and resolve previously divergent findings. As Atlantification is projected to move northeastward along the Atlantic water pathways in the future (Årthun et al., 2019), a better understanding of recent warming trends in the Barents Sea and Fram Strait has implications for how we understand the ocean's role in ongoing and future Arctic climate change.

Data Availability Statement

The ECCOv4-r3 ocean state estimate is available online (at https://ecco.jpl.nasa.gov/drive/files/Version4/Release3/). ERA-Interim reanalysis is available online (athttps://www.ecmwf.int/en/forecasts/datasets/archive-datasets/reanalysis-datasets/era-interim/). Time series of BSO and Kola temperatures are available online (at https://ocean.ices.dk/iroc/).

Acknowledgments

This study was funded by the Research Council of Norway projects PATHWAY (Grant 263223) and Nansen Legacy (Grant 276730), the Blue-Action project (European Union's Horizon 2020 research and innovation program; Grant 727852), and the Trond Mohn Foundation (Grant BFS2018TMT01). The authors thank Christopher Piecuch and one anonymous reviewer for their constructive comments that improved the manuscript.

References

Aagaard, K., Foldvik, A., & Hillman, S. R. (1987). The West Spitsbergen Current: Disposition and water mass transformation. *Journal of Geophysical Research*, *92*(C4), 3778–3784. https://doi.org/10.1029/JC092iC04p03778

Aksenov, Y., Bacon, S., Coward, A. C., & Nurser, A. J. G. (2010). The North Atlantic inflow to the Arctic Ocean: High-resolution model study. *Journal of Marine Systems*, *79*(1-2), 1–22. https://doi.org/10.1016/J.JMARSYS.2009.05.003

Årthun, M., Eldevik, T., & Smedsrud, L. H. (2019). The role of Atlantic heat transport in future Arctic winter sea ice loss. *Journal of Climate*, *32*, 3327–3341. https://doi.org/10.1175/JCLI-D-18-0750.1

Årthun, M., Eldevik, T., Smedsrud, L. H., Skagseth, O., & Ingvaldsen, R. B. (2012). Quantifying the influence of Atlantic heat on Barents Sea ice variability and retreat. *Journal of Climate*, *25*(13), 4736–4743. https://doi.org/10.1175/JCLI-D-11-00466.1

Asbjørnsen, H., Årthun, M., Skagseth, O., & Eldevik, T. (2019). Mechanisms of ocean heat anomalies in the Norwegian Sea. *Journal of Geophysical Research: Oceans*, *124*, 2908–2923. https://doi.org/10.1029/2018JC014649

Buckley, M. W., Ponte, R. M., Forget, G., & Heimbach, P. (2015). Determining the origins of advective heat transport convergence variability in the North Atlantic. *Journal of Climate*, *28*(10), 3943–3956. https://doi.org/10.1175/JCLI-D-14-00579.1

Carmack, E., Polyakov, I., Fer, I., Hunke, E., Hutchings, J., Jackson, J., et al. (2015). Toward quantifying the increasing role of oceanic heat in sea ice loss in the new Arctic. *Bulletin of the American Meteorological Society*, *96*(12), 2079–2105. https://doi.org/10.1175/BAMS-D-13-00177.1

Carton, J. A., Penny, S. G., & Kalnay, E. (2019). Temperature and salinity variability in the SODA3, ECCO4r3, and ORAS5 ocean reanalyses, 1993-2015. *Journal of Climate*, *32*(2), 2277–2293. https://doi.org/10.1175/JCLI-D-18-0605.1

Dee, D. P., Uppala, S. M., Simmons, A. J., Berrisford, P., Poli, P., Kobayashi, S., et al. (2011). The ERA-Interim reanalysis: Configuration and performance of the data assimilation system. *Quarterly Journal of the Royal Meteorological Society*, *137*(656), 553–597. https://doi.org/10.1002/qj.828

Descamps, S., Aars, J., Fuglei, E., Kovacs, K. M., Lydersen, C., Pavlova, O., et al. (2017). Climate change impacts on wildlife in a High Arctic archipelago—Svalbard, Norway. *Global Change Biology*, *23*(2), 490–502. https://doi.org/10.1111/gcb.13381

Ellingsen, I., Slagstad, D., & Sundfjord, A. (2009). Modification of water masses in the Barents Sea and its coupling to ice dynamics: A model study. *Ocean Dynamics*, *59*(6), 1095–1108. https://doi.org/10.1007/s10236-009-0230-5

Elmendorf, S. C., Henry, G. H. R., & Hollister, R. D. (2012). Plot-scale evidence of tundra vegetation change and links to recent summer warming. *Nature Climate Change*, *2*, 453–457. https://doi.org/10.1038/NCLIMATE1465

Forget, G., Campin, J.-M., Heimbach, P., Hill, C. N., Ponte, R. M., & Wunsch, C. (2015). ECCO version 4: An integrated framework for non-linear inverse modeling and global ocean state estimation. *Geoscientific Model Development*, *8*, 3071–3104. https://doi.org/10.5194/gmd-8-3071-2015

Forget, G., Ferreira, D., & Liang, X. (2015). On the observability of turbulent transport rates by Argo: Supporting evidence from an inversion experiment. *Ocean Science*, *11*(5), 839–853. https://doi.org/10.5194/os-11-839-2015

Fossheim, M., Primicerio, R., Johannesen, E., Ingvaldsen, R. B., Aschan, M. M., & Dolgov, A. V. (2015). Recent warming leads to a rapid borealization of fish communities in the Arctic. *Nature Climate Change*, *5*, 673–677. https://doi.org/10.1038/nclimate2647

Foukal, N. P., & Lozier, M. S. (2018). Examining the origins of ocean heat content variability in the eastern North Atlantic subpolar gyre. *Geophysical Research Letters*, *45*, 11,275–11,283. https://doi.org/10.1029/2018GL079122

Fukumori, I., Wang, O., Fenty, I., Forget, G., Heimbach, P., & Ponte, R. M. (2017). ECCO Version 4 Release 3.

Gent, P. R., & Mcwilliams, J. C. (1990). Isopycnal mixing in ocean circulation models. *Journal of Physical Oceanography*, *20*(1), 150–155. https://doi.org/10.1175/1520-0485(1990)020<0150:IMIOCM>2.0.CO;2

Hamed, K. H., & Rao, R. A. (1997). A modified Mann-Kendall trend test for autocorrelated data. *Journal of Hydrology*, *204*, 182–196. https://doi.org/10.1016/S0022-1694(97)00125-X

Heimbach, P., Hill, C., & Giering, R. (2005). An efficient exact adjoint of the parallel MIT General Circulation Model, generated via automatic differentiation. *Future Generation Computer Systems*, *21*(8), 1356–1371. https://doi.org/10.1016/J.FUTURE.2004.11.010

Kim, K.-Y., Kim, J.-Y., Kim, J., Yeo, S., Na, H., Hamlington, B. D., & Leben, R. R. (2019). Vertical feedback mechanism of winter Arctic amplification and sea ice loss. *Scientific Reports*, *9*, 1184. https://doi.org/10.1038/s41598-018-38109-x

Koenigk, T., & Brodeau, L. (2014). Ocean heat transport into the Arctic in the twentieth and twenty-first century in EC-Earth. *Climate Dynamics*, *42*, 3101–3120. https://doi.org/10.1007/s00382-013-1821-x

Kohnemann, S. H. E., Heinemann, G., Bromwich, D. H., & Gutjahr, O. (2017). Extreme warming in the Kara sea and Barents Sea during the winter period 2000-16. *Journal of Climate*, *30*(22), 8913–8927. https://doi.org/10.1175/JCLI-D-16-0693.1

Large, W., & Yeager, S. G. (2004). Diurnal to decadal global forcing for ocean and sea-ice models: The data sets and flux climatologies. https://doi.org/10.5065/D6KK98Q6

Lee, T., Fukumori, I., & Tang, B. (2004). Temperature advection: Internal versus external processes. *Journal of Physical Oceanography*, *34*(8), 1936–1944. https://doi.org/10.1175/1520-0485(2004)034<1936:TAIVEP>2.0.CO;2

Liang, X., Spall, M., & Wunsch, C. (2017). Global ocean vertical velocity from a dynamically consistent ocean state estimate. *Journal of Geophysical Research: Oceans*, *122*, 8208–8224. https://doi.org/10.1002/2017JC012985

Lind, S., Ingvaldsen, R. B., & Furevik, T. (2018). Arctic warming hotspot in the northern Barents Sea linked to declining sea-ice import. *Nature Climate Change*, *8*, 634–639. https://doi.org/10.1038/s41558-018-0205-y

Loeng, H. (1991). Features of the physical oceanographic conditions of the Barents Sea. *Polar Research*, *10*(1), 5–18. https://doi.org/10.3402/polar.v10i1.6723

Onarheim, I. H., & Årthun, M. (2017). Toward an ice-free Barents Sea. *Geophysical Research Letters*, *44*, 8387–8395. https://doi.org/10.1002/2017GL074304

Ottersen, G., Ådlandsvik, B., & Loeng, H. (2000). Predicting the temperature of the Barents Sea. *Fisheries Oceanography*, *9*(2), 121–135. https://doi.org/10.1046/j.1365-2419.2000.00127.x

Piecuch, C. G., Ponte, R. M., Little, C. M., Buckley, M. W., & Fukumori, I. (2017). Mechanisms underlying recent decadal changes in subpolar North Atlantic Ocean heat content. *Journal of Geophysical Research: Oceans*, *122*, 7181–7197. https://doi.org/10.1002/2017JC012845

Polyakov, I. V., Pnyushkov, A. V., Alkire, M. B., Ashik, I. M., Baumann, T. M., Carmack, E. C., et al. (2017). Greater role for Atlantic inflows on sea-ice loss in the Eurasian Basin of the Arctic Ocean. *Science*, *356*(6335), 285–291. https://doi.org/10.1126/science.aai8204

Sandø, A. B., Nilsen, J. E., Gao, Y., & Lohmann, K. (2010). Importance of heat transport and local air-sea heat fluxes for Barents Sea climate variability. *Journal of Geophysical Research*, *115*, C07013. https://doi.org/10.1029/2009JC005884

Schlichtholz, P. (2019). Subsurface ocean flywheel of coupled climate variability in the Barents Sea hotspot of global warming. *Scientific Reports*, *9*, 13,692. https://doi.org/10.1038/s41598-019-49965-6

Screen, J. A., Deser, C., Smith, D. M., Zhang, X., Blackport, R., Kushner, P. J., et al. (2018). Consistency and discrepancy in the atmospheric response to Arctic sea-ice loss across climate models. *Nature Geoscience*, *11*, 155–163. https://doi.org/10.1038/s41561-018-0059-y

Signorini, S. R., & McClain, C. R. (2009). Environmental factors controlling the Barents Sea spring-summer phytoplankton blooms. *Geophysical Research Letters*, *36*, L10604. https://doi.org/10.1029/2009GL037695

Skagseth, Ø, Eldevik, T., Årthun, M., Asbjørnsen, H., Lien, V. S., & Smedsrud, L. H. (2020). Reduced efficiency of the Barents Sea cooling machine. *Nature Climate Change*, *10*, 661–666. https://doi.org/10.1038/s41558-020-0772-6

Smedsrud, L. H., Esau, I., Ingvaldsen, R. B., Eldevik, T., Haugan, P. M., Li, C., et al. (2013). The role of the Barents Sea in the Arctic climate system. *Reviews of Geophysics*, *51*, 415–449. https://doi.org/10.1175/JCLI-D-15-0046.1

Smedsrud, L. H., Ingvaldsen, R., Nilsen, J. E., & Skagseth, O. (2010). Heat in the Barents Sea: Transport, storage, and surface fluxes. *Ocean Science*, *6*, 219–234. https://doi.org/10.5194/os-6-219-2010

Sorokina, S. A., Li, C., Wettstein, J. J., & Kvamstø, N. G. (2016). Observed atmospheric coupling between Barents Sea ice and the warm-Arctic cold-Siberian anomaly pattern. *Journal of Climate*, *29*, 495–511. https://doi.org/10.1029/2019GL083837

Wang, Q., Wang, X., Wekerle, C., Danilov, S., Jung, T., Koldunov, N., et al. (2019). Ocean heat transport into the Barents Sea: Distinct controls on the upward trend and interannual variability. *Geophysical Research Letters*, *46*, 13,180–13,190. https://doi.org/10.1029/2019GL083837

Woods, C., & Caballero, R. (2016). The role of moist intrusions in winter Arctic warming and sea ice decline. *Journal of Climate*, *29*(12), 4473–4485. https://doi.org/10.1175/JCLI-D-15-0773.1

Supporting Information for "Mechanisms underlying recent Arctic Atlantification"

Helene Asbjørnsen[1], Marius Årthun[1], Øystein Skagseth[2], Tor Eldevik[1]

[1]Geophysical Institute, University of Bergen, and Bjerknes Centre for Climate Research, Bergen, Norway

[2]Institute of Marine Research, and Bjerknes Centre for Climate Research, Bergen, Norway

Contents of this file

Figures S1, S2, S3, and S4.

Introduction

Figure S1. Map showing in situ profiles used as observational constraints in the ECCOv4-r3 ocean state estimate.

Figure S2. Comparison between observed and ECCOv4-r3 temperatures in the BSO and Kola sections.

Figure S3. Comparison between observed and ECCOv4-r3 summer hydrography in the northwestern Barents Sea.

Figure S4. Trend in vertical velocity in the northwestern Barents Sea to show the positive trend found in winter in the ice-covered region.

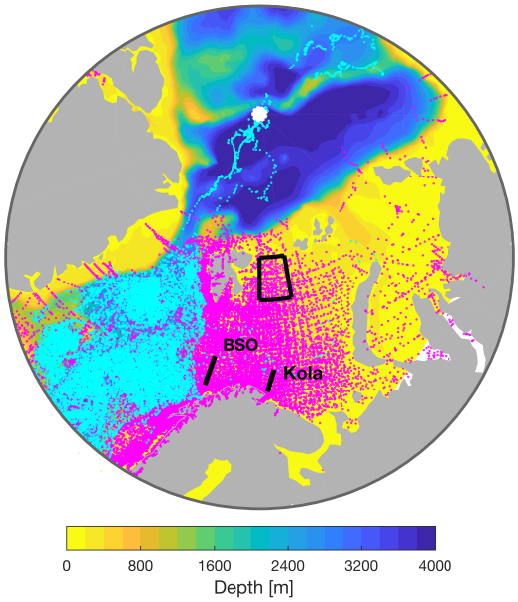

Figure S1. Bathymetry with in situ profiles used as observational constraints in the ECCOv4-r3 ocean state estimate. CTD profiles in magenta and profiles from Argo floats in turquoise. The Barents Sea Opening (BSO) and Kola sections are marked (used in Figure S2), together with the 77-80°N, 30-40°E box in the northwestern Barents Sea (used in Figure S3).

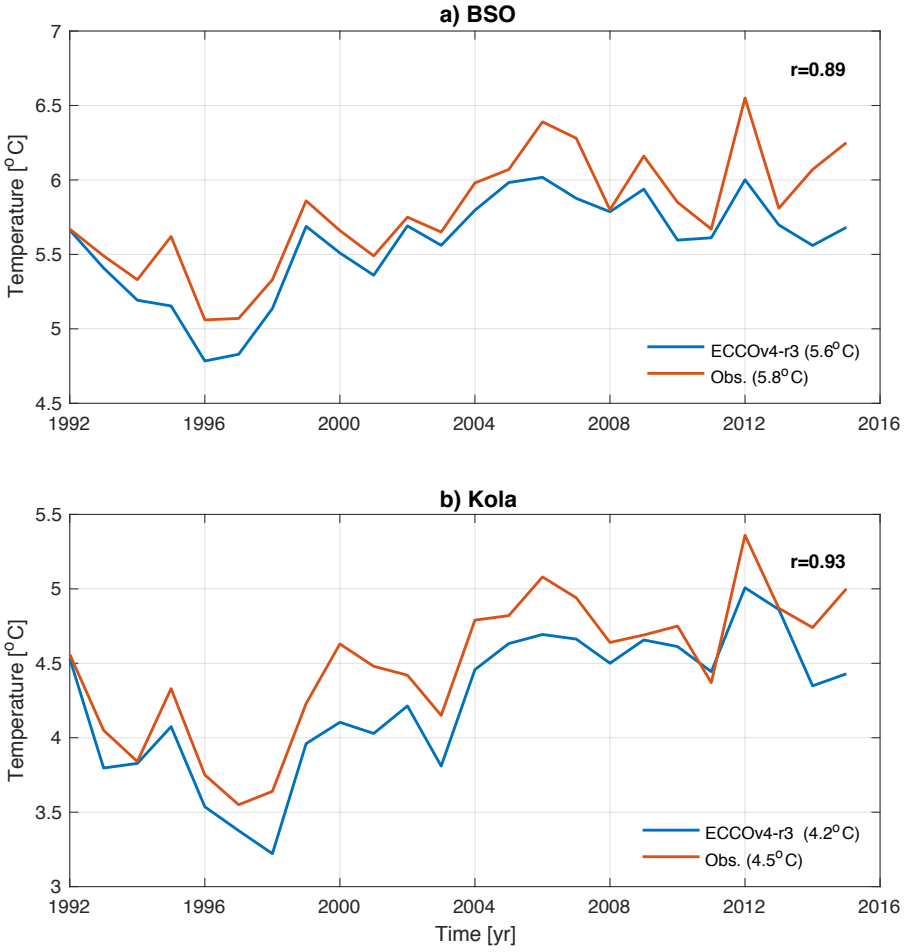

Figure S2. Comparison to observations. Annual mean temperature in the Barents Sea Opening (BSO; 50-200m) and the Kola section (0-200m) in observations (acquired from the ICES Report on Ocean Climate) and ECCOv4-r3. The time-mean temperature are noted in parentheses in the lower right-hand corner. Correlations between the respective time series are noted in the upper right-hand corner

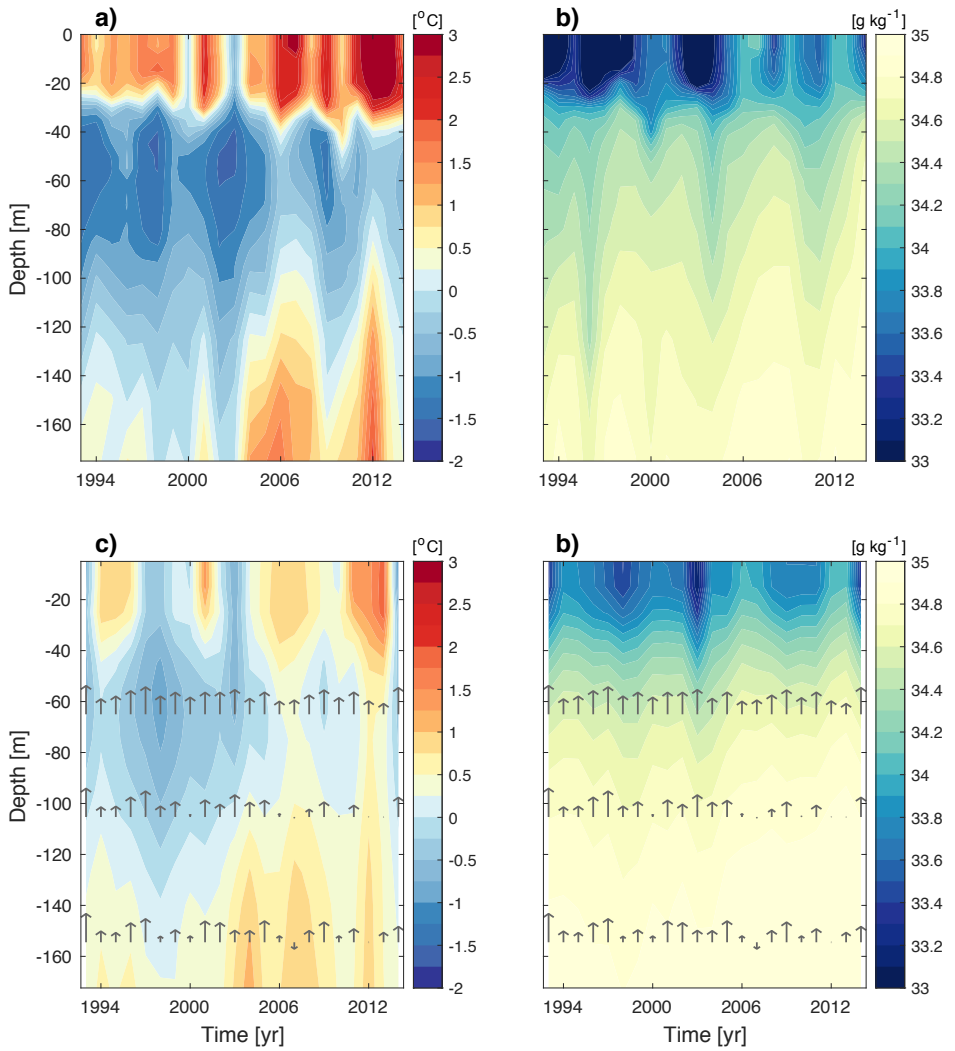

Figure S3. Summer hydrography in the northwestern Barents Sea (77-80°N, 30-40°E). September temperature and salinity in observations (a-b) and in ECCOv4-r3 (c-d). Observations are the in situ profiles going into the ECCOv4-r4 state estimate (ECCOv4 extended to 2017; available at https://ecco.jpl.nasa.gov/drive/files/Version4/Release4/input_ecco/input_insitu). September vertical velocities at 65m, 105m, and 155m depth are shown in arrows (c-d).

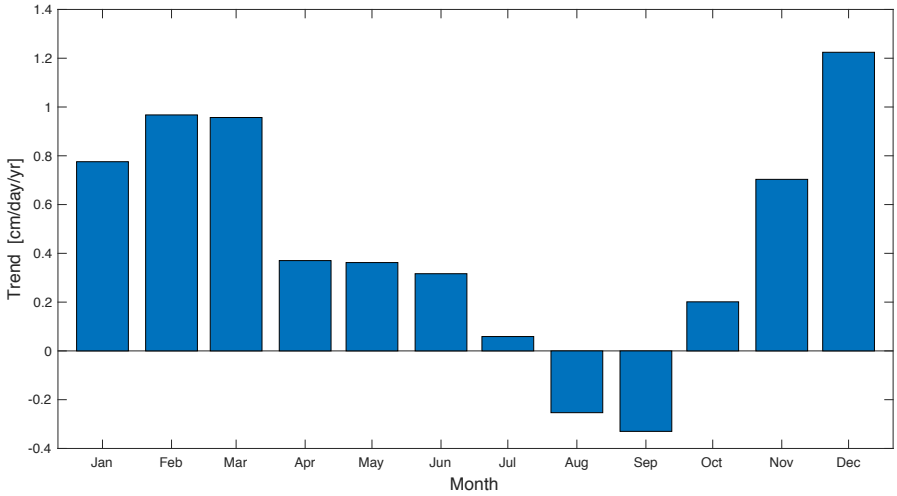

Figure S4. Trend in vertical velocity by season. Linear trend between 1993-2014 in mean vertical velocities (includes both resolved and unresolved (bolus) velocity) over the 55-95m depth layer, for the northwestern Barents Sea (77-80°N, 30-40°E).

Chapter 6

Additional contributions

Bibliography

Aagaard, K., L. Coachman, and E. Carmack (1981), On the halocline of the Arctic Ocean, *Deep Sea Research Part A. Oceanographic Research Papers*, *28*(6), 529–545, doi:10.1016/0198-0149(81)90115-1. 1.2

Årthun, M., and T. Eldevik (2016), On Anomalous Ocean Heat Transport toward the Arctic and Associated Climate Predictability, *Journal of Climate*, *29*(2), 689–704, doi:10.1175/JCLI-D-15-0448.1. 1.3

Årthun, M., T. Eldevik, L. H. Smedsrud, Ø. Skagseth, and R. B. Ingvaldsen (2012), Quantifying the Influence of Atlantic Heat on Barents Sea Ice Variability and Retreat, *Journal of Climate*, *25*(13), 4736–4743, doi:10.1175/JCLI-D-11-00466.1. 1.2

Årthun, M., T. Eldevik, E. Viste, H. Drange, T. Furevik, H. L. Johnson, and N. S. Keenlyside (2017), Skillful prediction of northern climate provided by the ocean, *Nature Communications*, *8*, doi:10.1038/ncomms15875. 2.1, 4

Årthun, M., B. Bogstad, U. Daewel, N. S. Keenlyside, A. B. Sandø, C. Schrum, and G. Ottersen (2018a), Climate based multi-year predictions of the Barents Sea cod stock, *PLOS ONE*, *13*(10), doi:10.1371/journal.pone.0206319. 1.3

Årthun, M., E. W. Kolstad, T. Eldevik, and N. S. Keenlyside (2018b), Time Scales and Sources of European Temperature Variability, *Geophysical Research Letters*, *45*(8), 3597–3604, doi:10.1002/2018GL077401. 1.3

Årthun, M., T. Eldevik, and L. H. Smedsrud (2019), The Role of Atlantic Heat Transport in Future Arctic Winter Sea Ice Loss, *Journal of Climate*, *32*(11), 3327–3341, doi:10.1175/JCLI-D-18-0750.1. 1.2

Barnier, B., G. Madec, T. Penduff, J.-M. Molines, A.-M. Treguier, J. Le Sommer, A. Beckmann, A. Biastoch, C. Böning, J. Dengg, C. Derval, E. Durand, S. Gulev, E. Remy, C. Talandier, S. Theetten, M. Maltrud, J. McClean, and B. De Cuevas (2006), Impact of partial steps and momentum advection schemes in a global ocean circulation model at eddy-permitting resolution, *Ocean Dynamics*, *56*, 543–567, doi:10.1007/s10236-006-0082-1. 2.2.1

Bersch, M. (2002), North Atlantic Oscillation-induced changes of the upper layer circulation in the northern North Atlantic Ocean, *Journal of Geophysical Research*, *107*(C10), doi:10.1029/2001JC000901. 1.3

Berx, B., B. Hansen, S. Østerhus, K. M. Larsen, T. Sherwin, and K. Jochumsen (2013), Combining in situ measurements and altimetry to estimate volume, heat and

salt transport variability through the Faroe-Shetland Channel, *Ocean Science*, *9*(4), 639–654, doi:10.5194/os-9-639-2013. 4

Blanke, B., and S. Raynaud (1997), Kinematics of the Pacific Equatorial Undercurrent: An Eulerian and Lagrangian Approach from GCM Results, *Journal of physical oceanography*, *27*(6), 1038–1053, doi:10.1175/1520-0485(1997)027<1038:KOTPEU>2.0.CO;2. 2.2.2

Bosse, A., and I. Fer (2019), Mean Structure and Seasonality of the Norwegian Atlantic Front Current Along the Mohn Ridge From Repeated Glider Transects, *Geophysical Research Letters*, *46*(22), 13,170–13,179, doi:10.1029/2019GL084723. 1.2

Bouillon, S., M. Morales Maqueda, V. Legat, and T. Fichefet (2009), An elastic-viscous-plastic sea ice model formulated on Arakawa B and C grids, *Ocean Modelling*, *27*(3-4), 174–184, doi:10.1016/J.OCEMOD.2009.01.004. 2.2.1

Bringedal, C., T. Eldevik, Ø. Skagseth, M. A. Spall, and S. Østerhus (2018), Structure and Forcing of Observed Exchanges across the Greenland-Scotland Ridge, *Journal of Climate*, *31*(24), 9881–9901, doi:10.1175/JCLI-D-17-0889.1. 1.2

Broome, S., L. Chafik, and J. Nilsson (2019), Mechanisms of the time-varying sea surface height and heat content trends in the eastern Nordic Seas, *Ocean Science*, *16*, 715–728, doi:10.5194/os-2019-109. 1.3, 4

Buckley, M. W., and J. Marshall (2016), Observations, inferences, and mechanisms of the Atlantic Meridional Overturning Circulation: A review, *Reviews of Geophysics*, *54*(1), 5–63, doi:10.1002/2015RG000493. 1.1

Buckley, M. W., R. M. Ponte, G. Forget, and P. Heimbach (2014), Low-Frequency SST and Upper-Ocean Heat Content Variability in the North Atlantic, *Journal of Climate*, *27*(13), 4996–5018, doi:10.1175/JCLI-D-13-00316.1. 2.2.3

Buckley, M. W., R. M. Ponte, G. Forget, and P. Heimbach (2015), Determining the Origins of Advective Heat Transport Convergence Variability in the North Atlantic, *Journal of Climate*, *28*(10), 3943–3956, doi:10.1175/JCLI-D-14-00579.1. 1.3, 2.2.3

Burgard, C., and D. Notz (2017), Drivers of Arctic Ocean warming in CMIP5 models, *Geophysical Research Letters*, *44*(9), 4263–4271, doi:10.1002/2016GL072342. 1.2

Carmack, b. E., I. Polyakov, I. Fer, E. Hunke, J. Hutchings, J. Jackson, C. Layton, H. Melling, D. Perovich, O. Persson, B. Ruddick, M.-L. Timmermans, J. Toole, T. Ross, S. Vavrus, and P. Winsor (2015), Toward quantifying the increasing role of oceanic heat in sea ice loss in the new Arctic, *Bulletin of the American Meteorological Society*, *96*(12), 2079–2105, doi:10.1175/BAMS-D-13-00177.1. 1.2, 4

Carton, J. A., G. A. Chepurin, J. Reagan, and S. Häkkinen (2011), Interannual to decadal variability of Atlantic Water in the Nordic and adjacent seas, *Journal of Geophysical Research*, *116*(C11), doi:10.1029/2011JC007102. 1.3, 2.2.3

Carton, J. A., G. A. Chepurin, and L. Chen (2018), SODA3: A New Ocean Climate Reanalysis, *Journal of Climate*, *31*(17), 6967–6983, doi:10.1175/JCLI-D-18-0149.1. 2.2.3

Chafik, L., J. Nilsson, Ø. Skagseth, and P. Lundberg (2015), On the flow of Atlantic water and temperature anomalies in the Nordic Seas toward the Arctic Ocean, *Journal of Geophysical Research: Oceans*, *120*(12), 7897–7918, doi:10.1002/2015JC011012. 1.2

Chaudhuri, A. H., R. M. Ponte, G. Forget, and P. Heimbach (2013), A Comparison of Atmospheric Reanalysis Surface Products over the Ocean and Implications for Uncertainties in Air-Sea Boundary Forcing, *Journal of Climate*, *26*, 153–170, doi: 10.1175/JCLI-D-12-00090.1. 2.2

Chepurin, G. A., and J. A. Carton (2012), Subarctic and Arctic sea surface temperature and its relation to ocean heat content 1982-2010, *Journal of Geophysical Research: Oceans*, *117*(C6), doi:10.1029/2011JC007770. 1.3, 4

Daniault, N., H. Mercier, P. Lherminier, A. Sarafanov, A. Falina, P. Zunino, F. F. Pérez, A. F. Ríos, B. Ferron, T. Huck, V. Thierry, and S. Gladyshev (2016), The northern North Atlantic Ocean mean circulation in the early 21st century, *Progress in Oceanography*, *146*, 142–158, doi:10.1016/J.POCEAN.2016.06.007. 1.2

Dee, D. P., S. M. Uppala, A. J. Simmons, P. Berrisford, P. Poli, S. Kobayashi, U. Andrae, M. A. Balmaseda, G. Balsamo, P. Bauer, P. Bechtold, A. C. M. Beljaars, L. van de Berg, J. Bidlot, N. Bormann, C. Delsol, R. Dragani, M. Fuentes, A. J. Geer, L. Haimberger, S. B. Healy, H. Hersbach, E. V. Hólm, L. Isaksen, P. Kållberg, M. Köhler, M. Matricardi, A. P. McNally, B. M. Monge-Sanz, J.-J. Morcrette, B.-K. Park, C. Peubey, P. de Rosnay, C. Tavolato, J.-N. Thépaut, and F. Vitart (2011), The ERA-Interim reanalysis: configuration and performance of the data assimilation system, *Quarterly Journal of the Royal Meteorological Society*, *137*(656), 553–597, doi:10.1002/qj.828. 2.2.1, 2.2.3

Deser, C., and M. L. Blackmon (1993), Surface Climate Variations over the North Atlantic Ocean during winter: 1900-1989, *Journal of Climate*, *6*(9), 1743–1753, doi: 10.1175/1520-0442(1993)006<1743:SCVOTN>2.0.CO;2. 1.3

Döös, K. (1995), Interocean exchange of water masses, *Journal of Geophysical Research*, *100*, 13,499–13,514, doi:10.1029/95JC00337. 2.2.2

Dussin, R., B. Barnier, L. Brodeau, and J. M. Molines (2016), The making of the DRAKKAR forcing set DFS5, *Tech. rep.*, Laboratoire de Glaciologie et Géophysique de l'Environnement, Grenoble, url: https://www.drakkar-ocean.eu/publications/reports/report_DFS5v3_April2016.pdf. 2.2.1

Ekman, V. W. (1905), On the influence of the Earth's rotation on ocean currents, *Arch. Math. Astron. Phys.*, *2*(11), 1–52. 1.1

Eldevik, T., J. E. Ø. Nilsen, D. Iovino, K. Anders Olsson, A. B. Sandø, and H. Drange (2009), Observed sources and variability of Nordic seas overflow, *Nature Geoscience*, *2*(6), 406–410, doi:10.1038/ngeo518. 1.2

Fasullo, J. T., and K. E. Trenberth (2008), The Annual Cycle of the Energy Budget. Part II: Meridional Structures and Poleward Transports, *Journal of Climate*, *21*(10), 2313–2325, doi:10.1175/2007JCLI1936.1. 1.1

Fer, I. (2009), Weak Vertical Diffusion Allows Maintenance of Cold Halocline in the Central Arctic, *Atmospheric and Oceanic Science Letters*, *2*(3), 148–152, doi:10.1080/16742834.2009.11446789. 1.2

Forget, G., J.-M. Campin, P. Heimbach, C. N. Hill, R. M. Ponte, and C. Wunsch (2015a), ECCO version 4: an integrated framework for non-linear inverse modeling and global ocean state estimation, *Geoscientific Model Development*, *8*, 3071–3104, doi:10.5194/gmd-8-3071-2015. 2.2.3, 2.2

Forget, G., D. Ferreira, and X. Liang (2015b), On the observability of turbulent transport rates by Argo: supporting evidence from an inversion experiment, *Ocean Science*, *11*(5), 839–853, doi:10.5194/os-11-839-2015. 2.2.3

Fossheim, M., R. Primicerio, E. Johannesen, R. B. Ingvaldsen, M. M. Aschan, and A. V. Dolgov (2015), Recent warming leads to a rapid borealization of fish communities in the Arctic, *Nature Climate Change*, *5*, 673–677, doi:10.1038/nclimate2647. 1.3

Foukal, N. P., and M. S. Lozier (2017), Assessing variability in the size and strength of the North Atlantic subpolar gyre, *Journal of Geophysical Research: Oceans*, *122*(8), 6295–6308, doi:10.1002/2017JC012798. 1.3, 4

Fox-Kemper, B., A. Adcroft, C. W. Böning, E. P. Chassignet, E. Curchitser, G. Danabasoglu, C. Eden, M. H. England, R. Gerdes, R. J. Greatbatch, S. M. Griffies, R. W. Hallberg, E. Hanert, P. Heimbach, H. T. Hewitt, C. N. Hill, Y. Komuro, S. Legg, J. Le Sommer, S. Masina, S. J. Marsland, S. G. Penny, F. Qiao, T. D. Ringler, A. M. Treguier, H. Tsujino, P. Uotila, and S. G. Yeager (2019), Challenges and Prospects in Ocean Circulation Models, *Frontiers in Marine Science*, *6*, 65, doi:10.3389/fmars.2019.00065. 2.2

Frajka-Williams, E., I. J. Ansorge, J. Baehr, H. L. Bryden, M. P. Chidichimo, S. A. Cunningham, G. Danabasoglu, S. Dong, K. A. Donohue, S. Elipot, P. Heimbach, N. P. Holliday, R. Hummels, L. C. Jackson, J. Karstensen, M. Lankhorst, I. A. Le Bras, M. S. Lozier, E. L. McDonagh, C. S. Meinen, H. Mercier, B. I. Moat, R. C. Perez, C. G. Piecuch, M. Rhein, M. A. Srokosz, K. E. Trenberth, S. Bacon, G. Forget, G. Goni, D. Kieke, J. Koelling, T. Lamont, G. D. McCarthy, C. Mertens, U. Send, D. A. Smeed, S. Speich, M. van den Berg, D. Volkov, and C. Wilson (2019), Atlantic Meridional Overturning Circulation: Observed Transport and Variability, *Frontiers in Marine Science*, *6*, 260, doi:10.3389/fmars.2019.00260. 1.1

Fukumori, I., O. Wang, I. Fenty, G. Forget, P. Heimbach, and R. M. Ponte (2017), ECCO Version 4 Release 3, *Tech. rep.*, MIT, Massachusetts, url: http://hdl.handle.net/1721.1/110380. 2.2.3

Furevik, T. (2001), Annual and interannual variability of Atlantic Water temperatures in the Norwegian and Barents Seas: 1980-1996, *Deep Sea Research Part I: Oceanographic Research Papers*, *48*(2), 383–404, doi:10.1016/S0967-0637(00)00050-9. 1.2, 1.3

Grégorio, S., T. Penduff, G. Sérazin, J.-M. Molines, B. Barnier, and J. Hirschi (2015), Intrinsic Variability of the Atlantic Meridional Overturning Circulation at

Interannual-to-Multidecadal Time Scales, *Journal of Physical Oceanography*, *45*, 1929–1946, doi:10.1175/JPO-D-14-0163.1. 2.2.1

Häkkinen, S., P. B. Rhines, and D. L. Worthen (2011), Warm and saline events embedded in the meridional circulation of the northern North Atlantic, *Journal of Geophysical Research*, *116*(C3), doi:10.1029/2010JC006275. 1.3, 4

Hansen, B., and S. Østerhus (2000), North Atlantic-Nordic Seas exchanges, *Progress in Oceanography*, *45*(2), 109–208, doi:10.1016/S0079-6611(99)00052-X. 1.2

Hansen, B., S. Østerhus, W. R. Turrell, S. Jónsson, H. Valdimarsson, H. Hátún, and S. M. Olsen (2008), The Inflow of Atlantic Water, Heat, and Salt to the Nordic Seas Across the Greenland-Scotland Ridge, in *Arctic-Subarctic Ocean Fluxes*, edited by Robert R. Dickson, Jens Meincke, and Peter Rhines, chap. 1, pp. 15–43, Springer Netherlands, doi:10.1007/978-1-4020-6774-7. 1.2

Hátún, H., and L. Chafik (2018), On the Recent Ambiguity of the North Atlantic Subpolar Gyre Index, *Journal of Geophysical Research: Oceans*, *123*(8), 5072–5076, doi:10.1029/2018JC014101. 1.3, 4

Hátún, H., A. B. Sandø, H. Drange, B. Hansen, and H. Valdimarsson (2005), Influence of the Atlantic Subpolar Gyre on the Thermohaline Circulation, *Science*, *309*, 1841–1844, doi:10.1126/science.1114777. 1.3

Hátún, H., K. Lohmann, D. Matei, J. Jungclaus, S. Pacariz, M. Bersch, A. Gislason, J. Ólafsson, and P. Reid (2016), An inflated subpolar gyre blows life toward the northeastern Atlantic, *Progress in Oceanography*, *147*, 49–66, doi:10.1016/J.POCEAN.2016.07.009. 1.3

Heimbach, P., C. Hill, and R. Giering (2005), An efficient exact adjoint of the parallel MIT General Circulation Model, generated via automatic differentiation, *Future Generation Computer Systems*, *21*(8), 1356–1371, doi:10.1016/J.FUTURE.2004.11.010. 2.2.3

Heimbach, P., I. Fukumori, C. N. Hill, R. M. Ponte, D. Stammer, C. Wunsch, J.-M. Campin, B. Cornuelle, I. Fenty, G. Forget, A. Köhl, M. Mazloff, D. Menemenlis, A. T. Nguyen, C. Piecuch, D. Trossman, A. Verdy, O. Wang, and H. Zhang (2019), Putting It All Together: Adding Value to the Global Ocean and Climate Observing Systems With Complete Self-Consistent Ocean State and Parameter Estimates, *Frontiers in Marine Science*, *6*, 55, doi:10.3389/fmars.2019.00055. 1.3, 4

Helland-Hansen, B., and F. Nansen (1909), The Norwegian Sea, *Fiskdir. Skr. Ser. Havunders*, *11*(2), 1–360. 1.1

Hogg, N. G. (1992), On the transport of the Gulf Stream between Cape Hatteras and the Grand Banks, *Deep Sea Research Part A. Oceanographic Research Papers*, *39*(7-8), 1231–1246, doi:10.1016/0198-0149(92)90066-3. 1.2

Holliday, N. P., S. L. Hughes, S. Bacon, A. Beszczynska-Möller, B. Hansen, A. Lavín, H. Loeng, K. A. Mork, S. Østerhus, T. Sherwin, and W. Walczowski (2008), Reversal

of the 1960s to 1990s freshening trend in the northeast North Atlantic and Nordic Seas, *Geophysical Research Letters*, *35*(3), doi:10.1029/2007GL032675. 1.3

Holliday, N. P., M. Bersch, B. Berx, L. Chafik, S. Cunningham, C. Florindo-López, H. Hátún, W. Johns, S. A. Josey, K. M. H. Larsen, S. Mulet, M. Oltmanns, G. Reverdin, T. Rossby, V. Thierry, H. Valdimarsson, and I. Yashayaev (2020), Ocean circulation causes the largest freshening event for 120 years in eastern subpolar North Atlantic, *Nature Communications*, *11*(1), 585, doi:10.1038/s41467-020-14474-y. 1.3

Hurrell, J. W. (1995), Decadal Trends in the North Atlantic Oscillation: Regional Temperatures and Precipitation, *Science*, *269*(5224), 676–679, doi:10.1126/science.269.5224.676. 1.3

Keenlyside, N. S., M. Latif, J. Jungclaus, L. Kornblueh, and E. Roeckner (2008), Advancing decadal-scale climate prediction in the North Atlantic sector, *Nature Geoscience*, *453*, 84–88, doi:10.1038/nature06921. 1.3

Koul, V., J.-E. Tesdal, M. Bersch, H. Hátún, S. Brune, L. Borchert, H. Haak, C. Schrum, and J. Baehr (2020), Unraveling the choice of the north Atlantic subpolar gyre index, *Scientific Reports*, *10*(1), 1005, doi:10.1038/s41598-020-57790-5. 1.3, 4

Krahmann, G., M. Visbeck, and G. Reverdin (2001), Formation and Propagation of Temperature Anomalies along the North Atlantic Current, *Journal of Physical Oceanography*, *31*(5), 1287–1303, doi:10.1175/1520-0485(2001)031<1287:FAPOTA>2.0.CO;2. 1.3

Kushnir, Y. (1994), Interdecadal Variations in North Atlantic Sea Surface Temperatures and Associated Atmospheric Conditions, *Journal of Climate*, *7*, 141–157, doi:10.1175/1520-0442(1994)007<0141:IVINAS>2.0.CO;2. 1.3

Lambert, E., T. Eldevik, and P. M. Haugan (2016), How northern freshwater input can stabilise thermohaline circulation, *Tellus*, *68*, doi:10.3402/tellusa.v68.31051. 1.1

Langehaug, H. R., A. B. Sandø, M. Årthun, and M. Ilcak (2019), Variability along the Atlantic water pathway in the forced Norwegian Earth System Model, *Climate Dynamics*, *52*, 1211–1230, doi:10.1007/s00382-018-4184-5. 1.3

Large, W., and S. G. Yeager (2004), Diurnal to Decadal Global Forcing for Ocean and Sea-Ice Models: The Data Sets and Flux Climatologies, *Tech. rep.*, NCAR, Boulder, Colorado, doi:10.5065/D6KK98Q6. 2.2.3

Lind, S., R. B. Ingvaldsen, and T. Furevik (2018), Arctic warming hotspot in the northern Barents Sea linked to declining sea-ice import, *Nature Climate Change*, *8*, 634–639, doi:10.1038/s41558-018-0205-y. 1.2, 4

Lique, C., A. M. Treguier, B. Blanke, and N. Grima (2010), On the origins of water masses exported along both sides of Greenland: A Lagrangian model analysis, *Journal of Geophysical Research*, *115*(C5), doi:10.1029/2009JC005316. 2.2.2

Loeng, H. (1991), Features of the physical oceanographic conditions of the Barents Sea, *Polar Research*, *10*(1), 5–18, doi:10.3402/polar.v10i1.6723. 1.2

Lozier, M. S., F. Li, S. Bacon, F. Bahr, A. S. Bower, S. A. Cunningham, M. F. de Jong, L. de Steur, B. deYoung, J. Fischer, S. F. Gary, B. J. W. Greenan, N. P. Holliday, A. Houk, L. Houpert, M. E. Inall, W. E. Johns, H. L. Johnson, C. Johnson, J. Karstensen, G. Koman, I. A. Le Bras, X. Lin, N. Mackay, D. P. Marshall, H. Mercier, M. Oltmanns, R. S. Pickart, A. L. Ramsey, D. Rayner, F. Straneo, V. Thierry, D. J. Torres, R. G. Williams, C. Wilson, J. Yang, I. Yashayaev, and J. Zhao (2019), A sea change in our view of overturning in the subpolar North Atlantic., *Science*, *363*(6426), 516–521, doi:10.1126/science.aau6592. 4

Lozier, S. M., S. Leadbetter, R. G. Williams, V. Roussenov, M. S. C. Reed, and N. J. Moore (2008), The Spatial Pattern and Mechanisms of Heat-Content Change in the North Atlantic, *Science*, *319*, 800–803, doi:10.1126/science.1146436. 1.3

Madec, G. (2015), *NEMO ocean engine*, Note du Pôle de modélisation, Institut Pierre-Simon Laplace, France, No 27, ISSN No 1288-1619. 2.2.1

Marshall, J., H. Johnson, and J. Goodman (2001), A Study of the Interaction of the North Atlantic Oscillation with Ocean Circulation, *Journal of Climate*, *14*(7), 1399–1421, doi:10.1175/1520-0442(2001)014<1399:ASOTIO>2.0.CO;2. 1.3

McWilliams, J. C. (1996), Modeling the Oceanic General Circulation, *Annual Review of Fluid Mechanics*, *28*(1), 215–248, doi:10.1146/annurev.fl.28.010196.001243. 2.2

Mork, K. A., Ø. Skagseth, V. Ivshin, V. Ozhigin, S. L. Hughes, and H. Valdimarsson (2014), Advective and atmospheric forced changes in heat and fresh water content in the Norwegian Sea, 1951-2010, *Geophysical Research Letters*, *41*(17), 6221–6228, doi:10.1002/2014GL061038. 1.3, 2.2.3

Mork, K. A., Ø. Skagseth, and H. Søiland (2019), Recent Warming and Freshening of the Norwegian Sea Observed by Argo Data, *Journal of Climate*, *32*(12), 3695–3705, doi:10.1175/JCLI-D-18-0591.1. 1.3, 4

Nguyen, A. T., V. Ocaña, V. Garg, P. Heimbach, J. M. Toole, R. A. Krishfield, and C. M. Lee (2017), On the Benefit of current and future ALPS data for improving Arctic coupled ocean-sea ice state estimation, *Oceanography*, *30*(2), 69–73, doi:10.5670/oceanog.2017.223. 4

Onarheim, I. H., and M. Årthun (2017), Toward an ice-free Barents Sea, *Geophysical Research Letters*, *44*(16), 8387–8395, doi:10.1002/2017GL074304. 1.2

Onarheim, I. H., T. Eldevik, M. Årthun, R. B. Ingvaldsen, and L. H. Smedsrud (2015), Skillful prediction of Barents Sea ice cover, *Geophysical Research Letters*, *42*(13), 5364–5371, doi:10.1002/2015GL064359. 1.2, 1.3, 2.1

Onarheim, I. H., T. Eldevik, L. H. Smedsrud, and J. C. Stroeve (2018), Seasonal and Regional Manifestation of Arctic Sea Ice Loss, *Journal of Climate*, *31*(12), 4917–4932, doi:10.1175/JCLI-D-17-0427.1. 1.2, 4

Orvik, K. A., and P. Niiler (2002), Major pathways of Atlantic water in the northern North Atlantic and Nordic Seas toward Arctic, *Geophysical Research Letters*, *29*(19), 1896, doi:10.1029/2002GL015002. 1.2

Orvik, K. A., and Ø. Skagseth (2005), Heat flux variations in the eastern Norwegian Atlantic Current toward the Arctic from moored instruments, 1995-2005, *Geophysical Research Letters*, *32*, L14,610, doi:10.1029/2005GL023487. 4

Orvik, K. A., and Skagseth (2003), Monitoring the Norwegian Atlantic slope current using a single moored current meter, *Continental Shelf Research*, *23*(2), 159–176, doi:10.1016/S0278-4343(02)00172-3. 1.2, 4

Østerhus, S., R. Woodgate, H. Valdimarsson, B. Turrell, L. de Steur, D. Quadfasel, S. M. Olsen, M. Moritz, C. M. Lee, K. M. H. Larsen, S. Jónsson, C. Johnson, K. Jochumsen, B. Hansen, B. Curry, S. Cunningham, and B. Berx (2019), Arctic Mediterranean Exchanges: A consistent volume budget and trends in transports from two decades of observations, *Ocean Science*, *15*, 379–399, doi:10.5194/os-15-379-2019. 1.2

Palter, J. B. (2015), The Role of the Gulf Stream in European Climate, *Annual Review of Marine Science*, *7*, 113–137, doi:10.1146/annurev-marine-010814-015656. 1.1, 1.1

Perovich, D. K., B. Light, H. Eicken, K. F. Jones, K. Runciman, and S. V. Nghiem (2007), Increasing solar heating of the Arctic Ocean and adjacent seas, 1979-2005: Attribution and role in the ice-albedo feedback, *Geophysical Research Letters*, *34*(19), doi:10.1029/2007GL031480. 1.2

Piecuch, C. G., R. M. Ponte, C. M. Little, M. W. Buckley, and I. Fukumori (2017), Mechanisms underlying recent decadal changes in subpolar North Atlantic Ocean heat content, *Journal of Geophysical Research: Oceans*, *122*(9), 7181–7197, doi:10.1002/2017JC012845. 1.3, 2.2.3

Polyakov, I. V., L. A. Timokhov, V. A. Alexeev, S. Bacon, I. A. Dmitrenko, L. Fortier, I. E. Frolov, J.-C. Gascard, E. Hansen, V. V. Ivanov, S. Laxon, C. Mauritzen, D. Perovich, K. Shimada, H. L. Simmons, V. T. Sokolov, M. Steele, and J. Toole (2010), Arctic Ocean Warming Contributes to Reduced Polar Ice Cap, *Journal of Physical Oceanography*, *40*, 2743–2755, doi:10.1175/2010JPO4339.1. 1.2

Polyakov, I. V., A. V. Pnyushkov, M. B. Alkire, I. M. Ashik, T. M. Baumann, E. C. Carmack, I. Goszczko, J. Guthrie, V. V. Ivanov, T. Kanzow, R. Krishfield, R. Kwok, A. Sundfjord, J. Morison, R. Rember, and A. Yulin (2017), Greater role for Atlantic inflows on sea-ice loss in the Eurasian Basin of the Arctic Ocean., *Science*, *356*(6335), 285–291, doi:10.1126/science.aai8204. 1.2, 4

Polyakov, I. V., T. P. Rippeth, I. Fer, M. B. Alkire, T. M. Baumann, E. C. Carmack, R. Ingvaldsen, V. V. Ivanov, M. Janout, S. Lind, L. Padman, A. V. Pnyushkov, and R. Rember (2020), Weakening of Cold Halocline Layer Exposes Sea Ice to Oceanic Heat in the Eastern Arctic Ocean, *Journal of Climate*, *33*(18), 8107–8123, doi:10.1175/JCLI-D-19-0976.1. 1.2

Reigstad, M., P. Wassmann, C. Wexels Riser, S. Øygarden, and F. Rey (2002), Variations in hydrography, nutrients and chlorophyll a in the marginal ice-zone and the central Barents Sea, *Journal of Marine Systems*, *38*(1-2), 9–29, doi:10.1016/S0924-7963(02)00167-7. 1.2

Rheinlaender, J. W., D. Ferreira, and K. H. Nisancioglu (2020), Topological Constraints by the Greenland-Scotland Ridge on AMOC and Climate, *Journal of Climate*, *33*(13), 5393–5411, doi:10.1175/JCLI-D-19-0726.1. 1.2

Rhines, P., S. Häkkinen, and S. A. Josey (2008), Is Oceanic Heat Transport Significant in the Climate System?, in *Arctic-Subarctic Ocean Fluxes*, edited by Robert R. Dickson, Jens Meincke, and Peter Rhines, chap. 4, pp. 87–109, Springer Netherlands, doi:10.1007/978-1-4020-6774-7. 1.1, 1.1

Roberts, C. D., M. D. Palmer, R. P. Allan, D. Desbruyères, P. Hyder, C. Liu, and D. Smith (2017), Surface flux and ocean heat transport convergence contributions to seasonal and interannual variations of ocean heat content, *Journal of Geophysical Research: Oceans*, *122*(1), 726–744, doi:10.1002/2016JC012278. 1.3

Robson, J., P. Ortega, and R. Sutton (2016), A reversal of climatic trends in the North Atlantic since 2005, *Nature Geoscience*, *9*(7), 513–517, doi:10.1038/ngeo2727. 1.3

Robson, J. I., R. T. Sutton, and D. M. Smith (2012), Initialized decadal predictions of the rapid warming of the North Atlantic Ocean in the mid 1990s, *Geophysical Research Letters*, *39*(19), doi:10.1029/2012GL053370. 1.3

Sarafanov, A. (2009), On the effect of the North Atlantic Oscillation on temperature and salinity of the subpolar North Atlantic intermediate and deep waters, *ICES Journal of Marine Science*, *66*, 1448–1454, doi:10.1093/icesjms/fsp094. 1.3

Schauer, U., E. Fahrbach, S. Osterhus, and G. Rohardt (2004), Arctic warming through the Fram Strait: Oceanic heat transport from 3 years of measurements, *Journal of Geophysical Research*, *109*(C6), doi:10.1029/2003JC001823. 1.2

Schlichtholz, P. (2019), Subsurface ocean flywheel of coupled climate variability in the Barents Sea hotspot of global warming, *Scientific Reports*, *9*, doi:10.1038/s41598-019-49965-6. 1.3

Segtnan, O. H., T. Furevik, and A. D. Jenkins (2011), Heat and freshwater budgets of the Nordic seas computed from atmospheric reanalysis and ocean observations, *Journal of Geophysical Research*, *116*(C11), doi:10.1029/2011JC006939. 1.2

Sherwin, T. J., M. O. Williams, W. R. Turrell, S. L. Hughes, and P. I. Miller (2006), A description and analysis of mesoscale variability in the Färoe-Shetland Channel, *Journal of Geophysical Research*, *111*(C3), doi:10.1029/2005JC002867. 1.2

Signorini, S. R., and C. R. McClain (2009), Environmental factors controlling the Barents Sea spring-summer phytoplankton blooms, *Geophysical Research Letters*, *36*(10), doi:10.1029/2009GL037695. 1.2

Skagseth, Ø., T. Furevik, R. Ingvaldsen, H. Loeng, K. A. Mork, K. A. Orvik, and V. Ozhigin (2008), Volume and Heat Transports to the Arctic Ocean Via the Norwegian and Barents Seas, in *Arctic-Subarctic Ocean Fluxes*, edited by Robert R. Dickson, Jens Meincke, and Peter Rhines, chap. 2, pp. 45–64, Springer Netherlands, doi:10.1007/978-1-4020-6774-7. 1.2

Skagseth, Ø., T. Eldevik, M. Årthun, H. Asbjørnsen, V. S. Lien, and L. H. Smedsrud (2020), Reduced efficiency of the Barents Sea cooling machine, *Nature Climate Change*, *10*, 661–666, doi:10.1038/s41558-020-0772-6. 1.2, 2.1, 4

Steele, M., and T. Boyd (1998), Retreat of the cold halocline layer in the Arctic Ocean, *Journal of Geophysical Research: Oceans*, *103*(C5), 10,419–10,435, doi:10.1029/98JC00580. 1.2

Stommel, H. (1961), Thermohaline Convection with Two Stable Regimes of Flow, *Tellus*, *13*(2), 224–230, doi:10.1111/j.2153-3490.1961.tb00079.x. 1.1

Sutton, R. T., and M. R. Allen (1997), Decadal predictability of North Atlantic sea surface temperature and climate, *Nature*, *388*, 563–567, doi:10.1038/41523. 1.3, 4

Sverdrup, H. U. (1947), Wind-driven currents in a baroclinic ocean; with application to the equatorial currents of the eastern Pacific, *Proceedings of the National Academy of Sciences*, *33*(11), 318–326. 1.1

Trenberth, K. E., and J. M. Caron (2001), Estimates of Meridional Atmosphere and Ocean Heat Transports, *Journal of Climate*, *14*(16), 3433–3443, doi:10.1175/1520-0442(2001)014<3433:EOMAAO>2.0.CO;2. 1.1, 1.1

Trenberth, K. E., and J. T. Fasullo (2008), An Observational Estimate of Inferred Ocean Energy Divergence, *Journal of Physical Oceanography*, *38*, 984–999, doi:10.1175/2007JPO3833.1. 1.2

Uppala, S. M., P. W. Kållberg, A. J. Simmons, U. Andrae, V. D. C. Bechtold, M. Fiorino, J. K. Gibson, J. Haseler, A. Hernandez, G. A. Kelly, X. Li, K. Onogi, S. Saarinen, N. Sokka, R. P. Allan, E. Andersson, K. Arpe, M. A. Balmaseda, A. C. M. Beljaars, L. V. D. Berg, J. Bidlot, N. Bormann, S. Caires, F. Chevallier, A. Dethof, M. Dragosavac, M. Fisher, M. Fuentes, S. Hagemann, E. Hólm, B. J. Hoskins, L. Isaksen, P. A. E. M. Janssen, R. Jenne, A. P. Mcnally, J.-F. Mahfouf, J.-J. Morcrette, N. A. Rayner, R. W. Saunders, P. Simon, A. Sterl, K. E. Trenberth, A. Untch, D. Vasiljevic, P. Viterbo, and J. Woollen (2005), The ERA-40 re-analysis, *Quarterly Journal of the Royal Meteorological Society*, *131*(612), 2961–3012, doi:10.1256/qj.04.176. 2.2.1

van Sebille, E., S. M. Griffies, R. Abernathey, T. P. Adams, P. Berloff, A. Biastoch, B. Blanke, E. P. Chassignet, Y. Cheng, C. J. Cotter, E. Deleersnijder, K. Döös, H. F. Drake, S. Drijfhout, S. F. Gary, A. W. Heemink, J. Kjellsson, I. M. Koszalka, M. Lange, C. Lique, G. A. MacGilchrist, R. Marsh, C. G. Mayorga Adame, R. McAdam, F. Nencioli, C. B. Paris, M. D. Piggott, J. A. Polton, S. Rühs, S. H. Shah, M. D. Thomas, J. Wang, P. J. Wolfram, L. Zanna, and J. D. Zika (2018), Lagrangian ocean analysis: Fundamentals and practices, *Ocean Modelling*, *121*, 49–75, doi:10.1016/j.ocemod.2017.11.008. 2.2.2

Visbeck, M., E. P. Chassignet, R. G. Curry, T. L. Delworth, R. R. Dickson, and G. Krahmann (2003), The ocean's response to North Atlantic Oscillation variability, in *The North Atlantic Oscillation: Climatic Significance and Environmental Impact*, edited by J. W. Hurrell et al., pp. 113–145, AGU, Washington, D. C., doi: 10.1029/134GM06. 1.3

Wagner, P., F. U. Schwarzkopf, I. M. Koszalka, and A. Biastoch (2019), Can Lagrangian Tracking Simulate Tracer Spreading in a High-Resolution Ocean General Circulation Model?, *Journal of Physical Oceanography*, *49*, 1141–1157, doi: 10.1175/JPO-D-18-0152.1. 2.2.2

Weller, R. A., D. J. Baker, M. M. Glackin, S. J. Roberts, R. W. Schmitt, E. S. Twigg, and D. J. Vimont (2019), The Challenge of Sustaining Ocean Observations, *Frontiers in Marine Science*, *6*, doi:10.3389/fmars.2019.00105. 2.2

Wunsch, C. (2002), What is the Thermohaline Circulation?, *Science*, *298*(5596), 1179–1181, doi:10.1029/2001JC000888. 1.1

Wunsch, C., and R. Ferrari (2018), 100 Years of the Ocean General Circulation, *Meteorological Monographs*, *59*, doi:10.1175/AMSMONOGRAPHS-D-18-0002.1. 2.2

Wunsch, C., and P. Heimbach (2007), Practical global oceanic state estimation, *Physica D*, *230*, 197–208, doi:10.1016/j.physd.2006.09.040. 1.3, 2.2.3

Yeager, S., A. Karspeck, G. Danabasoglu, J. Tribbia, and H. Teng (2012), A Decadal Prediction Case Study: Late Twentieth-Century North Atlantic Ocean Heat Content, *Journal of Climate*, *25*, 5173–5189, doi:10.1175/JCLI-D-11-00595.1. 1.3

Yeager, S. G., and J. I. Robson (2017), Recent Progress in Understanding and Predicting Atlantic Decadal Climate Variability, *Current Climate Change Reports*, *3*(2), 112–127, doi:10.1007/s40641-017-0064-z. 1.3, 2.1

Zhao, J., A. Bower, J. Yang, X. Lin, and N. P. Holliday (2018), Meridional heat transport variability induced by mesoscale processes in the subpolar North Atlantic, *Nature Communications*, *9*(1), 1124, doi:10.1038/s41467-018-03134-x. 1.2

Zuo, H., M. A. Balmaseda, S. Tietsche, K. Mogensen, and M. Mayer (2019), The ECMWF operational ensemble reanalysis-analysis system for ocean and sea ice: a description of the system and assessment, *Ocean Science*, *15*, 779–808, doi:10.5194/os-15-779-2019. 2.2.3

Graphic design: Communication Division, UiB / Print: Skipnes Kommunikasjon AS

uib.no

ISBN: 9788230843482 (print)
9788230866177 (PDF)